MULTISCALE MODELING AND VALIDATION OF PARTICULATE PROCESSES

BY MAITRAYE SEN

A dissertation submitted to the

Graduate School—New Brunswick

Rutgers, The State University of New Jersey

in partial fulfillment of the requirements

for the degree of

Doctor of Philosophy

Graduate Program in Chemical and Biochemical Engineering

Written under the direction of

Dr. Rohit Ramachandran

and approved by

_____

_____

_____

_____

New Brunswick, New Jersey

May, 2015

ABSTRACT OF THE DISSERTATION

MULTISCALE MODELING AND VALIDATION OF PARTICULATE PROCESSES

by MAITRAYE SEN

Dissertation Director: Dr. Rohit Ramachandran

Since solid handling and processing have a wide application in many chemical and pharmaceutical industries, it is important to understand the powder dynamics. The objective of this work is to build multiscale models (with the aid of different modeling techniques; PBM (population balance model), DEM (discrete element model) and CFD (computational fluid dynamics) for various solid/powder handling operations and design an integrated flowsheet model connecting the continuous API (active pharmaceutical ingredient) purification/processing and downstream tablet manufacturing operations (as applicable in case of pharmaceutical industries). At present there is no existing link between the API processing and purification and downstream tablet manufacturing operation. However it has been seen that the physical properties of API (size, shape etc.) have considerable effect on the critical quality attributes (CQAs) of the product obtained from the downstream tablet manufacturing operations. Therefore, such a flowsheet will allow a detailed study of the effect of upstream (API purification and processing) process parameters on the downstream (tablet manufacturing) product attributes.

A multiscale modeling approach has been adapted in order to develop a novel PBM for powder mixing (an important unit operation in tablet manufacturing framework),

which can track various CQAs such as RTD (residence time distribution), RSD (relative standard deviation) and composition of the final blended product. The model demonstrated good prediction when validated against experimental results. The mixing model has been used for developing a multiscale, continuous, integrated flowsheet model. In this flowsheet model, the mixing unit has been integrated with the API separation and purification steps (i.e. crystallization, filtration and drying). The crystallization model has been developed based on population balance methodology and experimentally validated. The flowsheet model has been further used to perform optimization studies and design an efficient hybrid MPC-PID control system.

A multiscale CFD-DEM-PBM model has been developed for a fluid bed granulation process as well, which is an important operation present in the downstream tablet manufacturing framework (often present after the mixing operation). This model can be used to study the dynamics of the process and determine the CQAs of the granulated product. The multiscale model thus developed can be used to develop a reduced order model (ROM) which can be integrated with the flowsheet model.

This work will make a significant contribution towards understanding the process dynamics, process design and optimization in order to enhance the efficiency of the pharmaceutical manufacturing processes.

Acknowledgements

The very fact that I have reached this point, where I am writing my doctoral thesis, wouldn't have been possible without the three most important people in my life. My parents (Ms. Jaya Sen and Dr. Binay Sen) and JP (goes by "Japess" sometimes too!). I want to thank them for being there for me through my "ups and downs", no matter what. My mother has been a constant source of motivation and inspiration for me. She is one of the strongest and honest person I have in my life.

My hearty thanks and gratitude to my PhD advisor and mentor, Prof. Rohit Ramachandran. I wouldn't have reached this far without his help and support. I want to thank him for giving me a chance to be a part of his group and for believing that I can be a "Modeler" too! I could not ask for a better mentor.

I would like to thank my thesis committee members- Prof. Benjamin Glasser, Prof. Meenakshi Dutt and Dr. Ravindra Aglave. They have provided me with crucial feedback which have been extremely helpful towards my research. I also appreciate the support from ERC-CSOPS, NIPTE/FDA and various other funding agencies.

The years I spent at Rutgers as a doctoral student has been a life-time experience for me. During my PhD I had the opportunity to work with wonderful colleagues and make many friends. I would like to thank Ravendra Singh for his extremely useful advice and suggestions towards my research work. His help is greatly appreciated. I would also like to thank my colleague/friend/office-mate, Anwesha Chaudhury for her help whenever I needed it. Thanks to Anik Chaturbedi and Subhodh Karkala for being good friends. I want to thank my other colleagues- Dana Barrasso, Savitha Panikar, Ashutosh Tamrakar and Sarang Oka.

Last but not the least, I want to thank my favorite cousins- Shreya, Samriddha, Auditi, Sauparna and Baidurya. They are the closest thing I have to a brother or a sister.

Thanks to the four other people who made me realize that friends are no less than family, at times- Monojit, Yindrila, Lipika and Shanta. At the end, I want to acknowledge the part played by my maternal grandparents and my two aunts (Jyotsna and Jharna) in my life. All these wouldn't have been possible without their love and support.

Being a person with faith, my final thanks and gratitude to that "supreme being" for looking after me and my loved ones.

Table of Contents

Chapter 1

Introduction

The solid handling or processing industries have to deal with the inherent variability of powders which is the main hindrance towards effective operation and control of the manufacturing framework. Since particulate materials have a wide range of application in many chemical industries (e.g. food, agrochemical, paint, catalyst manufacturing, pharmaceutical etc.), it is important to be able to understand and overcome the various challenges associated with powder flow. It is difficult to explain powder flow on the basis of first-principles unlike fluid flow since each solid particle is a discrete entity which can interact in several ways with each other as well as with the equipment boundary. Flowability of powders may be erratic due to the segregation effect caused by the presence of fines, particle size distribution and presence of moisture which renders the powder cohesive etc. This work discusses the development of mathematical models in order to study and improve various manufacturing processes, as applicable in case of pharmaceutical industries. Many manufacturing processes in pharmaceutical industries are currently carried out in batch mode. Though batch processes are favored under certain processing conditions, continuous processing also has several advantages [1], such as it permits the same equipment to be used for small and large scale operations thereby minimizing the need for scale-up studies [2]. As the continuous process can be performed in a smaller area, it reduces plant footprint and is an environmental friendlier option than running batch-wise processes. It is also an energy and labor efficient process and gives more yield in principle [3]. A transition from batch to continuous mode of operation could require process re-designing and regulatory approval. The high cost of research and development required for developing new processes has always been an obstacle when implementing new manufacturing practices. In some cases, a batch mode

of operation may have certain shortcomings (e.g. inconsistency between batches, high cost) [4, 2, 5], which may be overcome by following a continuous processing strategy. Making use of model based approaches and continuous mode of production have the potential to reduce costs and improve the product quality [4, 5, 6, 7, 8, 9]. Modeling and simulation tools can aid the transition from batch to continous processing. A well developed, tuned, calibrated and validated model can be an effective tool in order to study the process dynamics or perform design, optimization and control studies. For instance, mathematical models can be developed that capture the dynamics of powder/solid processing operations, allowing for virtual experimentation and validation of new methodologies prior to implementation in the real plant. Design or optimization based studies require several trials; hence a model can be easily used for this purpose instead of conducting several experiments, which will also help to save resources.

In this work, some solid processing unit operations have been studied and implementation of continuous manufacturing framework in case of pharmaceutical industries has been discussed. The pharmaceutical industries have proven that it is innovative in the field of drug discovery and development by bringing novel drugs to market, however the area of improving the established manufacturing processes or introducing more efficient ones requires more focused attention [10]. In case of the pharmaceutical industries, the stringent regulatory requirements and the high cost of developing and understanding new processing techniques have made the transition difficult. The composition, purity, overall quality and effectiveness of the API being manufactured is of utmost importance. The high cost of drugs and the need for more efficient manufacturing methods makes it necessary to look towards more efficient production strategies that can meet these requirements and reduce the cost of healthcare without diminishing the quality [11]. The FDA (Food and Drug Administration, USA) mandates that all manufacturing stages meet the required GMP (Good Manufacturing Practices) in order to ensure good end product quality. Since it is necessary to closely monitor the product quality at every step in powder handling processes, the FDA has introduced the principles of QbD (Quality by design) and PAT (Process analytical technology). These guidelines allow consistent building of product quality at every step of the manufacturing framework

and help reduce production of inferior quality products. As the pharmaceutical industries are transitioning towards implementation of QbD and PAT guidelines, in order to improve the processing efficiency, there is a need to develop more science-based models which can be used to capture detailed process dynamics. Such a process model can be used for virtual experimentation and optimization, prior to testing in the actual plant. A mechanistic model developed from the first-principles can be more efficient in capturing the dynamics of a process compared to empirical or statistical models [12]. The pharmaceutical industries have two distinct upstream and downstream sets of operations. The upstream operation includes producing the drug molecule (API) followed by its purification and separation (i,e, reaction, separation, crystallization, filtration, drying etc.) [13]. The purified API crystals are further sent to the downstream processing framework where it is mixed with two or more excipient and the mixed product goes through several other unit operations (granulation, milling etc.) till the final tablet dosage forms are obtained [14]. The physical properties of the API crystal has a considerable effect on the downstream product quality. At present there is no connection between the upstream and downstream processes, therefore an important objective of this work is to establish such a connection in form of an continuously connected, integrated flowsheet model which can be used as an effective tool.

1.1 Summary of key results

It should be noted that the models which have been developed in this work are multiscale in nature. A multiscale model is able to store information from different scales or levels [15]. For example, a powder system consists of particles which can be treated as discrete entities. The powder particles interact with each other as well as the equipment wall/boundary in different manner. A process model developed based on population balance methodology alone is not able to track each and every individual particle. But it considers a particle population lumped based on certain characteristic (say size, shape, spatial location etc.). Therefore, PBMs are often referred to as meso-scale models. On the other hand, DEM is capable of simulating individual particles and thus store particle level information (on a particle scale). Similarly, continuum models (as

applicable in case of CFD) are associated with macro scale simulation. In this work, coupled PBM-DEM or CFD-DEM-PBM models have been developed for the different unit operations.

A novel PBM framework that can qualitatively capture the dynamics of a continuous powder mixing process has been developed. The PBM accounts for key design and process parameters such as mixer RPM, processing angle in terms of powder velocities, along with the effect of number of axial and radial compartments. Via this approach, results clearly show the qualitative validity of the PBM as a tool to capture the dynamics of the process that affect API composition, RSD and RTD. The model also demonstrates the use of the PBM as an overall multiscale modeling tool to combine particle-level models such as DEM in a multiscale framework. PBM interacts with DEM via one-way coupling which forms a basic framework for the multiscale modeling. The results thus obtained have been compared against a full DEM simulation which is a more fundamental particle-level model that elucidates the dynamics of the mixing process. Due to the relative computational simplicity of solving the PBM (as compared to DEM), the developed model can be used effectively in control and optimization of the mixing process. The developed PBM has been quantitatively validated by fitting experimentally obtained values of the above mentioned CQAs for different operating conditions. The model is dynamic and computationally tractable compared to traditional DEM descriptions of mixing processes. This lends credence to the use of the model as an effective tool in control and optimization of blending process and can have future implementation in designing a PAT system which will allow considerable improvements on the current manufacturing framework.

The mixer model has been connected with the API purification processes in form of an integrated flowsheet model which connects four unit operations, namely crystallization, filtration and drying followed by mixing. Crystallization, filtration and drying are the API separation and purification stages whereas mixing the purified API crystals with one or more desired excipient is a downstream pharmaceutical unit operation for tablet manufacturing. Since crystallization is an important separation step for the active ingredient, a parametric study on the crystallization model has been conducted

as well, by validating the model with experimental data. This particular flowsheet model has been optimized so that optimal operating conditions can be determined and the CQAs of the final product are satisfied. A multiscale MPC-PID control system has been designed for this particular flowsheet model. This will improve the process performance and maximize efficiency of the integrated process and also reduce the chance of producing rejects. The developed flowsheet process model can also be used as a modeling tool to implement control and optimization strategies *in-silico*.

A multiscale CFD-DEM-PBM model has been developed for a fluid bed granulation process, where both fluid and solid phases are present. In a fluid bed granulation process, the granules are formed by spraying the binder on the fluidized powder bed. The flow field can be solved by implementing CFD principles and the behavior of the solid particles can be modeled using DEM techniques. Presence of a link will help to understand how each phase interact with the other during the process.

The highlights of this work is to develop and validate a multiscale PBM for mixing process, integrating the mixing model with upstream API purification stages (crystallization, filtration and drying) in form of a continuous flowsheet model and presenting a multiscale framework to study the multiphase flow in fluid bed granulator (granulation being an important operation in the downstream tablet manufacturing framework and comes after the mixing operation). The overall objective is to establish a connection between the API purification/processing steps and the downstream tablet manufacturing operation which can be used to study the effect of the upstream process parameters on the downstream product quality and also provide control over the upstream parameters which can be manipulated in order to obtain the desired downstream product qualities.

1.2 Specific aims

This section lists the specific aims and the resulting publications for each aim.

Specific Aim I: Development of a multi-dimensional population balance model approach to continuous powder mixing process.

- **M. Sen**, R. Ramachandran, 2013. A multi-dimensional population balance model

approach to continuous powder mixing processes, Advanced Powder Technology, 24, 51-59.

Specific Aim II: Experimental validation of the population balance model, mathematical development and comparison of a multiscale PBM-DEM description of continuous powder mixing process.

- **M. Sen**, R. Singh, A. Vanarase, J. John, R. Ramachandran, 2012. Multi dimensional population balance modeling and experimental validation of continuous powder mixing processes, Chemical Engineering Science, 80, 349-360.
- **M. Sen**, A. Dubey, R. Singh, R. Ramachandran, 2013. Mathematical Development and Comparison of a Hybrid PBM-DEM description of a Continuous Powder Mixing Process, Journal of Powder Technology, DOI 10.1155/2013/843784

Specific Aim III: Multiscale model development, optimization and control of a continuous API purification/processing-downstream tablet manufacturing operation

- **M. Sen**, A. Chaudhury, R. Singh, R. Ramachandran, 2014. Two-dimensional population balance development and validation of a pharmaceutical crystallization process. American Journal of Modern Chemical Engineering, 1, 13-29.
- **M. Sen**, A. Chaudhury, R. Singh, J. John, R. Ramachandran, 2013. Multiscale flowsheet simulation of an integrated continuous purification-downstream pharmaceutical manufacturing process, International Journal of Pharmaceutics, 445, 29-38.
- **M. Sen**, A. Rogers, R. Singh, A. Chaudhury, J. John, M. G. Ierapetritou, R. Ramachandran, 2013. Flowsheet optimization of an integrated continuous purification-processing pharmaceutical manufacturing operation, Chemical Engineering Science, 102, 56-66.
- **M. Sen**, R. Singh, R. Ramachandran, 2014. Simulation-based design of an efficient control system for the continuous purification and processing of active pharmaceutical ingredients, Journal of Pharmaceutical Innovation, 9, 65-81.

- **M. Sen**, R. Singh, R. Ramachandran, 2014. A hybrid MPC-PID control system design for the continuous purification and processing of active pharmaceutical ingredients, Processes, 2, 392-418

Specific Aim IV: Development of a multiscale CFD-DEM-PBM description of a continuous fluid bed granulation process.

- **M. Sen**, D. Barrasso, R. Singh, R. Ramachandran, 2014. A multiscale hybrid CFD-DEM-PBM description of a fluid bed granulation process, Processes, 2, 89-111.

Chapter 2

Development of a multi-dimensional population balance model approach to continuous powder mixing process

- **M. Sen**, R. Ramachandran, 2013. A multi-dimensional population balance model approach to continuous powder mixing processes, Advanced Powder Technology, 24, 51-59.

The objective of this specific aim is to develop a novel PBM of a continuous mixing process which is able to qualitatively capture the dynamics of a typical powder mixing process. The effects of important process parameters and mixing performance (i.e, RSD, RTD, composition) have been investigated. The developed PBM can then be used as a multiscale tool (i.e., in combination with particle level models such as DEM) or for further model reduction (i.e., to obtain control relevant models for control and optimization).

A typical powder handling process will involve various unit operations, of which the most common are powder feeding, mixing, granulation etc. Considering the case-specific variability in the way in which the above processes are implemented, flexibility requires that any characterization be, to a large extent, modular (i.e., enabling multi-processing capabilities in a single manufacturing line) and this requires the modeling and characterization of a variety of different unit operations. This study focuses on continuous powder mixing which is an important unit operation and is almost always present no matter which route of processing is adapted.

Powder mixing is the act of bringing distinct bulk material particles into intimate contact in order to produce a mixture of consistent quality. Mixing of bulk solids occurs because of diffusive and convective velocity gradients within a given mixer. Segregation can also occur within the mixer, whereby the separation of distinct particles is

induced. Typically in pharmaceutical powder mixing processes that deal with fine cohesive powders, aggregation and segregation can occur whereby smaller particles can form agglomerates under the presence of cohesive forces triggering segregation due to differences in aggregation mobility (i.e., larger aggregation with greater mobility) [16].

Several experimental [17, 18, 19] and modeling approaches exist in the literature for powder mixing processes. The current modeling approaches can be categorized into Monte-Carlo methods [20], continuum and constitutive models [21], data-driven statistical models [22, 23, 24], compartment models [25, 26], RTD modeling approaches [27, 28, 29], multiscale-models [30, 31] and DEM based models [32, 33, 34, 35]. DEM models are typically very computationally intensive and require weeks/months of simulation which render it impractical for control and optimization. The other modeling approaches whilst having the advantage of being fast to solve, may often not contain detailed particle-level physics which experimental characterization and DEM simulations typically contain. A detailed review on the DEM method can be found in Dubey et al. [34]. The multiscale approach presented by Portillo et al. [30] presents an interesting use of combining a DEM plus statistical modeling approach to mixing processes and their results showed for a specific case study, mixing performance could be predicted reasonably accurately with huge savings in computational time. multiscale models have the potential to incorporate multiscale information from the particle level to the unit-operation level which is the motivating factor in this study, to consider an alternative approach (based on PBMs) to develop a multiscale framework to model continuous mixing processes.

2.1 Population Balance Model Methodology

Population balance models (PBMs) have been utilized substantially to model particulate processes such as crystallization [36, 37, 38, 39] and granulation [40, 41, 42, 43, 44] to name a few but till date have not been used to describe mixing processes.

2.1.1 Population Balance Equation

In its most general form, the population balance equation (PBE) is written as shown in Equation (2.1) [45]:

$$\frac{\partial F}{\partial t}(\mathbf{x},\mathbf{z},t) + \frac{\partial}{\partial \mathbf{x}}\left[F\frac{d\mathbf{x}}{dt}\right](\mathbf{x},\mathbf{z},t) + \frac{\partial}{\partial \mathbf{z}}\left[F\frac{d\mathbf{z}}{dt}\right](\mathbf{x},\mathbf{z},t) = \Re_{formation}(\mathbf{x},\mathbf{z},t) - \Re_{depletion}(\mathbf{x},\mathbf{z},t) + Inflow - Outflow \tag{2.1}$$

Here $\mathbf{x}$ is the vector of internal coordinates used to characterize the internal distribution, $\mathbf{z}$ is the vector of external coordinates and $F(\mathbf{x},\mathbf{z},t)$ is the population distribution function. In particulate processes, a single state variable, size, is often employed; and the resulting distribution is called the particle size distribution. The term $\frac{\partial}{\partial \mathbf{x}}\left[F\frac{d\mathbf{x}}{dt}\right](\mathbf{x},\mathbf{z},t)$ accounts for the evolution of the population distribution due to continuous growth. The term $\frac{\partial}{\partial \mathbf{z}}\left[F\frac{d\mathbf{z}}{dt}\right](\mathbf{x},\mathbf{z},t)$ accounts for the evolution of the population distribution with respect to spatial position. $\Re_{formation}(\mathbf{x},\mathbf{z},t)$ in Equation (2.2) accounts for formation of particles due to discrete phenomena such as aggregation and breakage, and $\Re_{depletion}(\mathbf{x},\mathbf{z},t)$ in Equation (2.3) accounts for depletion of particles by the same phenomena. Inflow and Outflow are the inlet and outlet flowrates respectively, in case of a continuous operation

$$R_{formation} = 0.5\int_{r_{min}}^{r-r_{min}} \beta(r', r-r')F(z,r',t)F(z,r-r',t)dr' + \int_{r}^{r_{max}} \Gamma(r')F(z,r',t) \tag{2.2}$$

$$R_{depletion} = \beta(r,r')F(z,r,t)F(z,r',t)dr' + \Gamma(r) + \phi(r)F(z,r,t) \tag{2.3}$$

Here $\beta(r,r')$ and $\Gamma(r)$ are the aggregation and breakage kernels respectively. $\phi(r)$ signifies a death-like phenomena. The first term in Equation (2.2) stands for the formation of particles of size r due to aggregation of two smaller particles. When two smaller particles combine, one larger particle is formed. Similarly the second term in Equation (2) represent formation of new particles due to breakage. r_{min} stands for the minimum

possible size of particles. In Equation (2.2) the first term stands for depletion of particles due to formation of new ones and the second term stands for depletion of particles due to breakage and death phenomena. See Ramachandran and Barton [44] for more details.

2.1.2 Multi-dimensional population balance model formulation

One-dimensional models have been well studied in particulate processes for model-based analysis [39, 46, 47]. They are often adequate for processes where the effect of key mechanisms (such as nucleation, aggregation and breakage) on the process dynamics can be accounted for through the consideration of a single particle characteristic. The modeling of continuous mixing processes requires the consideration of both internal and external coordinates and hence a multi-dimensional formulation of the PBE is required as shown in Equation (2.4) which represents a n three-dimensional formulation where n=2 to represent the the API and excipient components.

$$\begin{aligned}\frac{\partial}{\partial t}F(n,x,y,r,t)+\frac{\partial}{\partial x}\left[F(n,x,y,r,t)\frac{dx}{dt}\right]+\frac{\partial}{\partial y}\left[F(n,x,y,r,t)\frac{dy}{dt}\right]\\ +\frac{\partial}{\partial r}\left[F(n,x,y,r,t)\frac{dr}{dt}\right]=\Re_{formation}(n,x,y,r,t)-\Re_{depletion}(n,x,y,r,t)\\ +Inflow-Outflow \qquad (2.4)\end{aligned}$$

Here, x is the spatial co-ordinate in the axial direction, y is the spatial co-ordinate in radial direction, r is the internal co-ordinate which is particle size. The terms $\frac{dx}{dt}$ and $\frac{dy}{dt}$ represent the particle velocities in axial and radial directions respectively. The velocities act as an input to the PBM. The particle velocities can be obtained either experimentally or from a previously run simulation.

2.1.3 Aggregation Model

In this study, it has been assumed that no breakage of particles is taking place. Hence the breakage terms have been neglected although they can be incorporated into the

overall framework easily. The rationale is that particle cohesion leading to aggregation has been studied both experimentally [17] and via DEM simulations [16] as opposed to particle breakage. The aggregation rate process is defined in Equations (2.5) to (2.7)

$$\Re_{aggregation} = \Re_{formation} - \Re_{depletion} \tag{2.5}$$

where

$$R_{formation} = 0.5 \int_{r_{min}}^{r-r_{min}} \beta(n, x, y, r', r - r') F(n, x, y, r', t) F(n, x, y, r - r', t) dr \tag{2.6}$$

$$R_{depletion} = \beta(n, x, y, r, r') F(n, x, y, r, t) F(n, x, y, r', t) dr \tag{2.7}$$

$\beta(n, x, y, r, r')$ is the aggregation kernel and defined in Equation (2.8). The aggregation kernel is based on the kinetic theory of granular flow (KTGF) [48].

$$\beta(n, x, y, r, r') = K \sqrt{\frac{3\theta}{\rho}} (r + r')^2 \sqrt{\frac{1}{r^3} + \frac{1}{r'^3}} \tag{2.8}$$

Here K is a constant, ρ is the particle density and θ is a pseudo temperature termed as granular temperature (Equation (2.9)). v by definition is the random fluctuation velocity within a continuous granular medium but in this study is assumed to be the actual particle velocity for the purpose of establishing a baseline and can be used as a measure of its magnitude [49]. This assumption was deemed valid since it is the relative differences in the aggregation model that are important as opposed to the absolute differences. Although breakage of particles has not been considered in this study, it can be easily incorporated via previous work of Ramachandran et al. [43], which models particle breakage in a PBM framework.

$$\theta = \frac{1}{3} < v.v > \tag{2.9}$$

2.1.4 Numerical technique

In this study, a finite volume scheme has been used whereby the population distribution is first discretised into sub-populations and the population balance is formulated for each of these semi-lumped sub-populations. This is obtained by the integration of the population balance equation (see Equation (2.4)) over the domain of the sub-populations and re-casting the population into finite volumes. Thus, by this technique, the integro partial-differential equation as represented by the population balance equation, is reduced to a system of ordinary differential equations in terms of its rates. The ordinary differential equations are then integrated via a first order explicit Euler method. Stability conditions (e.g. CFL condition) have been checked similar to previous work in Ramachandran and Barton [44].

2.1.5 Mixer model development

The mixer is divided into multiple compartments both in the axial and radial direction. Mixing occurs in both directions via convective transfer. Dispersion is neglected since it is generally << than convection [26]. Particles are treated as discrete entities and their exchange between any two compartments is simulated dynamically to evaluate mixing performance defined by several metrics namely, API composition (y_{API}), RSD, average particle diameter (d_{30}) and the RTD, which are described in Equations (2.10) to (2.13). All of the above, represent CQAs which are required to be tightly monitored and controlled. It is crucial to maintain API composition within the blend since blend output is utilized in downstream processing such as granulation and tableting whereby the final granule/tablet composition must be within specification. RSD indicates the variability in API composition and typically quality control requires this variability to be between ±6%. RTD is a measure of the mixing performance of the mixer and monitoring the RTD can lead to improvements in the formulation and processing conditions to further optimize mixing performance.

$$y_{API} = \frac{\sum_{y=1}^{y_{max}} F(API, x_{max}, y, t)}{\sum_{n=1}^{n_{max}} \sum_{y=1}^{y_{max}} F(n, x_{max}, y, t)} \tag{2.10}$$

In the above equation, the numerator stands for the total number of API particles which come out of the last compartments at any point of time. The denominator represents total number of both API and excipient particles coming out of the last compartments at any point of time. Since there are only two components involved, hence the value of n_{max} is 2. x_{max} and y_{max} stand for the maximum number of grids in the axial and radial direction respectively.

$$RSD = \frac{\sqrt{\sum \frac{(y_i - y_{avg})^2}{n-1}}}{y_{avg}} \tag{2.11}$$

$$d_{30} = \left[\frac{(6r)}{\pi}\right]^{(1/3)} \tag{2.12}$$

$$E(t) = \frac{y_{API}(t)}{\int_0^\infty y_{API}(t)dt} \tag{2.13}$$

2.2 Simulation Results

The model simulations have been performed in MATLAB^{TM} (MathWorks) on a 8 GB RAM, 2.94 GHz desktop. The total discretized domain of the simulation comprised of 10, 10 and 10 finite volumes (bins) along the axial, radial and particle size coordinate axes. The width of the bin along the axial, radial and size coordinate was $4.4E^{-4}\,mm$, $1.0E^{-4}\,mm$, and $1E^{-5}\,m^3$ respectively.

2.2.1 Powder velocities

Powder velocities (i.e., the axial and radial velocities) need to be suitably described and incorporated into the PBM for effective dynamic simulation of the mixing process. In other work, the powder velocities have been determined experimentally along the axial length of the experimental vessel and constant velocities have been used [30] with the assumption that radial velocities are negligible and hence not considered. In this study, the assumption is relaxed and the powder velocities are determined firstly via a DEM simulation. The DEM simulation has been performed using EDEM^{TM} (DEM

Solutions) on a commercial mixer (Gericke GCM250^{TM}) at the actual scale with axial and radial dimensions of 330 mm and 100 mm respectively. The DEM simulation has been discussed in detail in specific aim 2.

Via post-processing of the data, axial and radial velocities can be determined at any point of time. However, in this study it has been obtained at $t = 180\,s$ once the steady state is reached. The purpose is to preserve the initial DEM velocities after which negligible change is observed and incorporate them into the PBM. Simulating the full DEM to obtain velocities would negate the utility of computationally cheaper model such as the PBM.

To illustrate the utility of the PBM to simulate the dynamics of the mixing process, a base case has been considered. Utilizing powder velocity information obtained from DEM simulation (mixer revolutions per minute set at 250 RPM), the PBM is simulated for a 10 by 10 grid for 1000 seconds. The base case represents a scenario of free-flowing particles which is generally considered in most works that utilize DEM based methods. Currently no work reports utilizing non DEM based methods on non free-flowing particles (i.e, cohesive particles). In this study, cohesive particles will be considered and addressed later in the section. API flowrate is fixed at one-fifth of the excipient flowrate (indicating a theoretical and desired y_{API} of 0.167). Total flowrate is 14.5 kg/h. An illustrative example (case 1) is presented whereby the powder velocities (obtained from the DEM simulation) are fed into the PBM to simulate the dynamics of the mixing process. In another example (case 2) constant powder velocities (as per the simulation in Portillo et al. [26]) have been considered to highlight the efficacy of the PBM as a tool to simulate mixing processes.

2.2.2 Case 1: Powder velocities from DEM simulation

Figure 2.1a illustrates the RSD (i.e, variability in the API composition) versus axial length at time end point(t=1000s). The axial length is represented in terms of the compartment number (1 to 10) in the axial direction. It can be seen that there is an overall decrease in the RSD over the length of the mixer as per what is typically observed from experimental data [26] and full DEM simulations [34]. It is interesting to note,

that in compartments 3 and 5, there is a spike in the RSD. This can be attributed to the high back-mixing (i.e, high proportion of negative powder velocities) and poorer radial mixing. Figure 2.1b depicts the RSD versus time profile taken at the mixer outlet. It can be seen that the variability decreases over time indicating that from a very initially segregated mixture (hence the extremely high RSDs), over time the mixing in the radial direction results in smoothening of the variability (0.35 at end-point). It can be noted that an RSD of < 0.06 is required for quality control in the pharmaceutical industry.

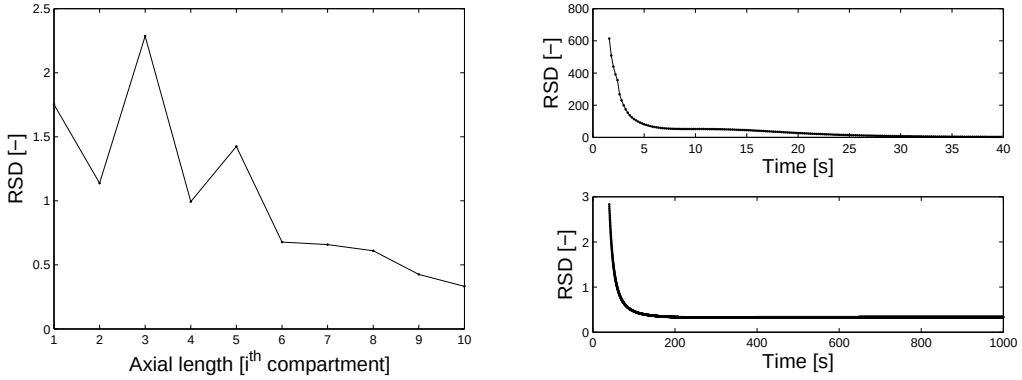

Figure 2.1: Plot of (a) RSD versus axial length at end time and (b) RSD versus time at mixer outlet for 0:40s and 40:1000s

Figure 2.2a shows the total mass flowrate at the inlet and outlet and confirms that the mass balance is satisfied. The time lag observed in the outlet flowrate can be attributed to the residence time in the mixer. Figure 2.2b indicates that the theoretical API composition is achieved at steady-state. This is a requirement of the total mass balance. Deviation from the composition can occur if there is a bias in the actual mixer (e.g. material stuck to the walls of the mixer due to cohesion). Figure 2.3 depicts the RTD of the API in the mixer upon injecting a pulse of API at $t = 100\,s$. The RTD curve indicates how long the API spends in the mixer and correlates to mixing performance. The width of the RTD curve can be set as a metric to optimize process performance as a function of formulation properties and processing conditions. Future sections will address the effect of certain processing parameters on RTD. Overall, the

PBM combined with the powder velocities obtained from DEM demonstrated that this integrated model can be a very useful tool in understanding the dynamics of the powder mixing process. Future sections will further address the effect of processing parameters on the earlier described CQAs.

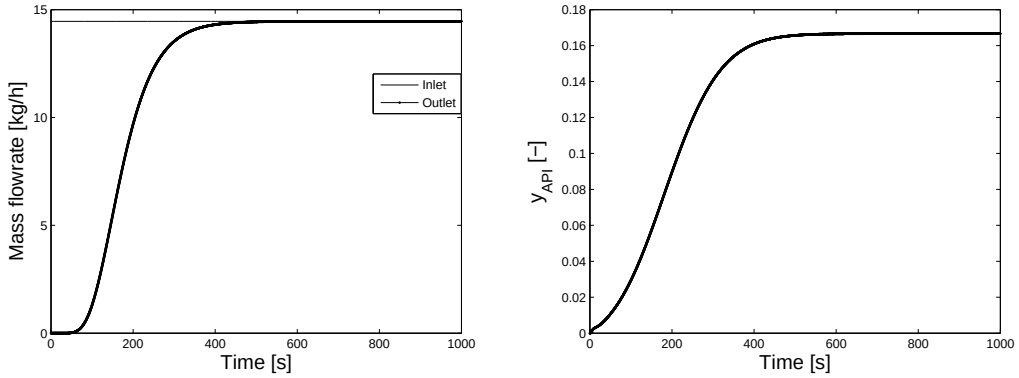

Figure 2.2: Plot of (a) Evolution of inlet and outlet mass flowrate and (b) evolution of API composition

2.2.3 Case 2: Constant powder velocities

The multiscale approach of combining PBM with DEM for powder mixing processes is a novel approach that has hitherto not been studied. It requires a detailed effort to understand each modeling tool well and more importantly the interface between them. The above section provides an illustrative example to demonstrate the utility and potential of this multiscale modeling approach as a robust modeling tool. In the next few sections, the DEM is decoupled from the PBM and only the PBM is considered. Constant values for the powder velocities are assumed (as opposed to obtaining them from DEM simulations) to investigate the robustness of the PBM by itself to qualitatively predict the trends of the CQAs as observed experimentally and *in silico* in the literature.

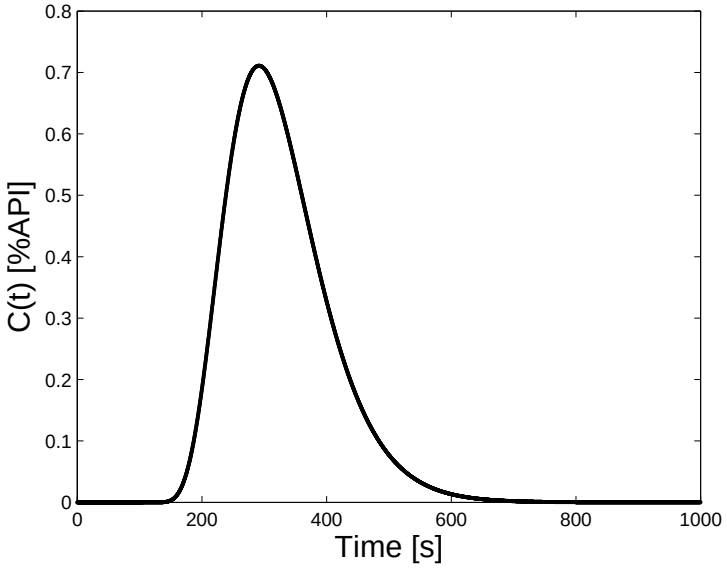

Figure 2.3: RTD of API upon injection of pulse at t=100s.

Effect of axial and radial mixing

Mixer RPM affects the degree of axial and radial mixing. To simulate impact of RPM, the axial and radial velocities are varied. Figure 2.5a illustrates the RSD versus axial length for differing axial powder velocities. It can be seen that as the axial powder velocities increases, the RSD increases, indicating de-mixing in the mixer. This can be attributed to powder moving faster through the mixer, thus spending reduced time in the mixer. This is also seen in Figure 2.5b whereby the RSD versus time at the mixer outlet is seen. Results show that as the axial powder velocities increase, the RSD as a function of time increases. Figures 2.4a and 2.4b show the effect of varying the radial powder velocities on the RSD versus axial length and RSD versus time. Results confirm that as radial mixing increases, the powder is more well-mixed and the RSD decreases. In Figure 2.6, the RTD for the different axial velocities can be seen confirming that for the larger axial velocities, the residence time of the powder in the mixer is reduced. .

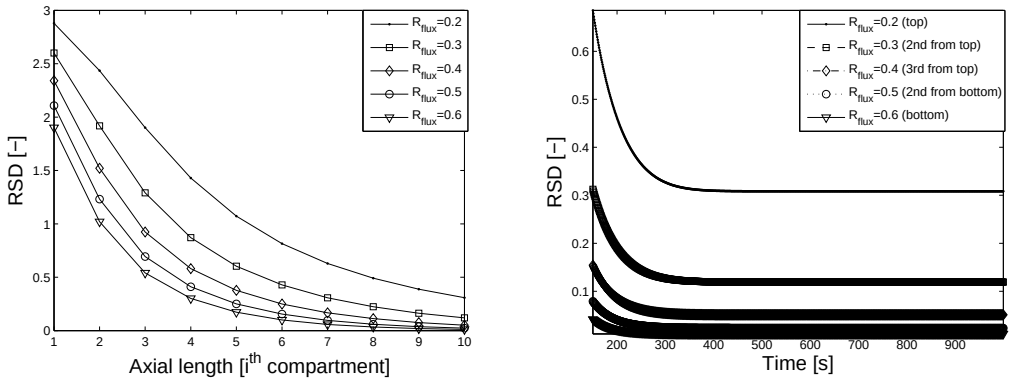

Figure 2.4: Plot of (a) RSD versus axial length at end time for different radial velocities and (b) RSD versus time at mixer outlet for different radial velocities

Effect of processing angle

Processing angle is an important design parameter in the operation of continuous mixing processes as it directly impacts both the mixing rates and the RTD of the powder. Conventional powder mixing design is to operate the mixer horizontally, but the mixer can also be upwardly or downwardly angled to affect mixing rates and RTD. To simulate varying processing angles, a range of axial and radial powder velocities have been considered. Note that varying the angle of the mixer changes both the axial and radial velocities proportionately (via component velocities derived from the linear velocity). Figure 2.7 depict the RSD versus axial length. It is interesting to note that there is an optimum achieved (lowest RSD value) at an intermediate axial and radial velocity. This qualitatively highlights that increased radial velocities promotes mixing but increased axial velocities promotes de-mixing, hence an optimum is achieved.

Effect of mixer dimensions

Mixer dimension is also an important design parameter that affects mixing performance. It is imperative that the minimal axial and radial dimensions are specified to ensure that the desired RSD is met. It should be noted that the mixer length and diameter in this work has been denoted in terms of number of axial and radial compartments

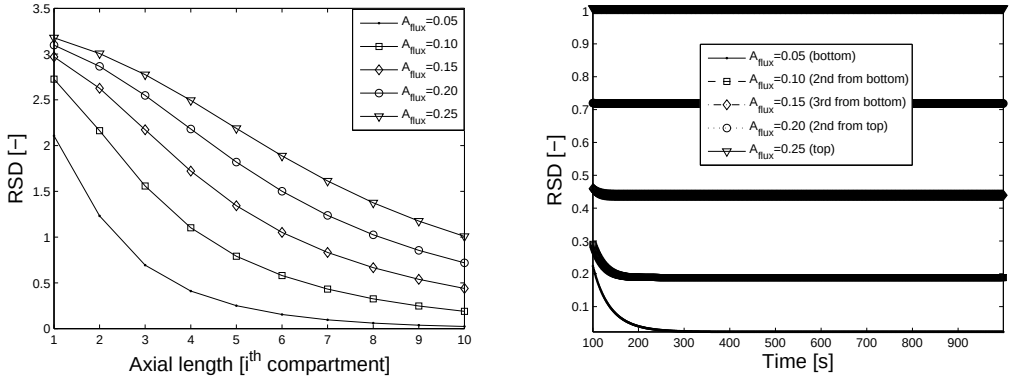

Figure 2.5: Plot of (a) RSD versus axial length at end time for different axial velocities and (b) RSD versus time at mixer outlet for different axial velocities

respectively. Figures 2.8a and 2.8b depict the RSD versus axial length and time respectively when the number of axial compartments is varied. It can be seen that as the number of compartments increases, RSD decreases. This is attributed to better mixing as the residence time of the powder in the mixer is increased. Figures 2.9a and 2.9b illustrate the effect of the number of radial compartments on RSD. It can be seen that as the number of radial compartments increases, RSD increases and this is attributed to poor mixing caused by increased segregation of the powders at t=0 (API and excipient are introduced into the mixer further apart).

Effect of cohesion

The effect of cohesion for powder mixing has been previously studied using DEM simulations [33, 50]. The conclusion is that cohesion plays a big role in the mixing and homogeneity of the blend. Cohesion typically leads to aggregation of particles. For instance API particles which are typically more cohesive tend to form larger agglomerates. As a result, this leads to a particle size differential which results in segregation of the larger particles and smaller particles in the mixer which in turn affects the mixing rates. Therefore, it is important to track the effect of cohesion on particle size via a

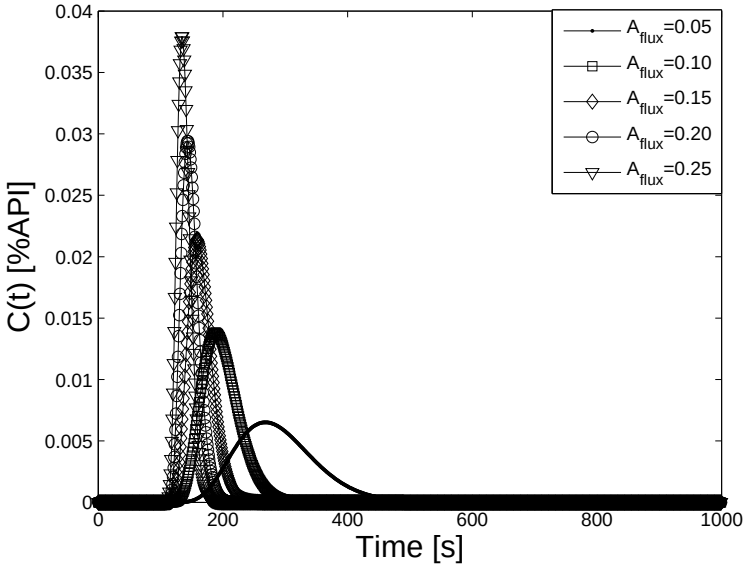

Figure 2.6: RTD of API upon injection of pulse at t=100s).

non DEM based approach such as the PBM utilized in this study. Figure 2.10 depicts the evolution of average diameter of the API and excipient as a result of cohesion which results in aggregation. The trend describes the qualitative effects of cohesion and illustrates the utility of the PBM to track size changes of particles which is also an important attribute to monitor. Detailed effects of cohesion can be studied via integrating DEM simulations with PBM in a multiscale manner. This is to account for changing velocity velocities (which can be calculated via DEM) as a result of cohesion-aggregation-segregation which lead to de-mixing. Nevertheless, the current PBM model demonstrates the coupling of an aggregation/cohesion kernel with the PBM framework to track size distributions.

2.3 Chapter Conclusions

A multi-dimensional PBM has been formulated to elucidate the dynamics of a continuous powder mixing process. The potential for a multiscale approach whereby DEM

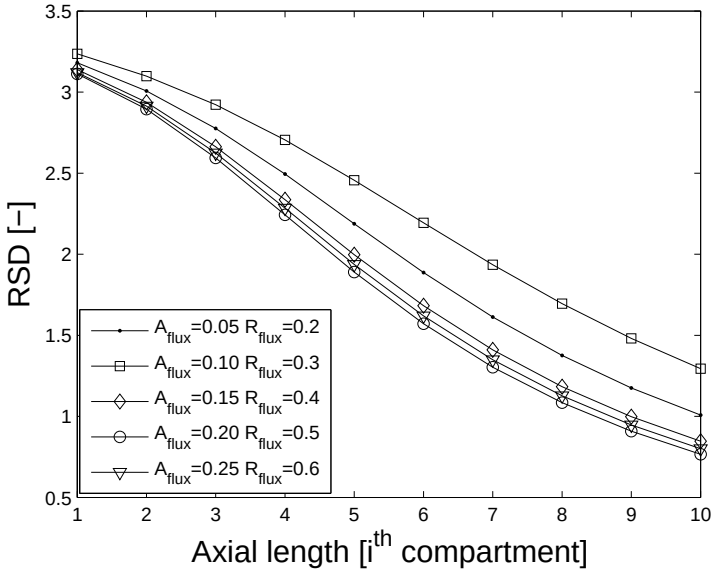

Figure 2.7: Plot of RSD versus axial length at end time

and PBM have been highlighted via an illustrative example with powder velocities obtained via DEM and used as inputs in the PBM to track key properties such as API composition and RSD. Focusing on the utility of the PBM as a robust model to describe mixing processes. This particular model can be used as an effective tool to study the effect of other processing and design parameters (i.e., mixer dimensions, processing angle, effect of mixer RPM). The effect of cohesion has been studied showcasing the ability of the PBM to incorporate monitoring of particle size (note: current non-DEM based models do not account for potential size enlargement of particles due to cohesion). Overall, results gives very good qualitative agreement with trends reported in the literature [30, 26] thus confirming the use of PBM along with other well established modeling tools (e.g. DEM) to describe the dynamics of the mixing process.

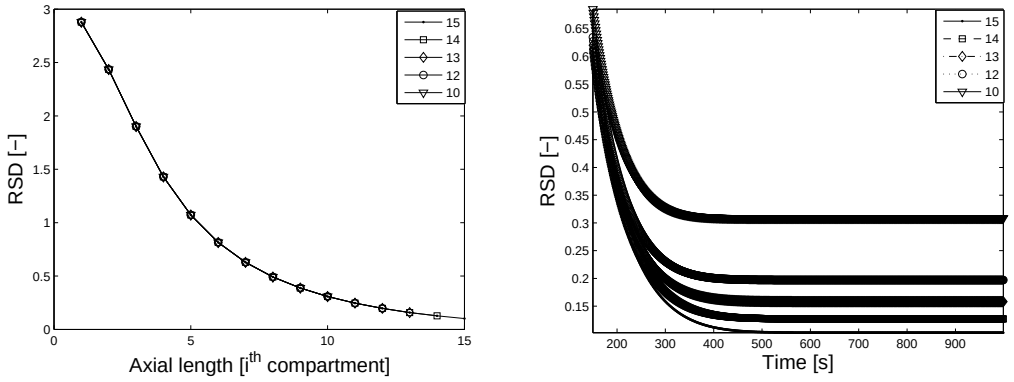

Figure 2.8: Plot of (a) RSD versus axial length at end time for different number of axial compartments and (b) RSD versus time at mixer outlet for different number of axial compartments

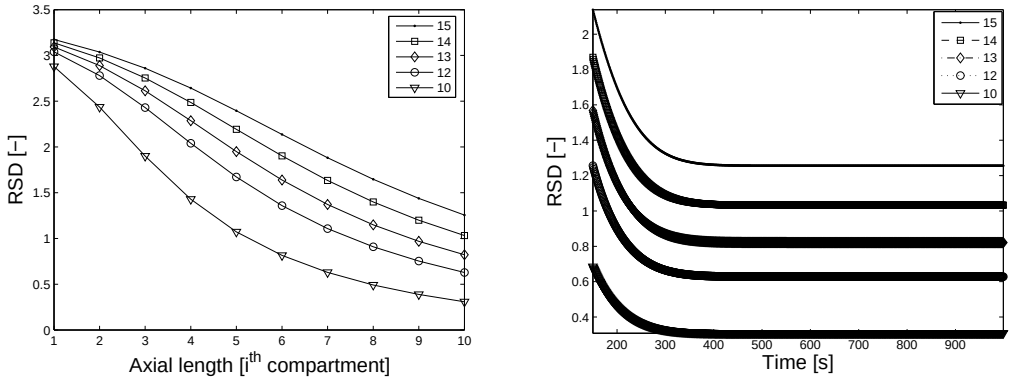

Figure 2.9: Plot of (a) RSD versus axial length at end time for different number of radial compartments and (b) RSD versus time at mixer outlet for different number of radial compartments

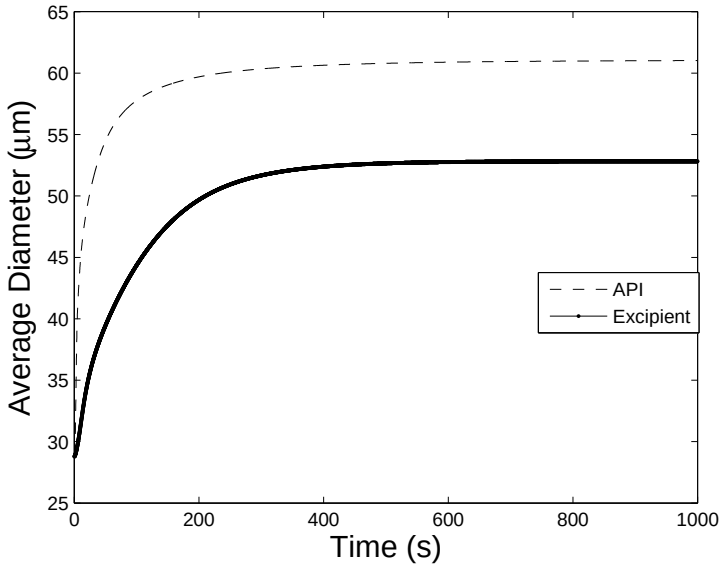

Figure 2.10: Evolution of average diameter for API and excipient.

Chapter 3

Experimental validation of the population balance model, mathematical development and comparison of a multiscale PBM-DEM description of continuous powder mixing process

- **M. Sen**, R. Singh, A. Vanarase, J. John, R. Ramachandran, 2012. Multi dimensional population balance modeling and experimental validation of continuous powder mixing processes, Chemical Engineering Science, 80, 349-360.
- **M. Sen**, A. Dubey, R. Singh, R. Ramachandran, 2013. Mathematical Development and Comparison of a Hybrid PBM-DEM description of a Continuous Powder Mixing Process, Powder Technology, DOI 10.1155/2013/843784

In this specific aim, one of the objectives is to quantitatively validate the multi-dimensional PBM of the continuous mixing model (developed in specific aim 1) with lab-scale experimental data. The optimization framework has been formulated using GAMS^{TM} (General Algebraic Modeling System). The velocity ratios between any two compartments have been estimated by optimizing the CQAs (RSD, Blend composition and RTD). The validated model can then be successfully used for design, analysis, control and optimization.

The other objective is to develop a dynamic one way coupled PBM-DEM model for continuous mixing process. This specific aim builds upon the previous study conducted in specific aim 1, which followed a steady state approach to develop a PBM to describe the dynamics of the mixing process. This dynamic and novel multiscale mixing model which combines DEM with PBM has been compared with the data from a full DEM simulation run on EDEM ^{TM}. The output of DEM has been post processed in order to extract the CQAs. As mentioned earlier, due to high computational time requirement,

DEM is not an effective tool for control and optimization. Hence in this work an offline coupling between DEM and PBM has been considered. DEM simulation can give information regarding particle properties (particle velocity) which are on particle level. These particle level information can be fed to the PBM from which the process-level variables (RSD, RTD, blend composition etc.) affecting the entire unit operation (mixing) can be extracted. In this way the model incorporates multiscale information and illustrates one way coupling where DEM provides the velocity information and is combined with the PBM which simulates key blend attributes as a function of time and thus applies the microscopic properties from particle level in order to capture process-level variables which characterize the mixing performance of the entire mixer.

The unpredictability of the powder blending operation is attributed to the uniqueness of the product formulation, which presents the challenge that no two mixing processes can ever be identical. The randomness in the process urged engineers to try to describe the process in quantitative terms and not empirically such that the accuracy of the predictive model is increased. The pharmaceutical industry is tightly regulated wherein all the production must comply with the good manufacturing practices (GMP) and the quality requirements are to be strictly satisfied [11]. It is due to inefficient control strategies [51, 52] and the non-predictive effects of process models that the final products obtained are often found to exhibit non-uniformity with a high degree of variability and do not meet the required specifications.

Since behavior of the powder processing units is still not well predicted, most pharmaceutical manufacturers employ a univariate trial and error strategy in their process development. Significant strides have been made to improve the process understanding by coupling science and a holistic risk-based assessment of both the product and the process by employing the QbD approach and PAT tools [53, 54, 55, 56, 57, 58].

In chemical-based product manufacturing, as in pharmaceutical, food and agrochemical industries, efficient and consistent process monitoring and analysis systems (PAT systems) have a very important role. These PAT systems ensure that the chemical based product is manufactured with the specified end product qualities [59]. The United

States FDA defines PAT as a mechanism to design, analyze, and control pharmaceutical manufacturing processes. It measures the Critical Process Parameters (CPP) which affects the CQAs of the final product. PAT aims at improving process understanding by defining their CPPs, and accordingly monitoring them in a timely manner (either on-line or in-line). This increases testing efficiency and also aids in time saving by avoiding unnecessary processing step, ensuring product consistency and reducing number of rejects [59, 60]. Hence it is important to have a well formulated and validated model of the unit operation so that there is significant reduction of time and expenses towards design of an efficient PAT system. Therefore, in this work an experimental validation of the mixing PBM has been carried out in order to show the ability of the model to capture or track experimental trends, followed by suggesting a multiscale framework which can capture the detailed process dynamics.

3.1 Multiscale modeling

PBM can incorporate the important design and process conditions and determine their effect on the various process variables on unit operation level. However the physics of any solid handling process is based on microscopic events which occur at particle level due to particle-particle and particle-wall interactions. The various particle characteristics (e.g. particle size distribution, particle shape, particle mass etc.) will govern the particle behavior. The gravitational and contact forces acting on the particles will have pronounced effect on the flow patterns [61, 62]. These particle-level phenomena will affect the path followed by the particles through different zones of the processing equipment [63]. A multiscale model for granulation has been reported in literature [64, 65], where a DEM has been used to determine the coalescence kernel and aggregation rate kernels in advance of solving a PBM. Abbas et al. [66] have reported a multiscale framework in case of crystallization where at the microscale, a PBM has been solved for predicting the crystal properties affected by fluid heat transfer on mesoscale and flow/temperature control on macroscale.

In multiscale modeling, the microscopic model is linked to the macroscopic model in a way such that the particle level information is used to track the CQAs of the final

product. A detailed summary on analysis and derivation of heterogeneous multiscale framework has been provided by Weinan et al. [67]. Although a model needs to be solved on macroscale but information is not always available. On the other hand, a model on microscale is available, but it is computationally intensive. Multiscale models can have two types of coupling (e.g. serial coupling and concurrent coupling) [68]. In serial coupling the microscopic model is solved beforehand and in concurrent coupling both the models (microscopic and macroscopic) are solved simultaneously.

DEM already exist in literature [32, 34, 69, 70] which are highly predictive in evaluation of particle-level physics. A PBM has been developed for the mixing process, as detailed in specific aim I. The coupling is serial in nature where the DEM simulation is run prior to simulating the PBM.

3.2 Discrete element model

Discrete element models treat each particle present in the granular flow as discrete entity unlike the continuum models which simulate the bulk behavior of the flow [34, 70]. The contact forces acting on the particles are calculated from Newton's second law of motion. The velocity and position of each particle are determined by integrating the particle's acceleration which is found from the contact force models. The particles are treated as spheres or collection of spheres and the distance between any two particles is computed as the distance between their centers. The distance between any two particles and the distance of any particle from the equipment boundary are computed at every time step. A particle-particle contact is detected if the distance between the centers of the particles is less than the sum of the particle radii and a particle-boundary contact is detected if the distance between the particle center and boundary is less than the particle's radius. A significantly small value for overlap is allowed in normal and tangential directions. Different types of contact models are available for DEM simulation [71, 72, 73]. Few of these models include continuous potential-based contact force models [74] and non-continuous contact force models [75, 76, 77]. DEM studies on different process equipments (e.g. hopper [78, 79], mixer [32, 34, 70], granulator [80, 81], crystallizer [82] etc.) are available in literature. DEM simulations

on the entire mixer has been performed by Dubey et al. [34]. These simulations are computationally expensive, hence a more economical approach of simulating a periodic slice of the mixer has also been suggested [32, 33].

3.3 Multiscale mixer model

The space is discretized into several compartments and it is assumed that homogenous mixing occurs in each of the compartments. Particles move from compartment to compartment in both axial and radial directions and this is governed by the axial and radial velocities. The exchange of mass between the compartments has been represented as number density of particles. Particles can either move forward to the compartment ahead of it or backward to the compartment behind it. On other hand, radial mixing conserves the total number of particles at a fixed axial location at any given point of time. Hence the mass balance of a single component can be simplified according to Equation (3.1):

$$\begin{aligned}\frac{\partial F(n,x,y,t)}{\partial t} = \frac{V_f[F_{n,x-1,y,t} - F_{n,x,y,t}]}{\Delta x} + \frac{V_b[F_{n,x+1,y,t} - F_{n,x,y,t}]}{\Delta x} \\ + V_r\frac{[F_{n,x,y+1,t} + F_{n,x,y-1,t} - 2F_{n,x,y,t}]}{\Delta y} + Inflow - Outflow \end{aligned} \tag{3.1}$$

The above equation can be written for component A and B (two components are being mixed). Component A can be treated as API and component B can be treated as the excipient. Here, V_f refers to the forward velocity in the axial direction, V_b refers to backward velocity in the axial direction and V_r refers to the radial velocity. Inflow is the rate at which the components are fed to the mixer. It is a constant value over time. If there are m×m compartments then outflow can be represented as $\sum_{n=1}^{2}\sum_{y=1}^{m} F(n,m,y,t)V_f$, where V_f is the forward flux.

The multiscale model does not require any of the particle properties (such as diameter, density, geometry etc.) or equipment geometry information as input, provided the velocities can be measured either experimentally or from detailed numerical simulations such as DEM. Once velocity parameters are selected, the simulation can be used to

provide information about the dynamics and the outcome of the process. It can be used to predict mixing performance in terms of a RSD of sample along the axial length at end time point, RSD at discharge as a function of time, API composition at discharge and RTD.

It can be noted that DEM will capture the particle properties and the effect of the equipment geometry in the velocity values. So if the particle size distribution is changed the velocity distribution is also going to change, which in turn will change the response of the PBM. Similarly, if the particle properties or mixer geometry are varied, the behavior of the output variables obtained from PBM will change accordingly.

3.4 Experimental validation of mixing model

Once a mathematical model is developed, it is an important task to validate the model with the help of experimental values in order to check if the model is able to track the experimentally determined trend. In this section the validation of the continuous mixer model has been discussed. The mixer has been divided into several compartments and the powder flow among these compartments has been expressed in terms of material balance equations. The model is dynamic in nature. Once the mathematical equations are formulated, the model parameters to be estimated need to be identified. The parameters in this case have been defined as the velocity ratios. Velocity ratios can be defined as the ratio of velocities (V_f,V_b,V_r as given in Equation (3.1)) of any two compartment between which particle transfer is taking place. Velocity ratios can take any value between -1 and 1. Forward axial velocity ratios are positive whereas backward axial velocity ratios are negative. Radial velocity ratios are always positive. In other words velocity ratios can be related to the relative number of particles being interchanged between any two compartments. These velocity ratios have been estimated at each point of time. The variables used to evaluate the mixing process are the RSD, API composition at the outlet and RTD. Several experiments have been carried out in order to obtain data sets of the above mentioned variables as a function of time. The objective is to fit the experimental data to the model following an optimization

algorithm which will minimize the sum of errors between the model predicted and experimental values. Since the problem is multi-dimensional and dynamic, time required to run the optimization program becomes an important factor. Hence the optimization framework has been solved on GAMS^{TM} using its built-in solver. The model has been validated for many experimental data sets and shown to be able to track these data with considerable accuracy. Figure 3.1 is a schematic of the steps followed.

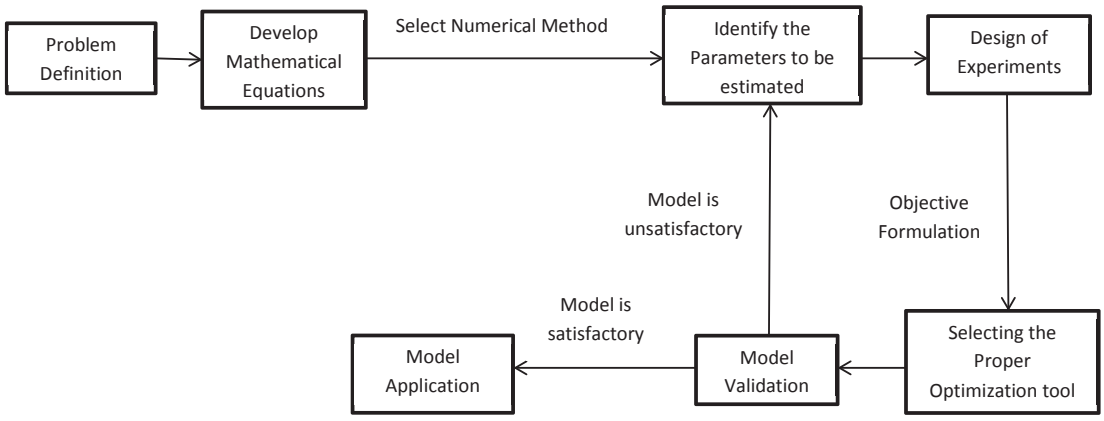

Figure 3.1: Problem formulation framework

The experimental data for RSD, API composition and RTD have been obtained from the work of Vanarase et al. [17, 83].

3.4.1 Parameter Estimation and Optimization

The optimization problem has been solved in GAMS^{TM}. Since RTD validation is from a different set of experiment, the RTD data has been fitted separately. The mixer optimization model is non-linear with 10101 number of constraints and 22561 number of variables. The Hessian of the Lagrangian has 5800 elements on the diagonal, 37256 elements below the diagonal and 19660 nonlinear variables. There are three families of solvers (CONOPT, MINOS and SNOPT) for nonlinear programming algorithms available on GAMS^{TM}. Each of these solvers behaves differently for a model. In this case CONOPT has been seen to be able to handle the model more effectively compared

to the rest. So the solver chosen is CONOPT. The non-linear programming algorithm is based on a generic GRG (Generalized reduced gradient) algorithm. The details of this algorithm has been explained by A. Drud [84, 85]. Since the model is likely to have multiple solutions, hence initial guesses have been provided so that the solution can be obtained in an appropriate region. This also reduces the time involved in finding the feasible solution. The mixer has been divided into a 5×5 compartment system with a total of 25 compartments. The simulation has been run for 100 seconds. There are two types of particles (Component A and component B) being mixed. The velocity ratios are a function of time, spatial position and particle type. The velocity ratios have been classified into three categories(e.g forward velocity ratios, backward velocity ratios and radial velocity ratios). Hence there are a total of 15000 velocity ratios which need to be estimated.

Parameter Estimation

The dynamic PBM after discretization can be represented functionally as given in Equations (3.2) and (3.3) [86]:

$$\dot{\mathbf{y}}(t, \mathbf{p}) = \mathbf{f}(\mathbf{y}(t, \mathbf{p}), \mathbf{p}), \forall t \in (0, t_f] \tag{3.2}$$

$$\mathbf{y}(0, \mathbf{p}) = y_o \tag{3.3}$$

where $\mathbf{y}$ is the population distribution function and $\mathbf{p}$ are the model parameters. The model parameters in this case are the forward, backward and radial velocity ratios between any two compartment.

Least square fitting has been used for parameter estimation. The objective is to decrease the squared error between the model predicted $\mathbf{x}_{predicted}$ and the experimental data $\mathbf{x}_{experimental}$. The data are usually the RSD and API composition values measured at different time points. It can be obtained by algebraic manipulations of the states such that $\mathbf{x}(t, \mathbf{p}) = g(\mathbf{y}(t, \mathbf{p}))$. The objective function to be minimized can be formulated as shown in Equation (3.4):

$$\Omega(p) = \sum_{z=1}^{n_z} \|\mathbf{x}_{predicted}(t_z, \mathbf{p}) - \mathbf{x}_{experimental}(t_z)\|^2 \tag{3.4}$$

where n is the total number of data points.

Gradient based optimization techniques are used to minimize Ω. The model sensitivities $\frac{\partial y_j}{\partial p_k}$ are integrated along with the model states $\mathbf{y}$ over the time domain, which are given as shown in Equations (3.5) and (3.6):

$$\frac{\partial \dot{\mathbf{y}}}{\partial \mathbf{p}}(t, \mathbf{p}) = \frac{\partial \mathbf{f}}{\partial \mathbf{y}}(t, \mathbf{p}) \frac{\partial \mathbf{y}}{\partial \mathbf{p}}(t, \mathbf{p}) + \frac{\partial \mathbf{f}}{\partial \mathbf{y}}(t, \mathbf{p}), \forall t \in (0, t_f] \tag{3.5}$$

$$\frac{\partial \mathbf{y}}{\partial \mathbf{p}}(0, \mathbf{p}) = 0 \tag{3.6}$$

Equation (3.7) below shows the sensitivity ODEs combined with the chain rule to obtain $\frac{\partial \Omega}{\partial \mathbf{p}}$:

$$\frac{\partial \Omega}{\partial \mathbf{p}}(\mathbf{p}) = \sum_{z=1}^{n_z} \sum_{m=1}^{n_m} 2(g_m(\mathbf{y}(t_z, \mathbf{p})) - x_{experimental,m}(t_z)) \frac{\partial g_m}{\partial \mathbf{y}}(t_z, \mathbf{p}) \frac{\partial \mathbf{y}}{\partial \mathbf{p}}(t_z, \mathbf{p}) \tag{3.7}$$

Objective function formulation

The RSD and API composition data were obtained from the experiments. The RSD and API composition have values of different orders. Hence the objective function for RSD has been multiplied by a constant (k) to fascilitate convergence. Individual objective functions can be formulated for each of the CQAs as shown in Equations (3.8) and (3.9).

$$\Omega^{APIComposition}(p) = \sum_{i=1}^{n} \|y_{API,predicted}(t_i, \mathbf{p}) - y_{API,experimental}(t_i)\|^2 \tag{3.8}$$

$$\Omega^{RSD}(p) = \sum_{i=1}^{n} k \| RSD_{predicted}(t_i, \mathbf{p}) - RSD_{experimental}(t_i) \|^2 \tag{3.9}$$

The overall objective function can then be formulated as shown in Equation (3.10):

$$\Omega^{Total}(p) = \Omega^{RSD}(p) + \Omega^{APIComposition}(p) \tag{3.10}$$

Since RTD measurement is a completely different set of experiment, hence the objective function has been formulated and optimized separately as shown below in Equation (3.11):

$$\Omega^{RTD}(p) = \sum_{i=1}^{n} \| E_{predicted}(t_i, \mathbf{p}) - E_{experimental}(t_i) \|^2 \tag{3.11}$$

Statistical Analysis

In order to test the robustness of the model, statistical tests have been conducted. A brief discussion on the various statistics which we considered in order to understand how effectively the model can fit the experimental data have been provided in this section.

The pearson correlation coefficient (R): The correlation coefficient measures the strength of a linear relationship or the degree of association between the model predicted (x) and experimental data (y). It can take any value between -1 and +1. A value of +1 will indicate a straight line between the experimental and predicted data.

$$R = \frac{\sum_{i=1}^{n} (x_i - \overline{x})(y_i - \overline{y})}{\sum_{i=1}^{n} (x_i - \overline{x})^2 \sum_{i=1}^{n} (y_i - \overline{y})^2} \tag{3.12}$$

Error sum of squares (SSE): It is a measure of the accuracy of predictions from model. Lower the value, better the model.

$$SSE = \sum (y_i - x_i)^2 \tag{3.13}$$

Regression Sum of Squares (SSR): It is again another measure for predicting the

accuracy of the model.

$$SSR = \sum (x_i - \overline{y})^2 \tag{3.14}$$

where $\overline{y} = \sum_{i=1}^{n} y_i/n$. $\overline{y}$ is also known as the mean value of the experimental data.

Coefficient of correlation (R^2) **and adjusted** R^2: It gives the extent of variance or fluctuation of the predictable variable. It is a measure of the certainty with which predictions can be made from the model. It can take any value between 0 and 1. If R^2 is equal to 1, it will indicate that regression line perfectly fits the data. However a large value of R^2 does not always imply that the model is a good one. For example, adding a variable to the model will always increase the value of R^2 regardless of whether the additional variable is statistically significant or not. To overcome this drawback, adjusted R^2 is often used. Its value is not affected by addition of any new variable to the model. Adjusted R^2 has the same significance as the R^2.

$$R^2 = 1 - \frac{SSE}{SST} \tag{3.15}$$

where $SST = \sum (y_i - \overline{y})^2$. SST is the total error.

3.5 Mixer model validation results

Several experimental data sets have been collected by varying the mixer speed (RPM) and feed rate. As demonstrated previously, mixer rpm is an important deciding factor as far as the blend quality is concerned. It affects the degree of axial and radial mixing. RTD model has been formulated and validated separately. RTD decreases with increase in mixer RPM. Experimental data points are highly scattered over time. This is because of the noisy and missing data which is caused by the measurement error of the sensor [23]. The flow of solid particles cannot be explained by first principle which is otherwise applicable in case of fluid flow. Hence a polynomial function has been first fitted to the data points. The main aim is to consider a mean of the scattered values so that a smooth curve can be obtained. The model has been validated for the fitted

trend line. The model optimization has been performed on an 8GB RAM, 2.94 GHz, 64-bit, 8-cored, Dell desktop. The optimization takes several minutes to run.

3.5.1 RSD and API composition

The model has been validated with four different experimental data sets [87]. Each experimental set provides with data for RSD and API Composition. A linearity test has also been conducted for each case by plotting model predicted data versus experimental data. Validation for the first two cases are being reported in this section.

Experiment 1

This data set has been obtained for a feedrate of 20 kg/hr and mixer speed of 200 RPM. API concentration in the mixture fed to the mixer inlet is 25%. Figure 3.2a and Figure 3.2b represent the comparision for API composition and RSD respectively. Figure 3.3a and Figure 3.3b show the linearity relationship for API composition and RSD respectively. Table 3.1 gives the value of the statistical parameters. As shown in Figure 3.2a, the predicted API composition is matching exactly with the experimental data (trendline) with very minor error. This can be further verified with the linearity plot as shown in Figure 3.3a, where a straight line between predicted API composition and experimental data can be seen. It is reflected in statistical analysis (see Table 3.1) as well. The R value is found to be 0.999805 which means that predicted API composition has a very strong linear relationship (straight line) with the experimental API composition. High value of R^2 (0.999388) and adjusted R^2 (0.99382) indicates a very high certainty in prediction of API composition. A very low value of SSE (0.000176) and SSR (0.001341) further verifies the accuracy of the model. Figure 3.2b as well as statistical analysis (see Table 3.1) show that the model is tracking the experimental RSD data (trendline) very well. Furthermore, figure 3.3b as well as the statistical analysis indicates that the predicted RSD and experimental RSD has a strong linear relationship (R=0.999411). Value of R^2 (0.998497) and adjusted R^2 (0.998482) are very high which means that through this model RSD could be predicted with high certainty. In this case the change in the initial and final values of RSD and API composition over the entire time period are 18.05% and 30.5% respectively.

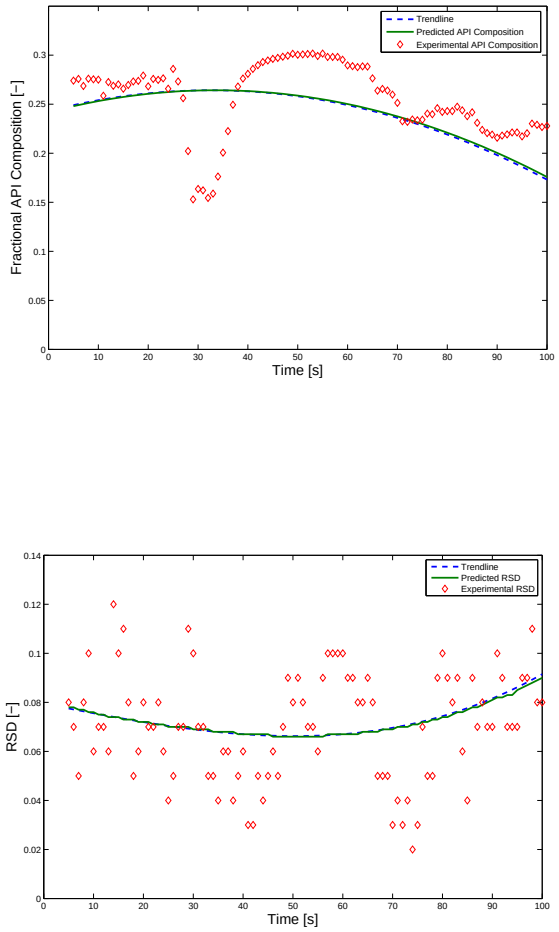

Figure 3.2: (a) Fractional API Composition versus time at mixer outlet for experiment 1 and (b) RSD versus time at mixer outlet for experiment 1

Experiment 2

Another experimental trial has been repeated for the same mixer speed of 200 RPM maintaining the feedrate at 20 kg/hr but with API concentration of 5% at the mixer inlet. Figure 3.4a is a comparision of the experimental and model predicted data for API composition whereas Figure 3.4b is the plot for RSD. Figure 3.5a and Figure 3.5b are the plots of linearity relationship for API composition and RSD respectively. Table 3.2 gives the value of the statistical parameters. Figure 3.4a shows a very good agreement

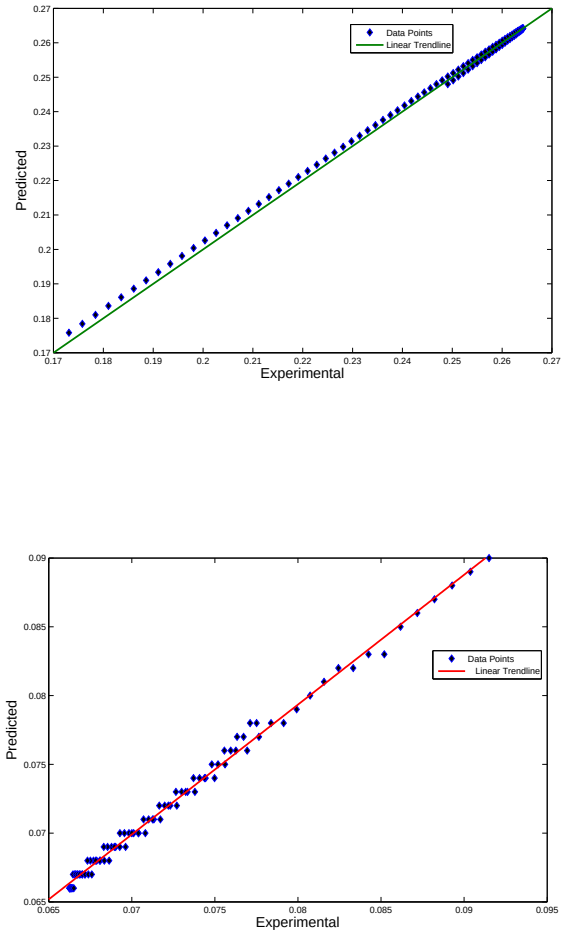

Figure 3.3: (a) Linearity plot for API Composition for experiment 1 and (b) Linearity plot for RSD for experiment 1

between the predicted and experimental (trendline) API composition. A strong linear relationship can be seen in Figure 3.5a. Statistical results as given in Table 3.2 further verify the accuracy of the model. As desired for a good model, the values of R (0.999366), R^2 (0.997179) and adjusted R^2 (0.997151) are very close to unity while the values of SSR (0.003026) and SSE (0.000897) are very close to zero. Similarly, predicted RSD and experimental RSD (trendline) has a good agreement as shown in Figure 3.4b. Figure 3.5b shows a good linear relationship between predicted and experimental RSD. Statistical analysis further verifies strong linearity (R=0.999346), good

API Composition	
Correlation	0.999805
R^2	0.999388
Adjusted R^2	0.99382
SSR	0.001341
SSE	0.000176
Relative Standard Deviation (RSD)	
Correlation	0.999411
R^2	0.998497
Adjusted R^2	0.998482
SSR	0.000607
SSE	$3.61E-05$

Table 3.1: Statistics for experiment 1

RSD prediction certainty (R^2=0.998425, adjusted R^2=0.998409) and a good model fitting (SSR=0.003148, SSE=0.000971). In this case the change in the initial and final values of RSD and API values over the entire time period are 44.4% and 41.43% respectively.

Experiment 3

This data set has been obtained for a feedrate of 20 kg/hr and mixer speed of 40 RPM. API concentration in the mixture fed to the mixer inlet is 10%. Figure 3.6a and Figure 3.6b show the comparision between the experimental and model predicted values of API composition and RSD respectively. As seen in Figure 3.6a, the model predicted API composition matches very well with the experimental data (trendline). Table 3.3 gives the value of the statistical parameters. Very high values of R (0.998423), R^2 (0.996064) and adjusted R^2 (0.996024) and very low values of SSR (0.001232), SSE (0.000149) shows a good fit of the mathematical model as well as high certainty in prediction of API composition. The match of predicted RSD with the experimental data can be seen in Figure 3.6b where a small deviation from the trendline has been observed. The statistical analysis (see Table 3.3) also reflects this. Values of R^2 (0.656826) and adjusted R^2 (0.653324) indicates an average certainty in prediction of RSD. Figure 3.7a represents the linearity relationship between the experimental and model predicted data for API composition. Figure 3.7b represents the linearity relationship between the two data sets for RSD. In this case the change in the initial and final values RSD and API

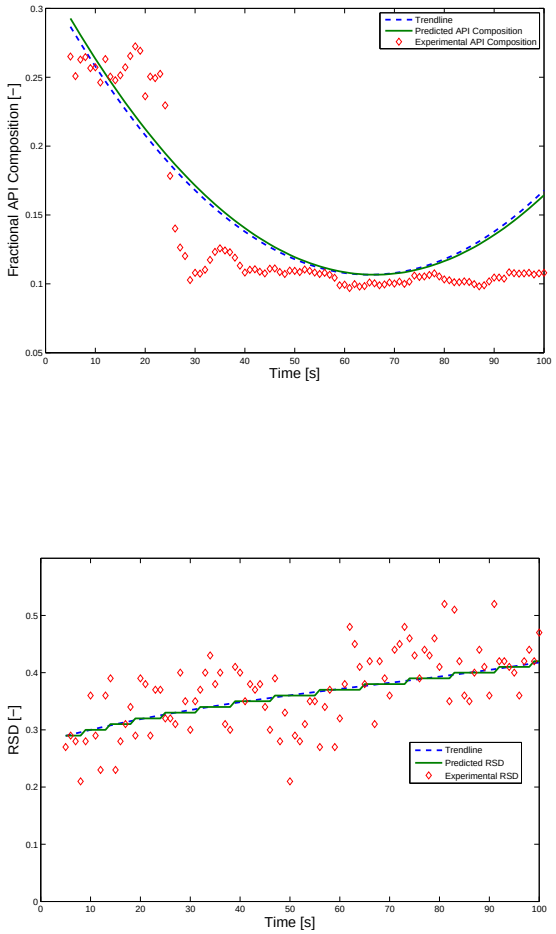

Figure 3.4: (a) Fractional API Composition versus time at mixer outlet for experiment 2 and (b) RSD versus time at mixer outlet for experiment 2

values over the entire time period are 0.00046% and 0.36% respectively. Since several data points are repeated over time, hence an average of the values have been taken to represent the linearity relationship.

Experiment 4

This data set has been obtained for a feedrate of 20 kg/hr and mixer speed of 320 RPM. API concentration in the mixture fed to the mixer inlet is 10%. Figure 3.8a and Figure 3.8b are the plots for API composition and RSD as obtained experimentally and predicted from the model. Figure 3.9a and Figure 3.9b show the linearity

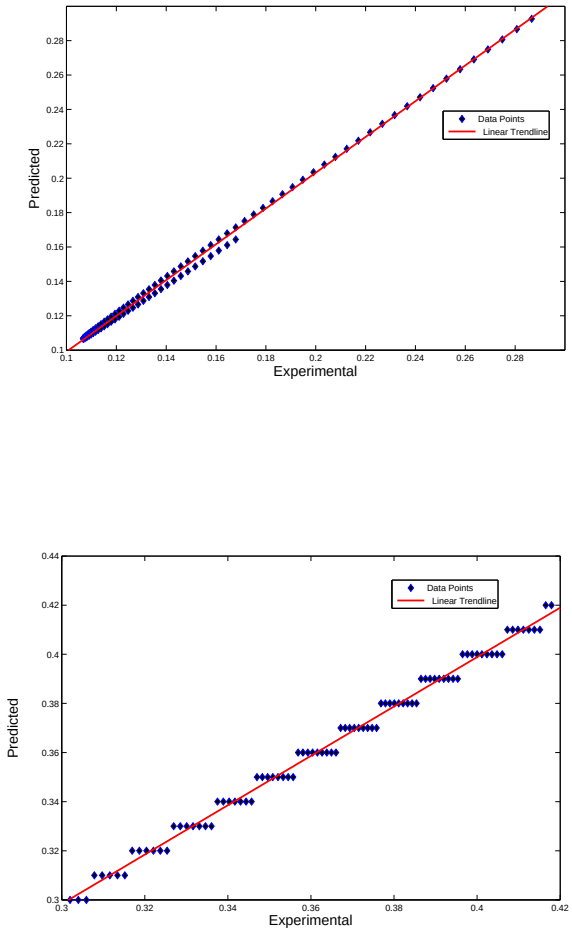

Figure 3.5: (a) Linearity plot for API Composition for experiment 2 and (b) Linearity plot for RSD for experiment 2

relationship for API composition and RSD respectively. Table 3.4 gives the value of the statistical parameters. As shown in Figure 3.8a, the predicted API composition approaches the experimental data with minor deviation. However, the statistical analysis (see Table 3.4) shows that the error is very less (SSR=0.007651, SSE=0.005737) and can be accepted. Furthermore, the predicted API composition shows a good linear relationship (R=0.987291) with the experimental data and the model can be used for the prediction of API composition with average certainty (R^2=0.973382, adjusted

API Composition	
Correlation	0.999366
R^2	0.997179
Adjusted R^2	0.997151
SSR	0.003026
SSE	0.000897
Relative Standard Deviation (RSD)	
Correlation	0.999346
R^2	0.998425
Adjusted R^2	0.998409
SSR	0.003148
SSE	0.000971

Table 3.2: Statistics for experiment 2

API Composition	
Correlation	0.998423
R^2	0.996064
Adjusted R^2	0.996024
SSR	0.001232
SSE	0.000149
Relative Standard Deviation (RSD)	
Correlation	0.996931
R^2	0.656826
Adjusted R^2	0.653324
SSR	0.15131
SSE	0.022438

Table 3.3: Statistics for experiment 3

R^2=0.973111). Similarly from Figure 3.8b predicted RSD is also approaching the experimental data with some minor error (SSR=0.007651, SSE=0.005737) that can be accepted. Measure of linearity (R=0.974142) and prediction certainty (R^2=0.940338, adjusted R^2=0.939729) is also acceptable. In this case the change in the initial and final values of RSD and API values over the entire time period are 19.5% and 0.85% respectively. Several data points are repeated over time, hence an average of the values have been taken to represent the linearity relationship.

3.5.2 Residence Time Distribution

RTD study has been conducted for mixer speed of 254 RPM at two different feed rates [87]. Validation result for one case is being reported here.

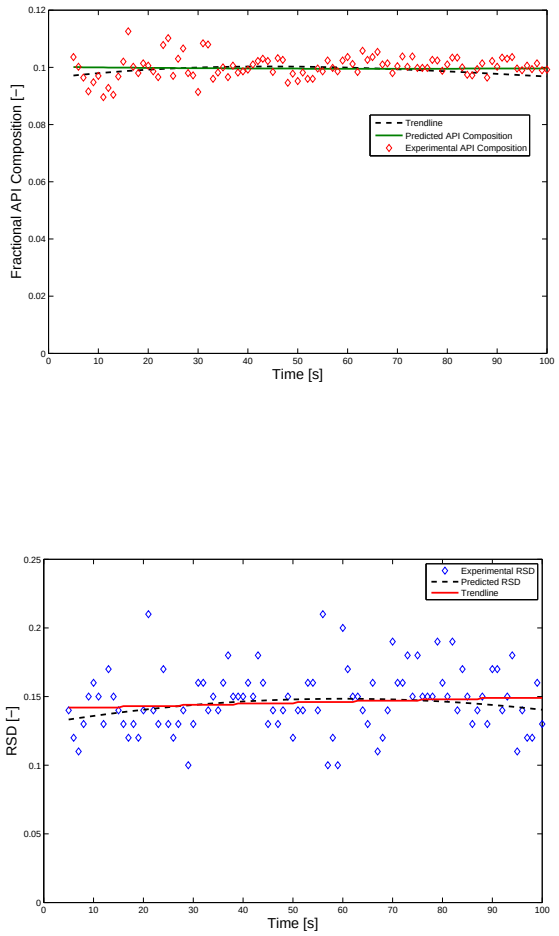

Figure 3.6: (a) Fractional API Composition versus time at mixer outlet for experiment 3 and (b) RSD versus time at mixer outlet for experiment 3

Run 1

The feed rate is maintained at 30 kg/hr. Figure 3.10 gives the comparison between the experimental and predicted data. Figure 3.11 is the linearity plot. Table 3.5 gives the statistics of the model. The nature of predicted RTD curve has a good agreement with the experimentally obtained RTD curve as shown in Figure 3.10. However, quantitatively a very small deviation has been observed. The predicted and experimental RTD also have a good linear relationship as shown in Figure 3.11. Furthermore, the statistical analysis (see Table 3.5) verifies quantitatively an average model fitting and

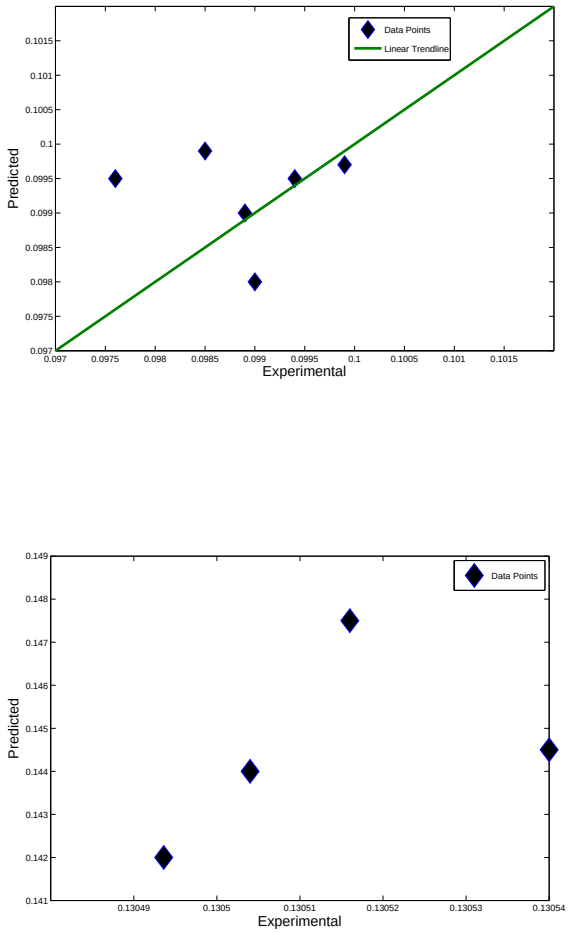

Figure 3.7: (a) Linearity plot for API Composition for experiment 3 and (b) Linearity plot for RSD for experiment 3

linearity.

Run 2

The feed rate is increased to 45 kg/hr. Figure 3.12 gives the comparison between the experimental and predicted data. Figure 3.13 is the linearity plot. Table 3.6 gives the statistics of the model. In this case also, the nature of predicted RTD curve shows a good agreement with the experimentally obtained RTD curve (see Figure 3.12). A small deviation has been also observed. However, the statistical analysis shows that this error is minor (SSE=0.005493, SSR=0.028012) and could be acceptable. The predicted RTD

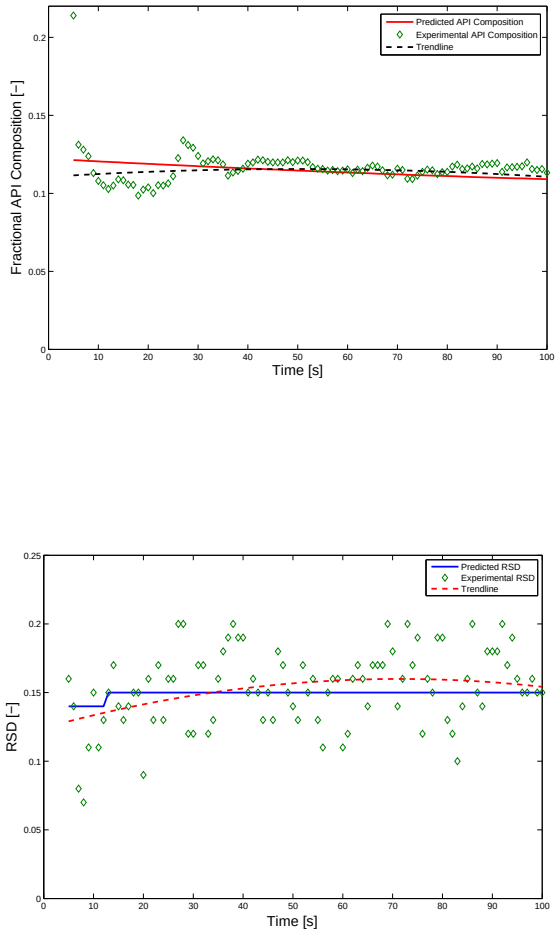

Figure 3.8: (a) Fractional API Composition versus time at mixer outlet for experiment 4 and (b) RSD versus time at mixer outlet for experiment 4

has a good linear relationship with the experimental RTD as shown in Figure 3.13 and further verified through statistical analysis (see Table 3.6).

3.6 Multiscale DEM-PBM model results

3.6.1 DEM Simulation (in collaboration with Dr. Atul Dubey)

In EDEM^{TM}, a commercial mixer (Gericke GCM250 ^{TM}) with impeller blades in alternating forward and backward orientation has been simulated. The details regarding the mixer blade geometry has been elaborated by Dubey et al [70]. Figure 3.14 gives

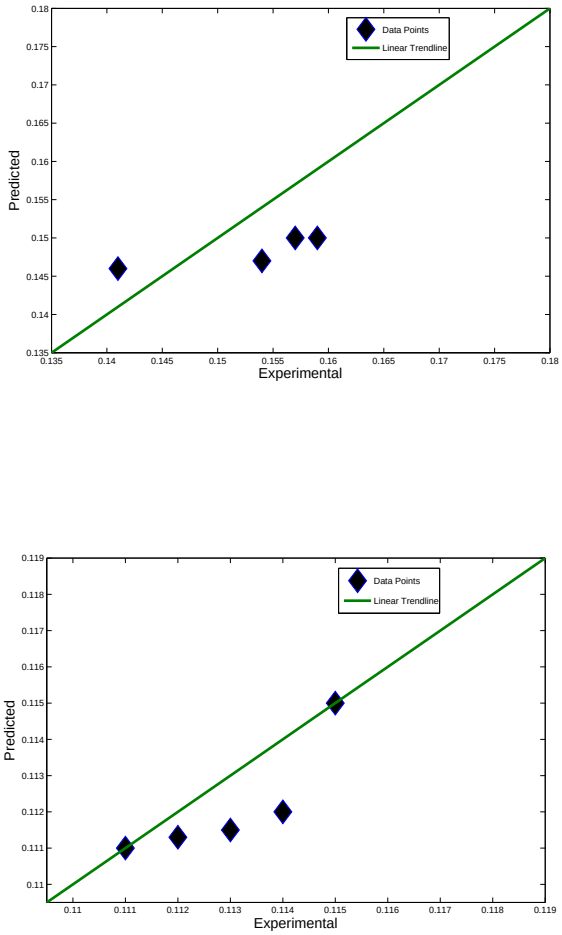

Figure 3.9: (a) Linearity plot for API Composition for experiment 4 and (b) Linearity plot for RSD for experiment 4

a snapshot of the mixer on EDEM^{TM}. The length and diameter of the mixer are 330 mm and 100 mm respectively. Equal number of partictles each of component A and B (or API and excipient as the system may be) are introduced into the mixer using two feeders discharging particles on either side of the inlet. The two components are completely segregated in the beginning. Table 3.7 gives the details about the particle properties, particle-particle, particle-blade and particle-wall interaction parameters used in the simulation. A feed rate of 1990 particles per second and an impeller speed of 250 rpm have been maintained. Normal particle size distribution with a mean radius of

API Composition	
Correlation	0.987291
R^2	0.973382
Adjusted R^2	0.973111
SSR	0.00369
SSE	0.001355
Relative Standard Deviation (RSD)	
Correlation	0.974142
R^2	0.940338
Adjusted R^2	0.939729
SSR	0.007651
SSE	0.005737

Table 3.4: Statistics for experiment 4

RTD	
Correlation	0.815995
R^2	0.540216
Adjusted R^2	0.494238
SSR	0.058952
SSE	0.034753

Table 3.5: Statistics for RTD-run 1

1mm with 5 % standard deviation has been used. The simulation runs for 260 seconds. The simulation is post-processed to obtain the axial velocities, radial velocities and particle IDs. In a DEM simulation, each particle is assigned a unique number known as the particle ID. These data are then used to obtain the RSD as a function of mixer length and time, rate of outflow, blend composition at discharge and RTD.

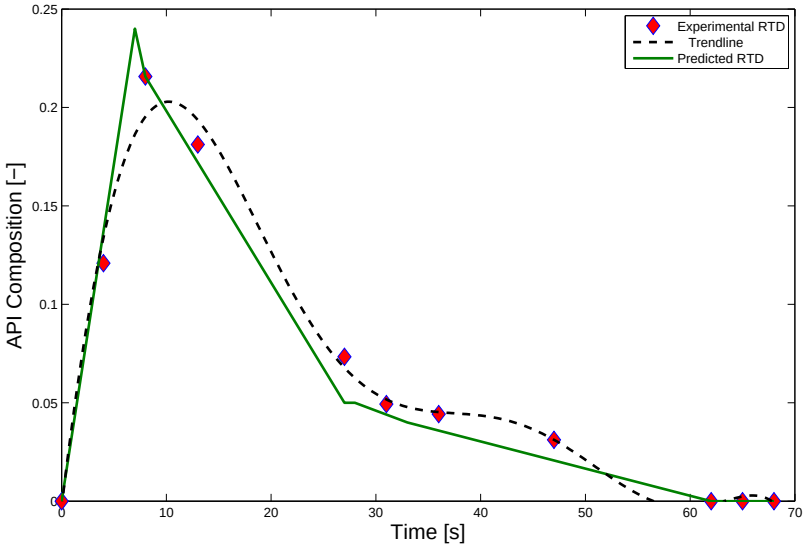

Figure 3.10: RTD vs Time for feedrate of 30 kg/hr (run 1)

RTD	
Correlation	0.831781
R^2	0.625658
Adjusted R^2	0.57218
SSR	0.028012
SSE	0.005493

Table 3.6: Statistics for RTD-run 2

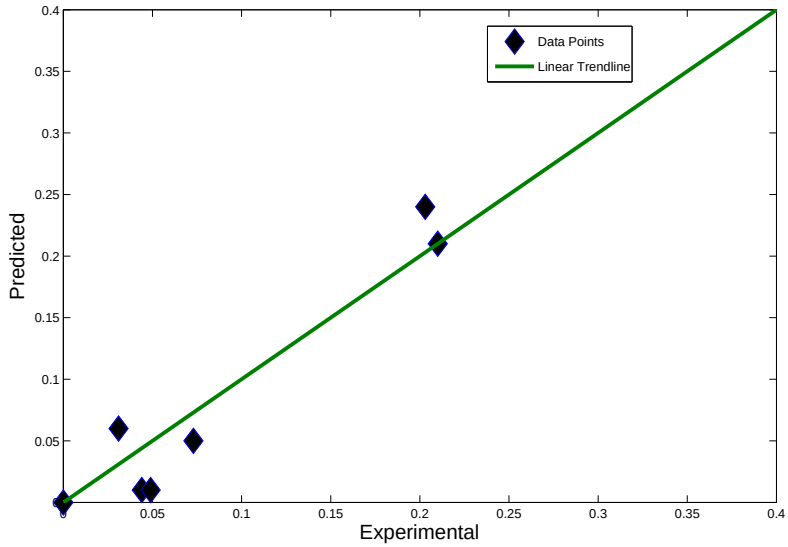

Figure 3.11: Linearity Plot for RTD at a feedrate of 30 kg/hr (run 1)

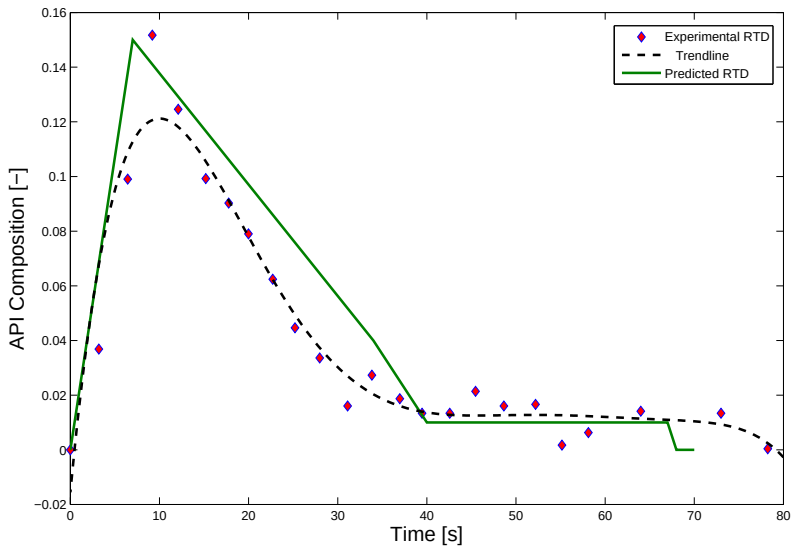

Figure 3.12: Linearity Plot for RTD at a feedrate of 45 kg/hr (run 2)

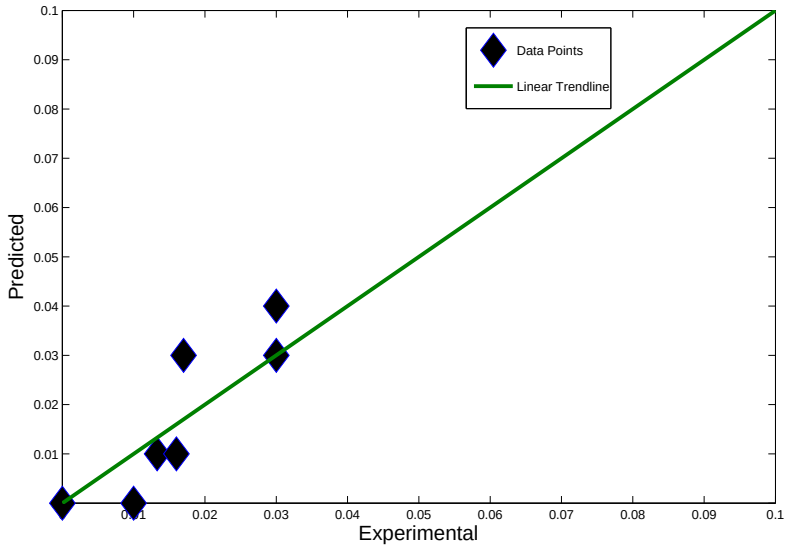

Figure 3.13: Linearity Plot for RTD at a feedrate of 45 kg/hr (run 2)

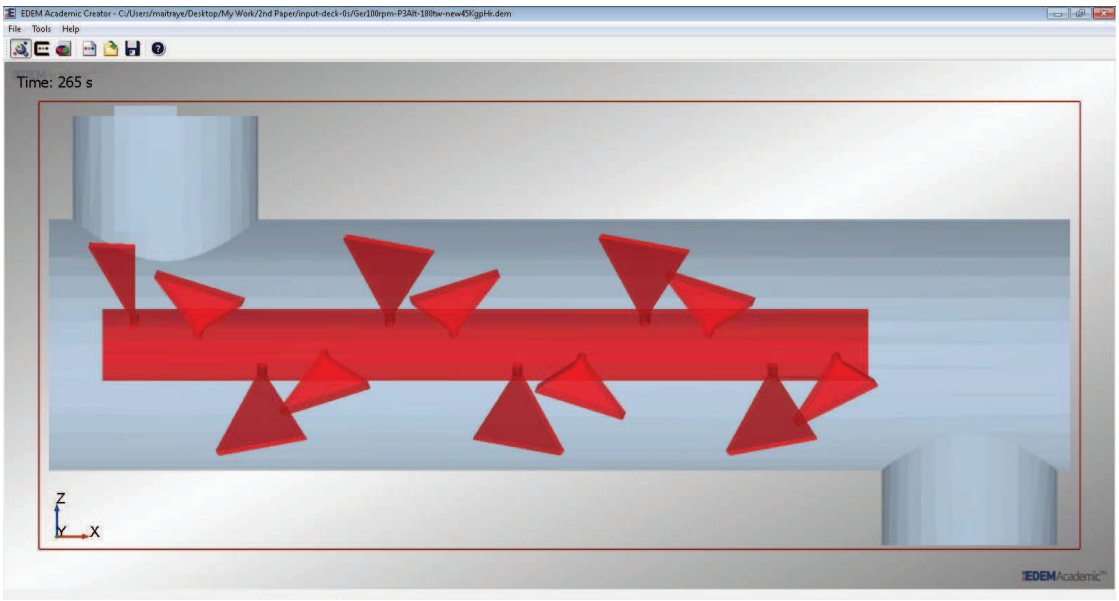

Figure 3.14: DEM snapshot of the mixer

Particle properties	
Shear modulus	$2E6Nm^{-2}$
Young's modulus	$6.06E6Nm^{-2}$
Poisson's ratio	0.33
Density	$1500kgm^{-3}$
Diameter	$2mm$
Normal size distribution with SD	0.2
Particle-particle interactions	
Coefficient of restitution	0.1
Coefficient of static friction	0.5
Coefficient of rolling friction	0.01
mixer walls	
Material	Steel
Shear modulus	$7.93E10Nm^{-2}$
Young's modulus	$2.403E11Nm^{-2}$
Poisson's ratio	0.33
Density	$8000kgm^{-3}$
Blades	
Material	Steel
Shear modulus	$7.93E10Nm^{-2}$
Young's modulus	$2.403E11Nm^{-2}$
Poisson's ratio	0.33
Density	$8000kgm^{-3}$
Particle-blade interactions	
Coefficient of restitution	0.1
Coefficient of static friction	0.4
Coefficient of rolling friction	0.01
Particle-wall interactions	
Coefficient of restitution	0.1
Coefficient of static friction	0.4
Coefficient of rolling friction	0.01

Table 3.7: DEM simulation parameters

In order to calculate the net outflow, a bin is formed at the discharge. The IDs of the particles present in this bin are obtained at each time step for one time frame. Few particle IDs may get repeated between any two consecutive time step because some particles stay in the bin for more than one time step. A code has been written to find the outflow in terms of total number of particles being discharged per time step. The code compares the particle IDs of every two consecutive time step, eliminates the particle IDs encountered in the previous time step and increases the particle count by one whenever a new particle ID appeares. Thus the total rate of particle flow at the outlet is calculated. In the next step, the particle IDs are obtained separately for each particle of component A and B at the discharge so that the individual flowrates can be calculated. From this information, component A composition and RSD can be calculated for every time step with the help of Equations 2.10 and 2.11 respectively. In order to determine the variation of RSD with the mixer length, the mixer is divided into 10×10 bins both axially and radially. The individual numbers of particles for components A and B in each bin are obtained at the last time step. RSD values averaged over the mixer length are calculated using equation 2.11.

In order to calculate RTD, the mixer run has been simulated until the mass hold-up in the mixer reached a near-constant value, indicating that a steady state has been achieved. The hold-up starts at zero at the beginning of the simulation and will rise quasi-linearly in the beginning as the particles collect inside the mixer. Once the particles start exiting the mixer, the curve will flatten and it turns into a horizontal line when steady state is reached. At this point the number of particles entering the mixer is about the same as those exiting. In the DEM simulation with the parameters shown in table 3.7, steady state has been typically achieved at around 50s. After the steady state has been achieved, the particles that are fed to the mixer within a 1-second window are tagged. These particles are tracked until they cross the weir at the outlet of the mixer. The time taken by each tagged particle to cross the weir is recorded as the residence time of the particle. The simulations are run at steady state for time intervals long enough so that at least 95 percent of the tagged particles are retrieved at the outlet. A histogram is created using 1-sec time bins and the number of particles in each time bin

is plotted against time. The RTD, E(t), has been calculated by normalizing the area under the concentration-time curve.

3.6.2 Multiscale DEM-PBM model

The multiscale model has been simulated with gPROMS^{TM} (Process Systems Enterprise) as the platform. The mixer domain has been discretised into 10 bins each in axial and radial coordinate axes. The width of the bin along the axial and radial coordinates are 33 mm and 10 mm respectively. It is important to determine and suitably incorporate the velocity values (i.e., the axial and radial velocities) into the PBM. Each compartment has its own radial and axial velocity values. The DEM output values (axial and radial particle velocity) have been extracted after every 5 seconds (starting from $t = 0$ till the final time point $t = 260s$) as excel sheets and then imported in the PBM (written in gPROMS^{TM}) as foreign object. The velocity values (V_f,V_b,V_r) have been updated every 5 seconds in the PBM for a total time of 260 seconds. It should be noted that a more frequent update of velocities can be implemented, given that in DEM the velocities are calculated each time in the order of micro-seconds. However, the focus of this study is on the computational efficiency of the model without compromising on too much accuracy of results. Equal number of components A and B particles have been introduced in the mixer. Equations 2.11-2.13 are used to determine the CQAs. In order to determine the RTD, first component B stream has been allowed to run through the mixer. A pulse input of component A particles has been introduced at t=50 seconds after the steady state is reached.

Combining DEM with PBM requires detailed understanding of both the models and the establishment of a well defined interface between them. The model generated CQAs as explained earlier depend on the input parameter space. In the following sections, the robustness of the multiscale model has been tested by varying few of the input parameters (i.e. dimensions of the mixer and introduction of noise in the feed rate).

Effect of the mixer dimensions

Knowledge of minimum mixer length and diameter required to fulfill the CQA requirements is essential from an equipment design point of view. Figure 3.15a and 3.15b represent the RSD versus time (at the mixer outlet) and axial length (at the end time point) respectively for change in mixer length while diameter is kept constant. The RSD decreases with time as well as over the axial length of the mixer. The axial length has been represented in terms of compartment number (1 to 10). It can be seen from the graphs that RSD decreases with increase in the mixer length. This is because as length increases, mixture is retained within the mixer for a longer time thus giving it more time to get mixed. And the final product obtained is more uniform with reduced variability. Similarly figures 3.16a and 3.16b show how RSD varies with change in diameter of the mixer when the length is fixed. It is seen that the mixture variability increases with increase in the diameter.

Effect of Noise

This section investigates how a mixer will respond to a possible perturbation in input flowrates. The usual source of disturbance at the inlet of the mixture is refilling of the feeder [88]. The flowrate fluctuations at the mixer inlet should be minimized so that the properties of the output stream from the mixer are not affected. It has been shown that a continuous mixer can dampen out variability from the feeder [29]. Noise has been added by adding a variance term to flowrate of the inlet stream which selects a value over a normal distribution. The standard deviation of the normal distribution has been varied in order to get an idea of the maximum allowable perturbation such that the output stream properties are not changed. Figure 3.17 shows how the fractional composition of component A varies at the outlet with time as the degree of perturbation changes. It can be seen that all the cases except the one where the standard deviation is 0.3 almost overlap. Figures 3.18a and 3.18b represent how the RSD changes with change in degree of perturbation. From figure 3.18a, it can be seen that the RSD deviates slightly for standard deviation of 0.3 whereas the rest overlap. Change in RSD

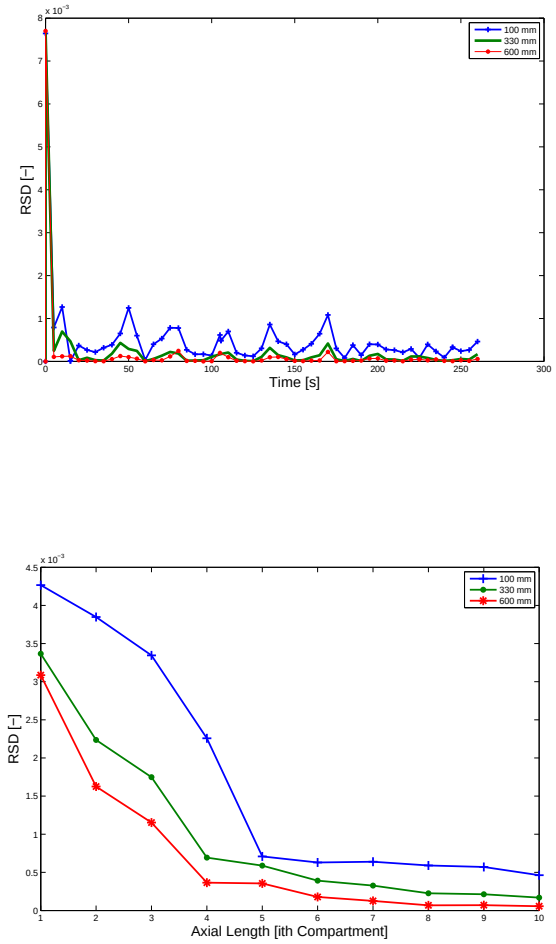

Figure 3.15: (a) RSD versus time at mixer outlet for change in mixer length and (b) RSD versus axial length at the time end-point for change in mixer length

with respect to time is not very evident as degree of perturbation changes because RSD approaches zero from a high initial value for all the cases.

This means that the developed model is robust and the mixer can eliminate any disturbance of small magnitude present in the inlet stream provided the degree of perturbation is within range.

The multiscale PBM-DEM model demonstrated good qualitative agreement with experimental studies as well as full featured DEM simulations [89, 17, 90].

Comparison of multiscale PBM-DEM with Full DEM Simulation

The model outputs (i.e., RSD, API composition and RTD) have been obtained from the multiscale model and compared with that obtained by post-processing the full DEM simulation. The values obtained from the two models have been normalized and then compared against each other. It should be noted that the legend "gPROMS" used in the plots stands for the multiscale DEM-PBM model written in gPROMS^{TM}. Figure 3.19 depicts the RTDs obtained from the DEM and gPROMs^{TM} model. The plot shows that there is good qualitative agreement between the methods. Residence time can be increased by increasing the length and decreasing the mixer speed. Increasing the length or decreasing the mixer speed will have considerable effect on other CQAs and cost. Hence it is crucial to optimize the mixer performance as a function of processing conditions and formulation properties. An RTD study may be helpful in such type of process optimization.

Figure 3.20a and 3.20b show how the RSD varies with mixer length and time respectively. The overall RSD decreases over the mixer length for both DEM simulations and the multiscale model (gPROMS^{TM}) simulation. It can be noted that in DEM there are spikes occurring in RSD for compartments 2,4,7 and 8. On the other hand the decrease in RSD in case of multiscale model is smooth. The RSD at discharge decreases over time for both the models as the system turns two segregated streams of components into more uniform blend. This shows that there is qualitative agreement between the two models as far as the mixing dynamics is concerned. Both the plots show that the DEM results are very noisy and this is an inherent property of the simulation which assumes large sized particles due to which relatively small number of particles reside in the mixer or exit the mixer at any moment of time. On the other hand the multiscale PBM-DEM model shows very gradual variation of the properties. Figure 3.21 represents the component A concentration of the mixture at the outlet as a function of time. The steady state value is 0.5 since same amount of both the components have been taken at the inlet. The fractional composition values for DEM again seem to highly fluctuate about the steady state whereas they change gradually in case of the multiscale

PBM-DEM model.

Figure 3.22 represents how the particle flowrate at the discharge vary with time. Both the multiscale model and DEM results fluctuate. This is because powder flow cannot be explained on the basis of first principles unlike fluid flow. In a continuum phase such as a fluid, a perfect steady-state is possible because the inlet and outlet flowrates can match exactly, which is not possible with discrete particles. Hence the concept of perfect steady state is not realised in powder system. There are several ways in which any two particles can interact with each other as well as with the mixer wall. As a result the particle-particle interactions and particle-wall interactions will have a pronounced effect on the powder flow. But the fluctuations seem to reduce over time. Overall, it can be seen that within acceptable error due to numerical noise, the multiscale is able to qualitatively capture the dynamics of the mixing process as demonstrated by a full DEM simulation. Moreover the multiscale PBM-DEM model is less noisy and more gradual while reporting the values of the CQAs.

Comparison of simulation time between DEM and PBM

All simulations have been performed using a desktop computer with a 2.94 GHz Intel (Core i7) processor with 8 GB RAM. The PBM-DEM model has been simulated for the same time interval as the DEM simulation. The full DEM took 6.5 days running on a 4 core and 2 threads/core processor with a total of 8 workers. The PBM simulation on the other hand took 30 minutes running on a single core processor using 1 worker. Moreover, the memory occupancy of the DEM is significantly more, taking up to 90% of available RAM compared to the PBM which uses up 50% RAM. This clearly demonstrates the efficacy of using the PBM for control and optimization as opposed to the full DEM simulation which is not amenable to provide signal feedback given the time (of the order of days) it takes to perform a simulation. DEM simulation can be run only once in order to extract the particle level data (particle velocity), which can be fed to the PBM. Then the PBM can be modified and run as many times as required to extract the required macroscopic scale variables which affect the overall unit operation and thus make control and optimization easier because of its lesser time requirement.

It should be noted that the current PBM simulation takes 30 min in a serial simulation. Parallel simulation of PBMs using multi-core CPU computing has shown to be efficient in further reducing the computational time of simulating a PBM thus enhancing its utility in control and optimization [91, 92].

3.7 Chapter Conclusions

The developed multi-dimensional PBM for the continuous mixing process has been validated. The model is shown to be able to track several experimental runs taken by varying the process parameters. The statistical analysis shows that the model predicted data matched very well with the experimental data and the proposed model has high prediction certainty. A multiscale framework of the multi-dimensional PBM and DEM has been developed. PBM coupled with DEM forms a basis of one-way coupling. Variation in several design and process parameters such as mixer dimension and presence of disturbance or noise in the inlet streams have been considered in order to test the robustness of the multiscale model. The results thus obtained from the multiscale framework have been compared with the full DEM simulation. It gives a good qualitative agreement with the trends as seen in DEM. The multiscale model has been shown to be faster compared to the DEM which is computationally intensive. Therefore, the multiscale model can be used more effeciently for design and optimization related studies since the simulation speed is faster and it is also able to store information from both particle and process levels.

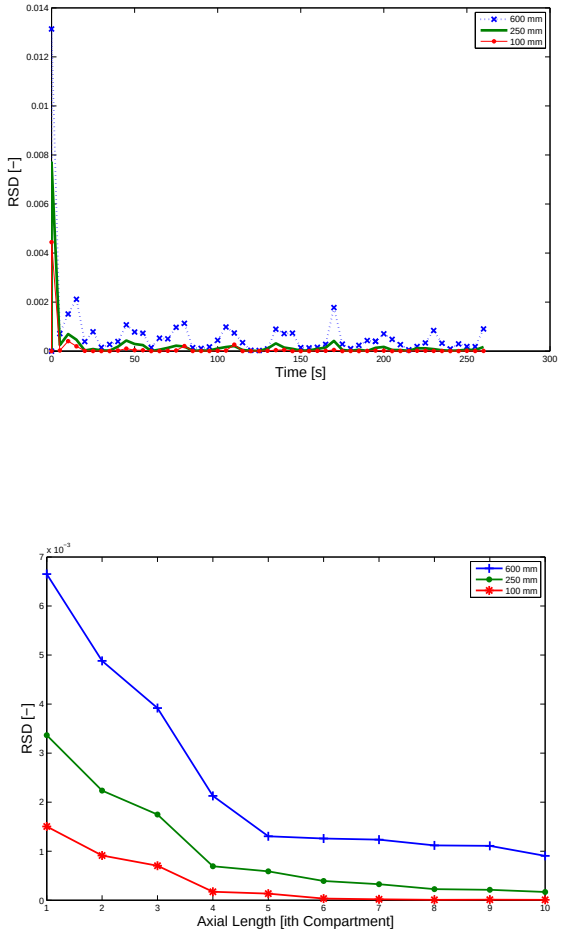

Figure 3.16: (a) RSD versus time at mixer outlet for change in diameter of the mixer and (b) RSD versus axial length at the time end-point for change in diameter of the mixer

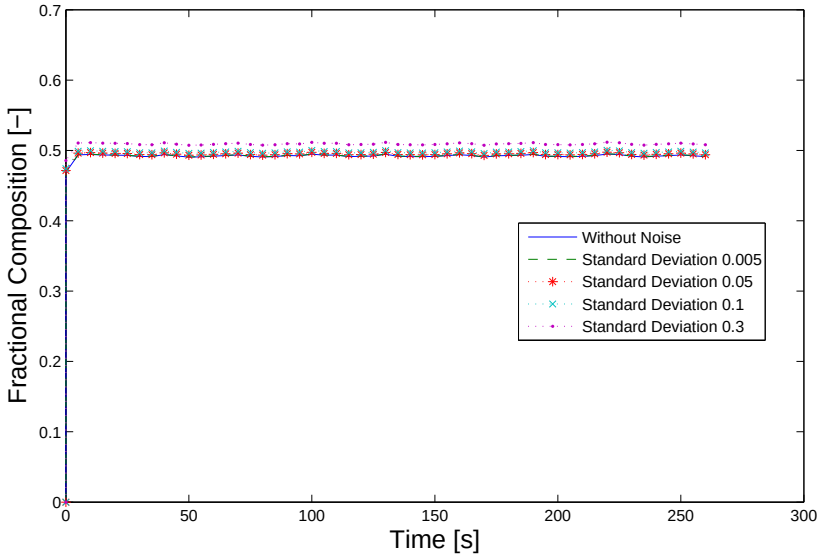

Figure 3.17: Evolution of fractional composition of component A

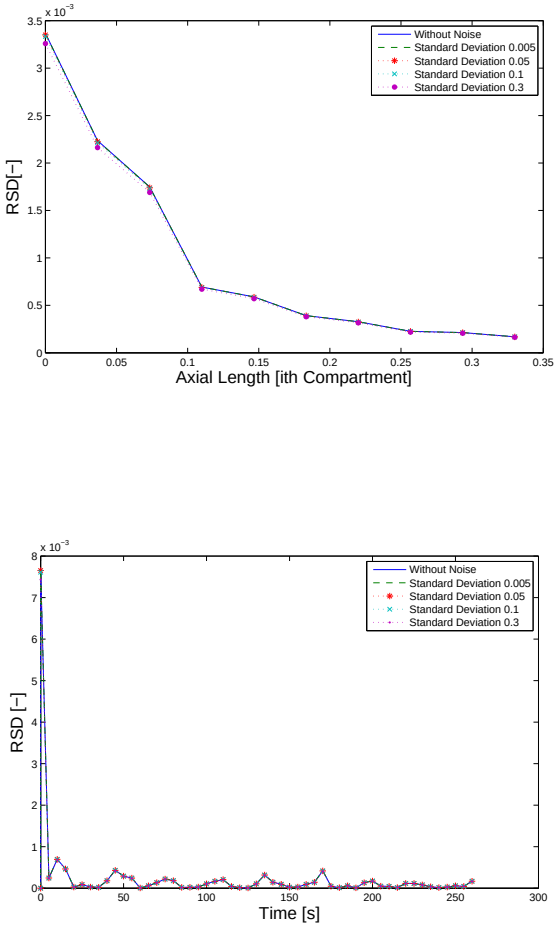

Figure 3.18: (a) RSD versus axial length at time end-point for noise addition and (b) RSD versus time at mixer outlet for noise addition

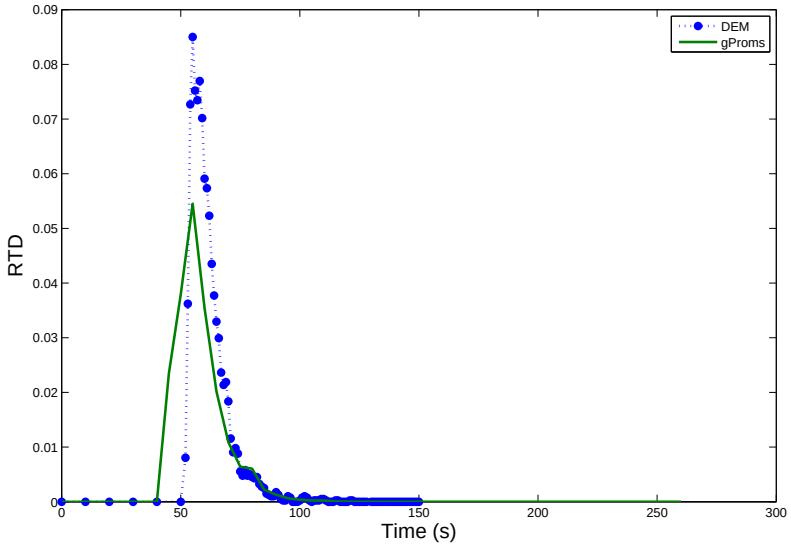

Figure 3.19: Comparison of RTD vs Time

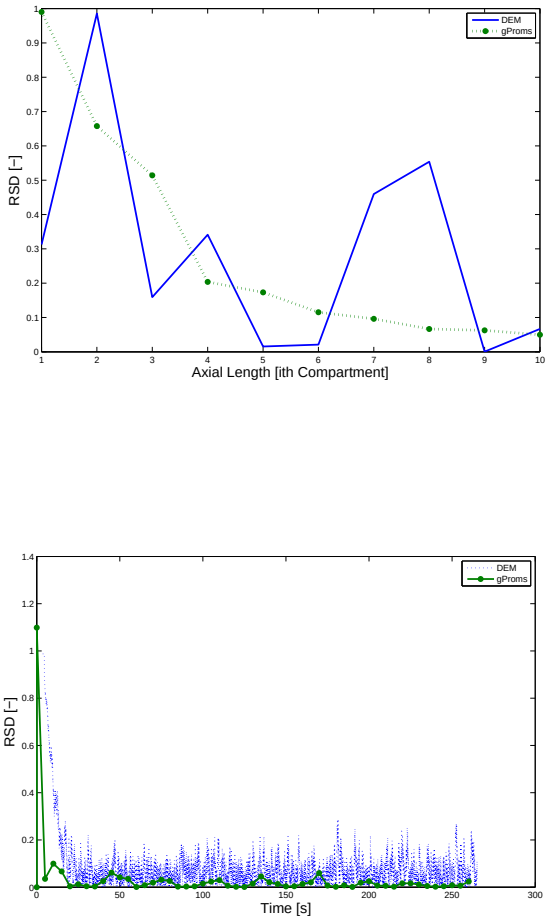

Figure 3.20: (a) Comparison of RSD versus axial length at time end point (b) Comparison of RSD versus time at mixer outlet

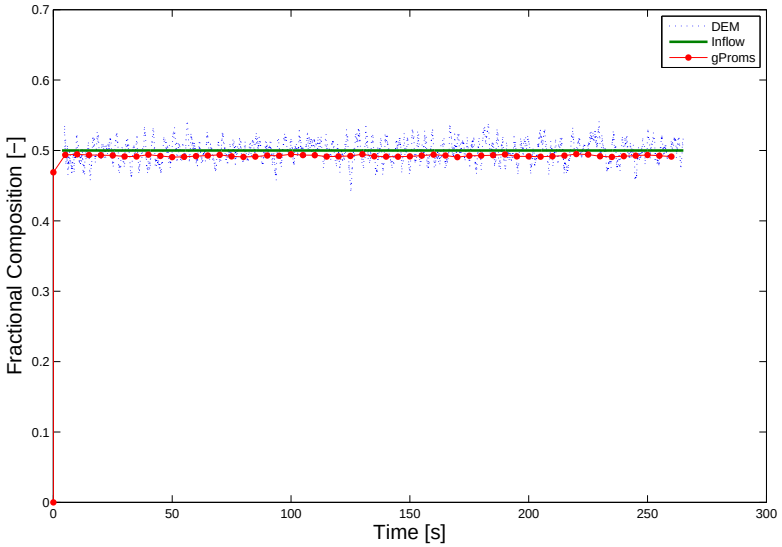

Figure 3.21: Comparison of evolution of fractional composition of component A

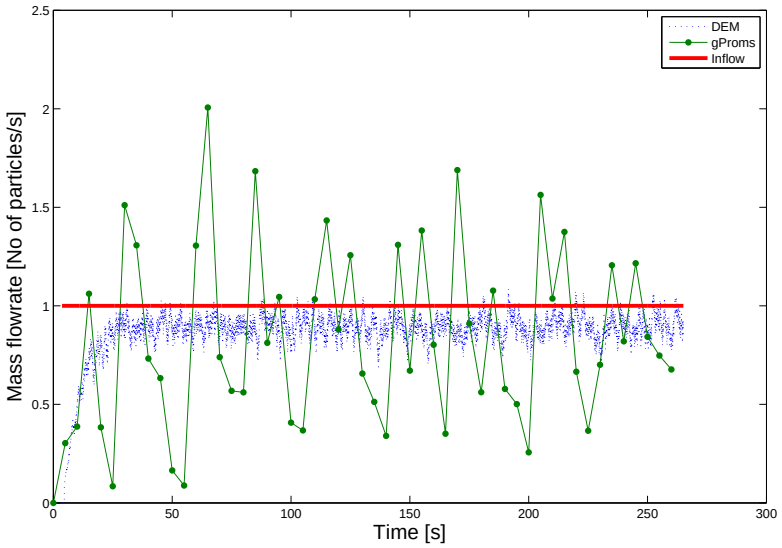

Figure 3.22: Comparison of evolution of outlet mass flowrate

Chapter 4

Multiscale model development, optimization and control of a continuous API purification/processing-downstream tablet manufacturing operation

- **M. Sen**, A. Chaudhury, R. Singh, R. Ramachandran, 2014. Two-dimensional population balance development and validation of a pharmaceutical crystallization process. American Journal of Modern Chemical Engineering, 1, 13-29.

- **M. Sen**, A. Chaudhury, R. Singh, J. John, R. Ramachandran, 2013. Multi-scale flowsheet simulation of an integrated continuous purification-downstream pharmaceutical manufacturing process, International Journal of Pharmaceutics, 445, 29-38.

- **M. Sen**, A. Rogers, R. Singh, A. Chaudhury, J. John, M. G. Ierapetritou, R. Ramachandran, 2013. Flowsheet optimization of an integrated continuous purification-processing pharmaceutical manufacturing operation, Chemical Engineering Science, 102, 56-66.

- **M. Sen**, R. Singh, R. Ramachandran, 2014. Simulation-based design of an efficient control system for the continuous purification and processing of active pharmaceutical ingredients, Journal of Pharmaceutical Innovation, 9, 65-81.

- **M. Sen**, R. Singh, R. Ramachandran, 2014. A hybrid MPC-PID control system design for the continuous purification and processing of active pharmaceutical ingredients, Processes, 2, 392-418

The objectives of this specific aim are to develop an optimized integrated model (in form of a continuous flowsheet model) which connects four unit operations, namely

crystallization, filtration and drying followed by mixing (multiscale model developed in specific aim II) and design an efficient hybrid MPC-PID control strategy for the same. Crystallization, filtration and drying are the API separation and purification stages whereas mixing the purified API crystals with one or more desired excipient is a downstream pharmaceutical unit operation for tablet manufacturing. This particular flowsheet model will be optimized so that optimal operating conditions can be determined and the CQAs of the final product are satisfied. This will improve the process performance and maximize efficiency of the integrated process and also reduce the chance of producing rejects.

Several recent studies on flowsheet modeling for solid handling processes have been conducted and reported in the literature [10, 14, 93, 94]. For example a continuous flowsheet model has been reported by Boukouvala et al [10, 14], which integrates downstream tablet manufacturing unit operations (such as powder mixing, roller compaction, wet granulation, milling and compaction). Such integrated flowsheet models are very efficient and useful for product quality control and process understanding. However the pharmaceutical industry needs to fulfill the good manufacturing practices (GMP) such that the CQAs of the final product are satisfied [11]. It has been seen that the physical properties of the API crystals (size, shape, purity etc.) has considerable effect on the product quality of the downstream tablet manufacturing processes. Hence, it is also necessary to have control over the starting material (API) properties. Since the physical properties of the API crystal depends on the upstream processing parameters, care should be taken to ensure that the desired API properties and purity are achieved by adapting effective separation and purification steps [51]. Since in reality there is no direct connection between the API purification and downstream processing steps at present, in this work a continuous process flowsheet integrating API purification, separation and downstream processing has been developed in order to study the effect of the upstream process parameters on the downstream product attributes. The development of such a model will prevent loss of data between each unit operation and also lead to better control and optimization of the process as the pharmaceutical industry transitions to a continuous upstream and downstream operation [95].

Flowsheet modeling is the latest tool for developing multiscale simulation models depicting continuous pharmaceutical unit operations and has proven to have a high level of accuracy and is cost efficient [10, 14]. There are some of the modeling techniques which can be used to develop these integrated multiscale models. Black box modeling is a cost efficient modeling tool whereas a modeling tool based on the first principles is often found to be more computationally expensive [96]. Optimization of a model based on a flowsheet simulation has several advantages as it can help to avoid production of rejects. Both the flow behavior of the particles and the complex interactions between particles should be accounted for in order to obtain an accurate and predictive model. There exists prior work on API purification [97, 98] and API/excipient processing [29, 99] but there is a need to study the integration of these unit operations and determine the effect of upstream API properties on the process variables of the downstream processing steps. Establishing a connection between the two will allow the operator to perform *in silico* studies to manipulate the upstream process parameters in such a way that the desired CQAs of the final product obtained from downstream processing steps can be achieved.

The concept of continuous manufacturing of API has been also evaluated from a techno-economic perspective to evaluate its economic feasibility [1]. A continuous design framework consisting of synthesis and separation of API has been suggested [100] and a plant-wide control model describing continuous synthesis and processing of API [95, 101] has been reported. However there is no work reported on mechanistic model-based analysis and flowsheet optimization of the proposed continuous manufacturing strategy.

In dealing with a continuous operation that consists of several unit operations connected with one another, there is a need for real-time process control and monitoring to minimize production of rejects due to faulty machinery or raw materials. This is where PAT tools are extremely beneficial [102, 103]. Most of the studies on pharmaceutical process control to date have been focussed on a batch mode of operation, without considering the connection of upstream and downstream unit operations or the recycle and bypass streams and their heat interactions. Although there is a need to develop complex models considering all of these elements, it can increase the overall complexity of the process

and result in poor control [5, 104]. At present laboratory scale tests are performed for optimization of solid handling processes, which are very expensive and time consuming [14]. By the application of various modeling tools and databases, several such tests can be performed incorporating various possible alternatives. Though there are numerous advantages of shifting production, purification and processing stages from batch to continuous mode, there are several bottlenecks such as process complexity, especially in solid flow process, that still need to be addressed. Monitoring and control strategies in place must be effective and timely otherwise the product could fail to conform to CQAs [2]. Therefore, an effective process control scheme has been suggested for the flowsheet model as well.

The typical challenges associated with industrial process control are the presence of multi-variable process interactions between manipulated and controlled variables, measured and unmeasured disturbances, process delays and several constraints on the input and output variables [105]. Therefore, the MPC module has been widely used in several process industries (i.e. petroleum refineries, petrochemicals, bulk chemical production etc.) as an advanced process control strategy [106]. Some of the advantages of MPC over conventional regulatory controllers are that it can be easily adjusted to handle the complex process dynamics; it can efficiently handle the strong interaction among the process variables; it can easily compensate for large process dead time; it can handle non-square systems and is easier to tune [107, 108]. However, MPC requires an accurate process model and a robust optimization scheme which may be computationally expensive. On the other hand, a PID controller is relatively simpler to design and implement and can be used to control the variables which are comparatively less interactive with the entire process and which result in a lesser process dead time. Therefore, an optimum control strategy is highly desired in which the advantages of both the control strategies (i.e. both MPC and PID) can be integrated. A hybrid MPC-PID design will help to optimize the control loop performance, usage of resources and time. Therefore, a hybrid MPC-PID control loop has been designed and presented in this chapter.

Several researchers have reported a model based control and design for continuous processing frameworks. Ramachandran et al. [109] have performed an assessment of

control loop performance for a continuous tablet manufacturing framework via direct compaction using a simple PID control strategy. Singh et al. [108] have proposed an advanced control scheme using a MPC-PID hybrid approach for the same. A design of control system for the continuous tablet manufacturing framework via roller compaction route [93] and wet granulation route [110] have been reported as well. The study of various control strategies on downstream tablet manufacturing process is well documented [111]. Hybrid control strategies have been suggested as a promising scheme for plant-wide control [112], but it is yet to be applied in pharmaceutical industries. Therefore, this work presents a scenario where the control loops have been designed with an advanced control system (MPC) or simple PID control depending on the complexity of the dynamics.

4.1 Integrated Process

There are several steps involved in the purification and downstream processing of a chemical compound. These steps can be enumerated as: separation of insolubles, product isolation followed by product purification and product polishing [113]. The first two steps namely separation of insolubles and product isolation mainly aim at capturing the product in a liquid solvent which is free of particulates and any form of insoluble impurities. Once this is done product needs to be purified. There are several steps available for product purification and polishing depending on the properties of the product. If the product is solid and present in the solution in considerable quantities and is not highly heat sensitive, then crystallization can be chosen followed by filtration and spray drying.

Assuming that the above steps are applicable in the processing of most pharmaceutical APIs, the integrated model discussed in this section has been developed. It comprises of purification and polishing of API followed by its mixing with excipient to get the final pharmaceutical blend.

In the integrated process, crystallization, filtration, drying and mixing have been connected with each other in the given order. Crystallization will decide the CSD (crystal

size distribution) primarily and liquid content of the API crystals. Output of the crystallizer (slurry of API crystals in the mother liquor) is connected to the input of the filter. During filtration the crystals will be removed from the mother liquor. The crystals will be retained in form of cake on the filter medium. The solid cake when dislodged from the filter medium will enter the dryer. The stream entering the dryer has crystals with definite size and considerable liquid content as decided during the crystallization step. In the dryer, wet crystals are dried by removal of the liquid. The liquid content of the crystals is also brought down to a much lower and acceptable value. Once the API crystals are separated, purified and dried, they are sent to the mixer where these are mixed with an excipient to obtain the final pharmaceutical blend. Figure 4.1 below gives a pictorial representation of the integrated process. Although there is some size change associated with the drying process, the assumption is that it is minimal and hence neglected. So the CSD has been decided based on the crystallization process. The development of first-principle model for each unit operations involved in the integrated flowsheet model is described in the section below.

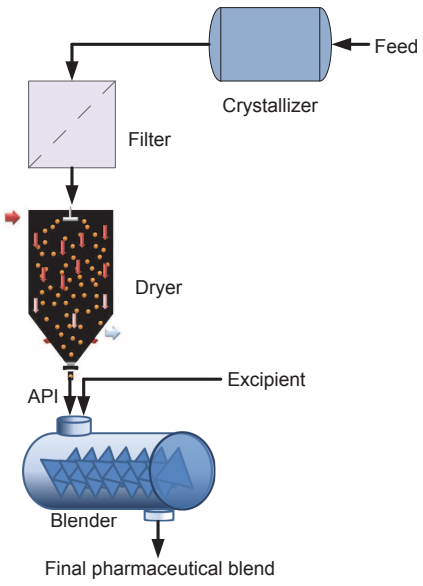

Figure 4.1: Schematic of the continuous process

4.2 Flowsheet Model Development

In this section the mathematical models of the crystallization, filtration and drying have been discussed. The mathematical model for mixing has been presented earlier in specific aim I amd II.

4.2.1 Crystallizer

The crystallization model has been adapted from the work of Chaudhury et al. [114]. The crystallization model has been developed based on PBM. In order to model the crystallization process, the external coordinates have been neglected since the main phenomenon during crystallization is the change in crystal size [38]. The population distribution function has been presented as a function of time and internal coordinates only, assuming homogeneity with respect to the flow.

In this study, a 2-D PBM considering growth in two directions has been implemented, as shown in Equation (4.1).

$$\frac{\partial F(L_1,L_2,t)}{\partial t} + \frac{\partial (G_1(L_1,t)F(L_1,L_2,t))}{\partial L_1} + \frac{\partial (G_2(L_2,t)F(L_1,L_2,t))}{\partial L_2} = B_0(C,t)\delta(L_1)\delta(L_2) + Inflow - Outflow \tag{4.1}$$

Here, the number density, F is a function of the two length directions (L_1 and L_2). L_1 and L_2 represent the internal coordinates to track the change in crystal size. G_1 and G_2 represent the growth terms in the L_1 and the L_2 directions respectively and B_0 represents the primary nucleation term. The delta dirac function indicates that the nucleation is taking place at the smallest grid of the length scale. The growth and the nucleation terms in Equation (4.1) can be written as shown in Equations (4.2), (4.3) and (4.4):

$$G_1 = k_{g1}\left(\frac{C - C_{sat}}{C_{sat}}\right)^{g_1} \tag{4.2}$$

$$G_2 = k_{g2} \left(\frac{C - C_{sat}}{C_{sat}} \right)^{g_2} \tag{4.3}$$

$$B_0 = k_b \left(\frac{C - C_{sat}}{C_{sat}} \right)^{b} \tag{4.4}$$

Here, C is the concentration of solute in the solution, C_{sat} is the solubility of the solute at the particular thermodynamic conditions (room temperature and pressure), $k_{g1},\ k_{g2},\ k_b,\ g_1,\ g_2,\ b$ are the various empirical parameters used to represent growth and nucleation in the form of a power law expression. Secondary nucleation, dissolution, aggregation and breakage of crystals are neglected but can be incorporated into the overall model if needed. The empirical parameters have been determined by aligning the model with realistic experimental conditions [114]. The crystallization model has been validated against experimental data from Bristol-Myers Squibb Co., NJ.

Another internal coordinate is added to the PBE which tracks the amount of liquid present in the crystals. From the works of Miki et al. [115], we have adapted the calculations for the mother liquor inclusion in a KDP crystal. The size coordinate considered in the paper is uni-dimensional, whereas in our work we have considered two length dimensions. In our case an averaged equivalent length has been obtained by calculating the diameter of a sphere with an equal amount of volume as the cuboidal crystal. Considering the width of the crystal to be L_1, the equivalent length of the crystal can be expressed as shown in Equation (4.5).

$$L_{eq}(L_1, L_2) = (\frac{6}{\pi} \times L_1^2 L_2)^{\frac{1}{3}} \tag{4.5}$$

The curve representing a residence time of 0.75 hr in figure 6 (refer to Miki et al. [115]), which is a plot of liquid inclusion rate versus crystal size, has been considered for our study. The expression shown in Equation (4.6) has been obtained after fitting the data using a linear regression.

$$Liq(L_{eq}) = 2 \times 10^{-5} L_{eq}^2 - 3 \times 10^{-9} L_{eq} + 10^{-13} \tag{4.6}$$

From Equation (4.1), it can be seen that the number density of particles is dependant

on the solute concentration thus indicating the need for a mass balance equation for updating the solute concentration in the solution over time. The mass balance equation can be written as shown in Equation (4.7) [38].

$$\frac{dC}{dt} = -\rho_c \int_0^\infty \int_0^\infty F(L_1, L_2, t)(2G_1(L_1L_2 - L1^2) + G_2L1^2)dL_1dL_2 \qquad (4.7)$$

where, ρ_c is the density of the crystal. The solubility of the solute in the solution is also a function of the temperature of the crystals. Hence, an energy balance equation is also needed to quantify the change in the temperature, T over time. Since this is a case of cooling crystallization, the temperature profile (cooling schedule) is an important factor in determining the efficiency of the process. The cooling schedule can be expressed as a function of time. Figure 4.2 presents the three different temperature profiles.

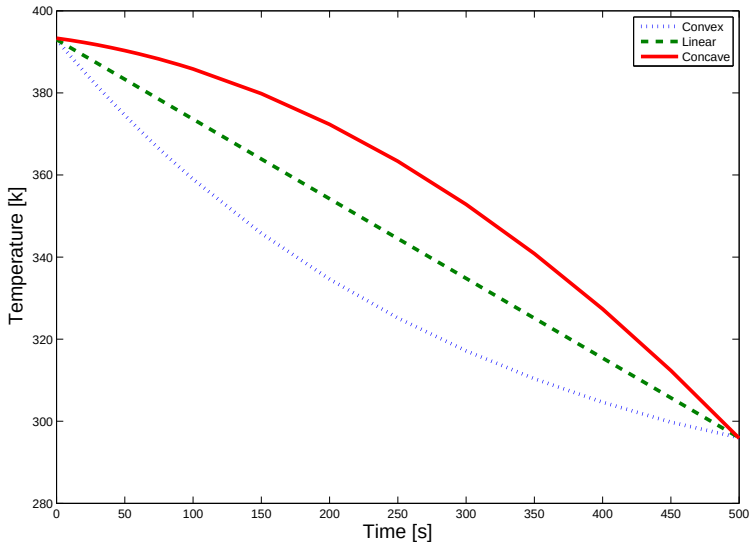

Figure 4.2: Cooling schedule for crytallization

C_{sat} has been expressed as a function of temperature as shown in Equation (4.8). The expression has been obtained by fitting experimental data as obtained from Bristol-Myers Squibb Co., NJ [114].

$$C_{sat} = 2.7357T - 40.925 \tag{4.8}$$

The output variables of interest from crystallization are population distribution function F, particle diameter D_p and porosity of crystals ϵ. These output variables become the inputs for the filtration process.

4.2.2 Filter and dryer

The filtration and drying model have been adapted from McCabe et al. [116] and Mezhericher et al. [117] respectively. Both the models have been described in detail in the work of Sen et al. [118]

4.2.3 Filter

Main design equations of cake filter can be given as in Equation (4.9)(adapted from [116]:

$$\frac{dV(L_1, L_2, L_3, t)}{dt} = \frac{A^2 \Delta P}{\mu(\alpha(L_1, L_2, L_3, t)cV(L_1, L_2, L_3, t) + R_m A)} \tag{4.9}$$

Here L_1 and L_2 are the two solid length directions and L_3 is the counter for liquid length which gets occluded into the solid crystals. $V(L_1, L_2, L_3, t)$ is filtrate volume, A is the fliter surface area, ΔP is pressure drop across the filtering medium, μ is viscosity of the fluid being sucked in through the septum, α is specific cake resistance, c is the mass of particles deposited in the filter per unit volume of filtrate and R_m is filter medium resistance.

c and α can be found as given in Equations (4.10) and (4.11):

$$c = \frac{C_F}{1 - (\frac{m_F}{m_c} - 1)C_F/\rho_s} \tag{4.10}$$

where C_F is concentration of solids in the slurry and ρ_s is density of solid. m_F and m_c are mass of wet and dry cake respectively.

$$\alpha(L_1, L_2, L_3, t) = \frac{150(1 - \epsilon(L_1, L_2, L_3, t))}{d_p(L_1, L_2, L_3, t)\epsilon(L_1, L_2, L_3, t)^3 \rho_s} \tag{4.11}$$

where ϵ is porosity of the cake (an input from crystallization) and d_p is the crystal diameter (an input from crystallization).

Assuming that there are no solid particles present in the filtrate, mass of wet cake deposited on the septum can be calculated as shown in Equation (4.12):

$$m_F(L_1, L_2, L_3, t) = F(L_1, L_2, L_3, t)V_p(L_1, L_2, L_3, t)\rho_s Na \tag{4.12}$$

where F is the population density function (an input from crystallization), V_p is particle volume and Na is avogadro number. The output of filtration will be connected to dryer. Since there is no size change associated in filtration hence population density function F and crystal diameter d_p will remain same as obtained from crystallization. m_F, F and d_p become inputs for the dryer.

4.2.4 Dryer

For drying a model has been developed where the liquid is being evaporated from the solid surface (adapted from Mezhericher et. al. [117])

The change in particle diameter with time is given by Equation (4.13):

$$\frac{dd_p(L_1, L_2, L_3, t)}{dt} = -\frac{m_v(L_1, L_2, L_3, t)}{\rho_l 2\Pi d_p(L_1, L_2, L_3, t)^2} \tag{4.13}$$

where m_v is evaporation rate and ρ_l is liquid density. The initial condition for diameter d_p is an input from filtration model.

Temperature profile of particle can be given as in Equation (4.14):

$$\begin{aligned} h_{fg} m_v(L_1, L_2, L_3, t) + c_{ps}\rho_{avg}(L_1, L_2, L_3, t)V_p(L_1, L_2, L_3, t)\frac{dT_p(L_1, L_2, L_3, t)}{dt} \\ = h(T_g - T_p(L_1, L_2, L_3, t))2\Pi d_p(L_1, L_2, L_3, t)^2 \end{aligned} \tag{4.14}$$

where h_{fg} is speacific heat of evaporation, ρ_{avg} is average density of wet particle, V_p is particle volume , h is heat transfer coefficient, c_{ps} and T_p are specific heat capacity and temperature of particle respectively.

Evaporation rate is given as shown in Equation (4.15):

$$m_v(L_1, L_2, L_3, t) = k(L_1, L_2, L_3, t)(x_p - x_{eql})2\Pi d_p(L_1, L_2, L_3, t)^2 \tag{4.15}$$

where k is mass transfer coefficient, x_p is liquid content of solid particle (an input from filtration) and $x_{eql} = \phi * Abosolute\ humidity$ such that ϕ is relative humidity.
The heat and mass transfer coefficients are given as shown below in Equations (4.16) and (4.17):

$$h(L_1, L_2, L_3, t) = \frac{Nu(L_1, L_2, L_3, t)k_g}{d_p(L_1, L_2, L_3, t)} \tag{4.16}$$

$$k(L_1, L_2, L_3, t) = \frac{Sh(L_1, L_2, L_3, t)D_v}{d_p(L_1, L_2, L_3, t)} \tag{4.17}$$

such that Nusselts number is given by Equation (4.18):

$$Nu(L_1, L_2, L_3, t) = (2+0.6Re(L_1, L_2, L_3, t)^{\frac{1}{2}}Pr^{\frac{1}{3}})(1+(C_{pv}*(T_g-T_p)/h_{fg}))^{-0.7} \tag{4.18}$$

and Sherwood number is given by Equation (4.19):

$$Sh(L_1, L_2, L_3, t) = (2+0.6Re(L_1, L_2, L_3, t)^{\frac{1}{2}}Sc^{\frac{1}{3}})(1+(Cpv*(T_g-T_p)/h_{fg}))^{-0.7} \tag{4.19}$$

k_g is the conductivity coefficient of drying gas, C_{pv} is the specific heat coefficient of vapour and Reynolds number $Re(L_1, L_2, L_3, t) = \rho_l U d_p(L_1, L_2, L_3, t)/\mu$ with U being the superficial velocity of the drying gas, Sc is Schimdt number and Pr is Prandtl number.
The outflow from dryer is given as shown below in Equation (4.20):

$$Mass_{out}(L_1, L_2, L_3, t) = m_F(L_1, L_2, L_3, t) - m_v(L_1, L_2, L_3, t) * F(L_1, L_2, L_3, t) * Na \tag{4.20}$$

m_F is obtained from filtration. The output of dryer is connected to the input of mixer. $Mass_{out}$ becomes the initial population density function for the mixer.

4.2.5 Numerical Technique

The PBM which is a multi-dimensional hyperbolic partial differential equation (PDE) has been discretized using a central finite difference scheme of order 6 followed by integration using an implicit backward differential formula (BDF) technique. Both the discretization and integration have been performed using $gPROMS^{TM}$ built-in functions, that ensure stability of the overall system and minimal numerical errors and numerical diffusion.

4.2.6 Input and Output Variables

Since the framework is continuous, hence all the input and output variables of each unit operation have been summarised in table 4.1. Inputs to crystallizer are seed rate and cooling schedule or cooling temperature profile (T). Outputs from crystallizer are crystal size distribution (CSD), average mean diameter (d_{50}) and liquid content of the crystals (x). All the output variables from crystallizer become the input for filter. The output from filter is the mass of wet cake (m_F) which becomes the input mass flowrate for dryer. Output mass flowrate from the dryer ($mass_{out}$) becomes the input mass flowrate of API crystals to the mixer. Outputs of the mixer are RSD and API composition which are two CQAs to decide the uniformity of the blend. The seed particles fed to the crystallizer are of uniform size, each having a surface area of 0.0225 μm^2. Table 4.2 lists the parameters used for crystallization. The usage of these empirical parameters has been justified by Chaudhury et. al [114].

Crystallizer	
Input Variables	Seed rate, T
Output Variables	CSD, D_{50}, x
Filter	
Input Variables	All output variables of crystallizer
Output Variables	m_F
Dryer	
Input Variables	Output of Filter
Output Variables	$mass_{out}$
Mixer	
Input Variables	$mass_{out}$ from dryer
Output Variables	RSD, API composition

Table 4.1: Input and output variables

Parameter	Value	Units
kg_1	9.4×10^{-6}	m/s
kg_2	7.8×10^{-6}	m/s
k_b	7.4×10^{-6}	$particles/m^3/s$
b	1.14	Dimensionless
g_1	1.3	Dimensionless
g_2	1.84	Dimensionless

Table 4.2: Kinetic parameters for crystallization

4.3 Multiscale coupling of DEM with PBM

The flowsheet model that has been developed can store multiscale information (i.e. both from DEM and PBM). CSD is primarily decided during the crystallization process. Therefore the PBM for crystallization has been run first. It is seen that the CSD does not change much beyond 250 seconds. The mean and standard deviation of the CSD as obtained from the crystallization process at time $t = 250$ seconds has been used to create the particle factory in the DEM simulation of the mixer. The details on the DEM simulation has been provided in specific aim II. Once the DEM simulation of the mixer is complete, it has been post-processed to obtain the axial and radial velocities. The axial and radial velocity values have been obtained every 25 seconds and imported into the PBM model of the mixer in $gPROMS^{TM}$ as a foreign object. In other words the velocity values for the mixer gets updated every 25 seconds. More frequent updating to improve accuracy can be performed at the expense of computational time. The schematic below figure 4.3 shows how DEM interacts with the PBM.

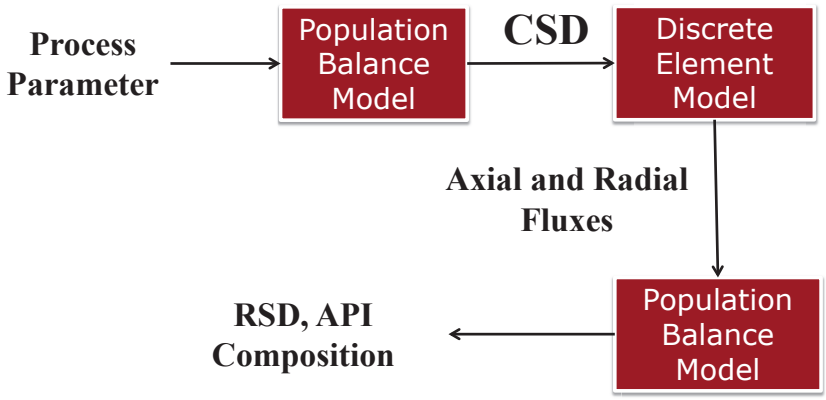

Figure 4.3: Coupling of DEM with PBM

4.4 Performance of the flowsheet model

4.4.1 Crystallization

The variables of interest from crystallization are average crystal diameter and CSD. The graph below as seen in figure 4.4 gives the average diameter of the crystals. The average crystal diameter increases with time as the crystal growth is taking place. Similarly figure 4.5 shows the CSD obtained. The mean size reported is 71.8 μ m. It is always desired to obtain a narrow CSD or uniform size distribution for a uniform quality blend. A uniform size distribution can be achieved by controlling the cooling profile of any given crystallization system. Figure 4.6a and 4.6b represent the crystal growth rate and rate of nucleation respectively. It can be seen that the crystal growth rate and the rate of nucleation increases with time initially, reaches a maxima and then starts decreasing as the solute saturation concentration decreases. Secondary nucleation (although not explicitly modeled) is not favored because it typically widens the range of CSD. Hence in an optimization framework, it is generally desired to maximize the crystal growth rate and minimize nucleation. Therefore, the model provides useful information about the respective growth and nucleation rates which can be utilized in an optimization framework.

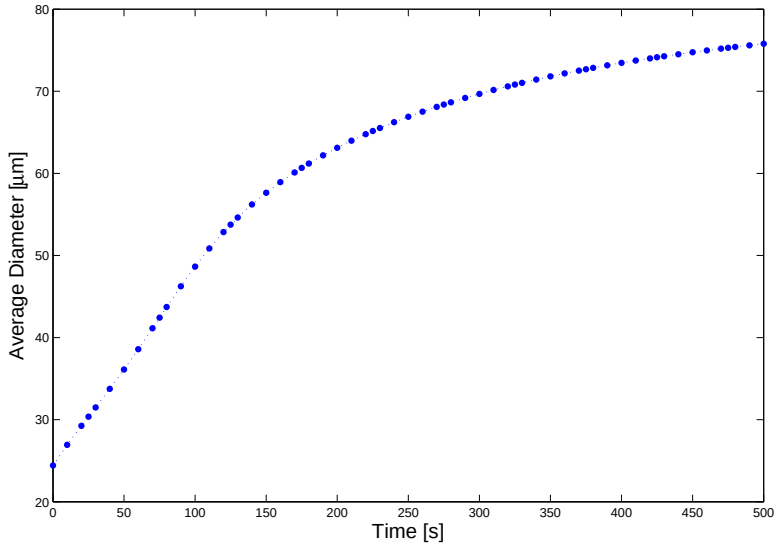

Figure 4.4: Average Diameter of crystal versus Time

Once the crystals are formed they are sent to the filter for separation of the crystals from the mother liquor.

4.4.2 Filtration and Drying

Filter pressure gradient is an important factor to decide the efficiency of the filtration process. By controlling the pressure gradient, one can optimize the filtration rate. Figure 4.7 represents the volume of filtrate obtained versus time. The graph gives a qualitative representation as how the total filtrate volume collected increases with time as the crystals are separated from mother liquor.

Once the crystals are separated from mother liquor they are sent to the dryer for removal of the occluded liquid. Temperature of the drying medium is one of the factors which is important for deciding the performance of the dryer. During drying the crystals are sprayed on a hot medium due to which the crystals will gain heat. The solvent considered for crystallization is ethylene glycol which has a boiling point of 470.3 K [119]. The particle surface temperature will increase and the occluded liquid will get evaporated

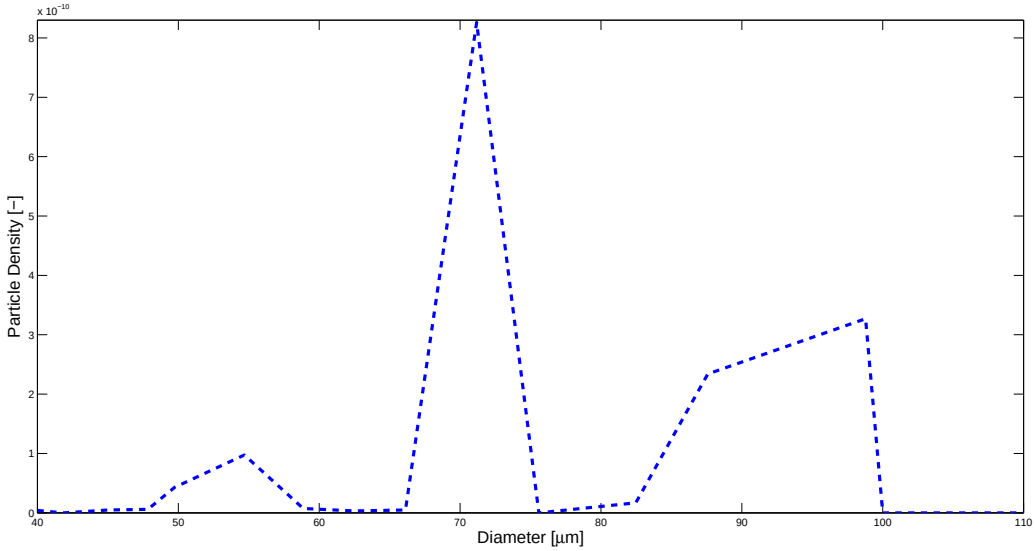

Figure 4.5: Crystal size distribution

as it gains the latent heat of vaporization. Figure 4.8 gives the temperature profile of the crystals. The graph gives a qualitative representation of increase in temperature with time.

Once the crystals are dried, they are sent to mixer to be mixed with the excipient.

4.4.3 Mixing

The CQAs associated with mixing which decide the blend uniformity are RSD and API composition of the final product blend. The lower the RSD, better is the uniformity of the blend. Figure 4.9a shows how RSD varies with time at the mixer outlet. Figure 4.9b shows how RSD varies with mixer length at the end time point. It can be seen that the RSD decreases over time as well as mixer length. This shows that the product gets well mixed with time. One of the important process parameters for mixing is mixer RPM. The axial and radial velocity values depends on the RPM value as well as the CSD. By controlling the mixer RPM, one can optimize the RSD and API composition. Figure 4.10 shows how the API composition (as a fraction) varies with time. The

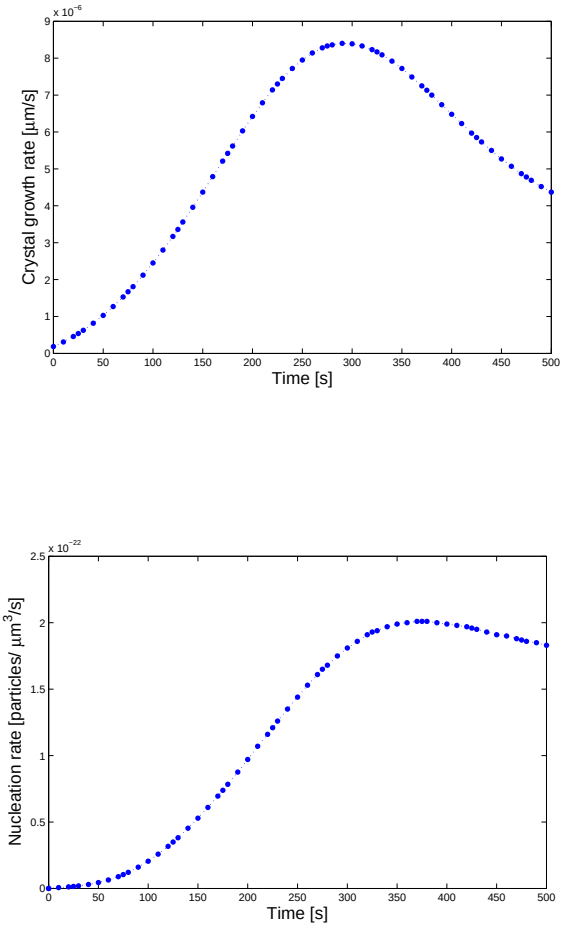

Figure 4.6: (a) Crystal growth rate and (b) Rate of nucleation

fractional API composition in the inlet stream is 0.4 and the mixer RPM has been maintained at 250. It can be seen that the outlet API fraction approaches the expected value (0.4) with time, which confirms the validity of the overall model.

4.4.4 Effect of different temperature cooling profiles

As previously highlighted, three kinds of temperature cooling profiles have been considered (Refer to Figure 4.2). As the cooling schedule changes, crystal size distribution will also change. Figure 4.11 presents the different CSD for each cooling schedule. Selecting the right cooling schedule for a particular process is very important and can be

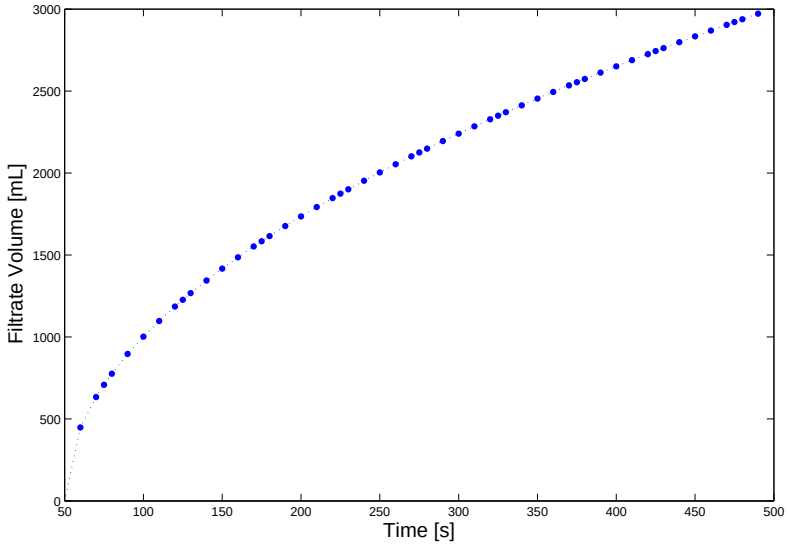

Figure 4.7: Total volume of filtrate collected versus Time

an interesting optimization study. The CSD information obtained from each cooling schedule has been used to run a DEM simulation of the mixer, for that particular case in order to obtain the particle velocities which are then fed to the mixing PBM. It is desired to design a process which will reduce the RSD (increase uniformity) of the final pharmaceutical blend. Figure 4.12 shows how the RSD varies along the mixer length. Although RSD decreases over the mixer length, the final RSD value of the linear cooling schedule is the least among three. Figure 4.13 shows how the API composition at the mixer outlet changes with change in the cooling schedule. The API composition approaches the expected value with time for all the cases. It can be seen from the plot that the linear profile reaches the expected value before the convex and concave profile. As the end time point approaches, all the three cases coincide with each other. However since the linear profile reaches the expected value faster than the other two profiles, hence in our system the linear profile is expected to give the optimized result. This fact is also supported by Figure 4.12 which shows that final RSD is the least for linear profile. However this will vary from one system to another and a detailed optimization

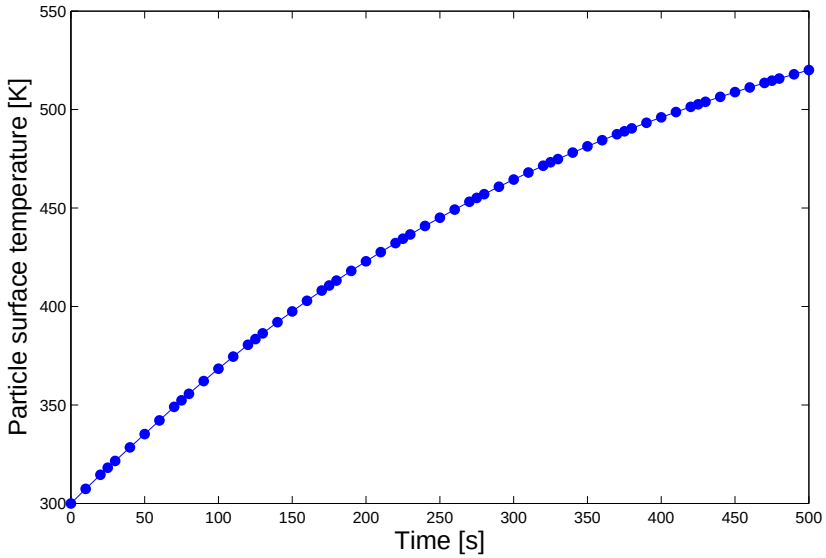

Figure 4.8: Particle temperature versus Time

study is necessary before deciding on the cooling schedule.

4.5 Flowsheet optimization

The flowsheet optimization has been performed with the help of built-in optimization solver of $gPROMS^{TM}$. The developed model consists of 11991 variables, of which 11978 are unknown (Algebraic: 11040 and differential: 938) and 13 are known. The number of equations is 12916, of which there are 938 initial conditions and 11978 are model equations. The $gPROMS^{TM}$ solver which has been used to solve this problem is known as CVP_SS ($gPROMS^{TM}$ terminology). This solver decides the duration of each control interval and values of the control variables over it. The dynamic model is then solved over the entire time horizon such that the time-variation of all variables in the system is calculated. The time variant values of the variables are used to determine the objective function value. The solver revises its choice at every step and the same procedure is repeated till convergence to the optimum is achieved. In this optimization framework all the decision variables are continuous, hence the SRQPD solver has been

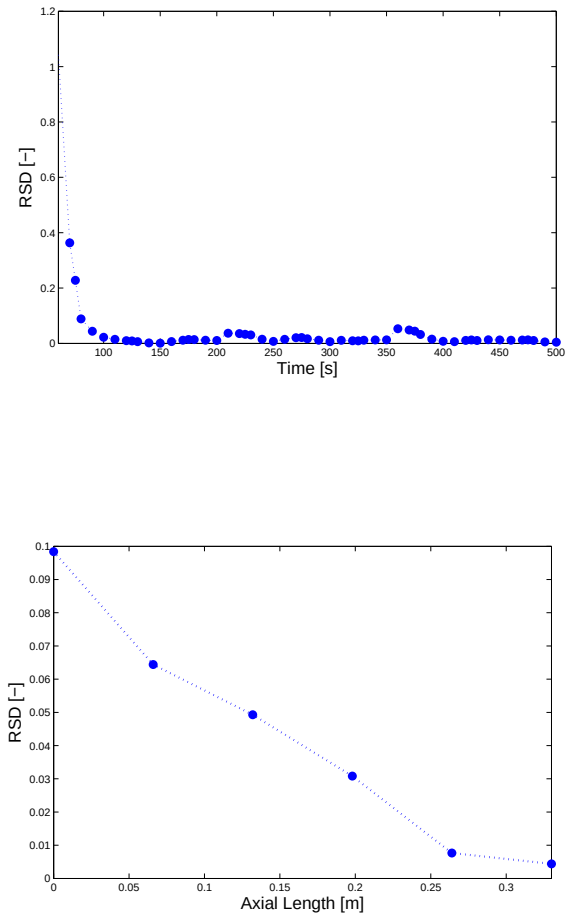

Figure 4.9: (a) RSD versus time at mixer outlet and (b) RSD versus axial length at final time point

chosen. The solver produces locally optimal values of the control variables. The basic algorithm followed by the $gPROMS^{TM}$ solver SRQPD is sequential quadratic programming (SQP). $gPROMS^{TM}$ follows a gradient based optimization schedule where the solver performs a sensitivity analysis to determine the direction of steepest descent along a line search. A step is taken along the line search trajectory and the values of objective function and constraints are evaluated. If there is a reduction in the value of the objective function then the step is accepted. A new iteration is started after one successful step from the newly accepted point, a new search direction is determined and the procedure is repeated. If there is an increase in the value of the objective

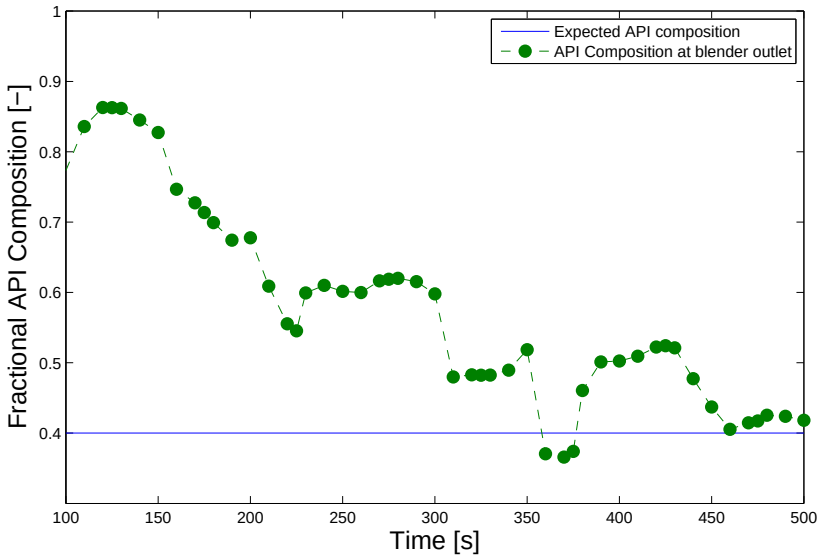

Figure 4.10: Fractional composition of API at outlet versus Time

function, then the step length is reduced and a new point of evaluation is located by maintaining the direction of search. The process of step reduction is repeated until the solver can determine an improved point of evaluation so that a new iteration can be started. The scaling options are built-in within the solver. Appropriate scaling to be applied to the optimization decision variables, control variables and length of the time horizon is chosen. The convergence criterion is improved estimate based which can be explained based on Equation (4.21) [120].

$$a + \frac{b}{|f| + 1} \leq \epsilon_o \tag{4.21}$$

a and b in Equation (4.21) can be given as shown in Equations (4.22)-(4.23)

$$a = \sum_{i=1}^{meq} |c_i| + \sum_{i=meq+1}^{m} max(0, -c_i) + \sum_{j=1}^{n} max(0, (x_j^L - x_j)(x_j - x_j^U)) \tag{4.22}$$

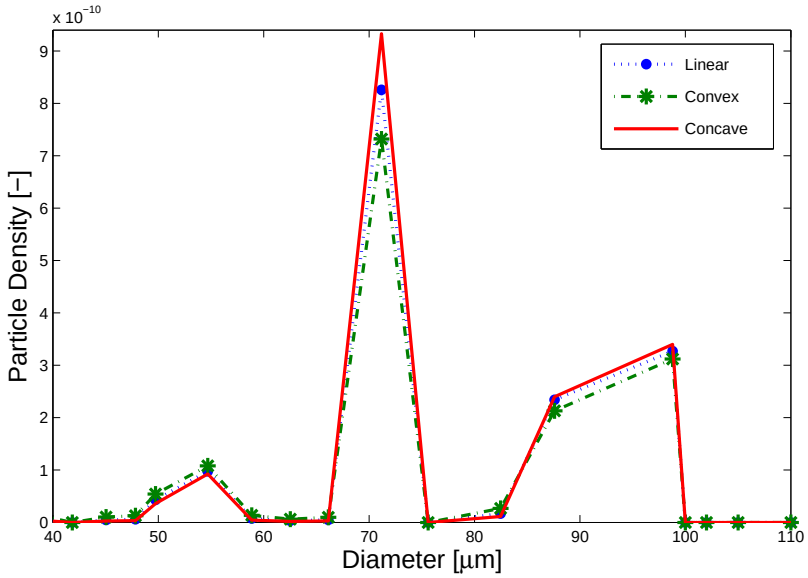

Figure 4.11: Comparison of crystal size distribution for different cooling schedule

$$b = |\nabla_x f^T d| + \sum_{i=1}^{m} |\lambda_i c_i| + \sum_{i=1}^{n} |\mu_i| max(0, (x_j^L - x_j)(x_j - x_j^U)) \tag{4.23}$$

In Equations (4.21)-(4.23) ϵ_o is the optimization tolerance, f is the objective function, c is the constraint vector, m_{eq} is the number of equality constraints, m is the total number of constraints, n is the size of the variable vector x (number of variables), x_j^L and x_j^U are the lower and upper bounds of variable x_j, λ_j is the Lagrangian multiplier corresponding to the equality constraint imposed on variable x_j, μ_j is the Lagrangian multiplier corresponding to the bound constraints imposed on variable x_j and d is the vector of corrections to x (i.e. the change in x during the current step). The value of ϵ_o is 1E-12. Maximum and minimum line search step length values are 1.0 and 1E-5 respectively. The maximum number of line search step is 20.

The simulation has been run for 400 seconds. The optimization took 11 iterations to converge and a total of 721 seconds to run with a total CPU time of 715.452 seconds running on a 4 core and 2 threads/core processor with a total of 8 workers.

The dynamic PBM after discretization can be represented functionally as given in

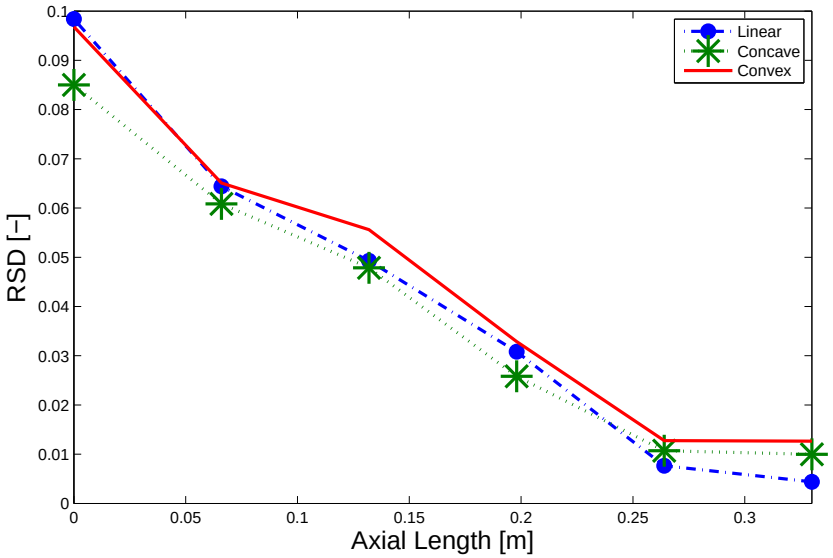

Figure 4.12: Comparison of RSD versus axial length at final time point for different cooling schedule

Equations (4.24) and (4.25) [86]:

$$\dot{\mathbf{y}}(t, \mathbf{p}) = \mathbf{f}(\mathbf{y}(t, \mathbf{p}), \mathbf{p}), \forall t \in (0, t_f] \tag{4.24}$$

$$\mathbf{y}(0, \mathbf{p}) = y_o \tag{4.25}$$

where $\mathbf{y}$ is the population distribution function and $\mathbf{p}$ are the model parameters. The process parameters in this case have been chosen to be cooling schedule during crystallization (T), pressure difference during filtration (ΔP), temperature of the drying medium (T_g) during drying and mixer rpm during mixing.

4.5.1 Objective function formulation

The objective can be formulated separately for each unit operation. The aim of the crystallization process is to obtain crystals with uniform size which can be achieved by minimizing rate of secondary nucleation and maximizing crystal growth rate [121]. This

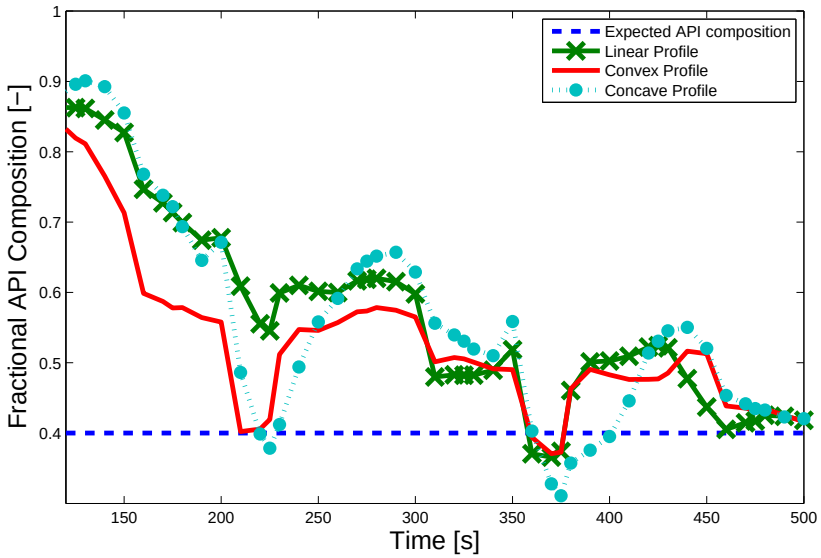

Figure 4.13: Comparison of API Composition versus time for different cooling schedule

can be achieved by manipulating the cooling schedule. In case of filtration, the rate of filtration should be maximized. This is possible by manupulating the pressure gradient across filter medium. During drying, the rate of evaporation should be maximized which can be achieved by manipulating the temperature of drying medium. The RSD and API composition of the final blend obtained from the mixer are the two most important CQAs of the final blend. Minimal RSD is desired and the API composition should be equal to the expected value (as desired in the final pharmaceutical formulation). The most important parameter which will affect the CQAs is mixer rpm (speed). Hence in case of mixer, RSD and the difference between API composition in final blend and the expected API composition in the final pharmaceutical formulation, should be minimized by manipulating the mixer rpm. The overall objective function can be written as shown in Equation (4.26).

$$\Omega^{Total}(p) = \frac{Rate - 0.5(Rate^{max} + Rate^{min})}{0.5(Rate^{max} - Rate^{min})} + \frac{\frac{1}{\dot{V}} - 0.5(\frac{1}{\dot{V}}^{max} + \frac{1}{\dot{V}}^{min})}{0.5(\frac{1}{\dot{V}}^{max} - \frac{1}{\dot{V}}^{min})} + \frac{\frac{1}{\dot{m_v}} - 0.5(\frac{1}{\dot{m_v}}^{max} + \frac{1}{\dot{m_v}}^{min})}{0.5(\frac{1}{\dot{m_v}}^{max} - \frac{1}{\dot{m_v}}^{min})} + \frac{RSD - 0.5(RSD^{max} + RSD^{min})}{0.5(RSD^{max} - RSD^{min})} + \frac{C_{diff} - 0.5(C_{diff}^{max} + C_{diff}^{min})}{0.5(C_{diff}^{max} - C_{diff}^{min})} \quad (4.26)$$

In Equation (4.26), $Rate = \frac{R_{secondary\ nucleation}}{R_{growth}}$ and $C_{diff} = abs(API\ composition\ at\ mixer\ outlet - Expected\ API\ composition)$

$R_{secondary\ nucleation}$ is rate of secondary nucleation, R_{growth} is rate of crystal growth, $\dot{V}$ is rate of filtration and m_v is rate of drying/evaporation. The overall objective function as given in Equation (4.26) should be minimized. Expected API composition is the desired amount of API in the final pharmaceutical blend. In this case the expected API composition is 0.4.

4.5.2 Principal Component Analysis based Reduced Order Model

(in collaboration with Amanda Rogers)

This discrete-element-reduced order model (DE-ROM) has been developed by Boukouvala et al. [122]. The DE-ROM has been applied for predicting the velocity values for the flowsheet model. The DEM simulations Have been used previously in order to obtain the velocity information for the mixer PBM. However, they are computationally very expensive and are therefore not readily integrated into flowsheets for process simulation and optimization. It is possible to take advantage of the information obtained from DEM simulations for process simulation purposes through the use of reduced order models (ROM). In the optimization study, a ROM based on principal component analysis (PCA) has been implemented in order to estimate the particle velocities within the mixer. This section will provide a brief overview of PCA based ROM as it pertains to the current work. Interested readers are referred to Boukouvala et al. and Lang et al. [122, 123, 124] for a detailed theoretical development and discussion of reduced order models based on PCA.

Principal component analysis (PCA) is a statistical tool that can be used to reduce

the dimensionlity of a dataset through orthogonal transformation resulting in a set of principal components that are orthogonal to one another. The components are arranged in order of decreasing percent variance explained (PVE) such that the first principal component explains the most variability in the original dataset and the last principal component explains the least. The number of components to use in a PCA model is selected such that the desired cumulative PVE is obtained. The dataset to be transformed using PCA is denoted as a matrix X consisting of n observations (rows) and m variables (columns). The results of PCA can be expressed in terms of scores, the transformed variables, and loadings, the weights by which the original data can be multiplied in order to obtain the corresponding scores. For a PCA model with a components, the scores matrix is denoted as T and is of size n by a. The loadings matrix is denoted as P and is of size m by a. Thus the original data matrix, X, can be reconstructed from the scores and loadings as shown in Equation (4.27), where E is an error term.

$$X = TP' + E \tag{4.27}$$

The objective of PCA based ROM is to develop a mapping between a vector or matrix of inputs U and the scores of the PCA model. U is of size n by k where k is the number of input variables under consideration and n is the number of observations for which data has been obtained. The form of this $U \rightarrow T$ mapping is determined by the modeler. Lang et. al [124] have described the use of Neural Networks, but other methods such as Kriging or multivariate regression may also be used provided a good fit can be obtained [123]. The mapping can be generalized as shown in Equation (4.28), where β is a matrix containing a rows of mapping coefficients and u_i is a specific instance of input variables $u_{1i}, u_{2i}...., u_{ki}$.

$$t_i = \beta u_i \tag{4.28}$$

Once the input to scores mapping has been developed, it is possible to predict the score vector t_i corresponding to a new set of inputs using Equation (4.28). From the score

vector, the corresponding data vector x_i can be obtained through multiplication of the score vector with the loadings matrix P as shown in Equation (4.27).

In the mixer case study of interest, the data matrix X consists of velocity information obtained from DEM simulation. The input matrix U contains two variables, $u_1 = rpm$ and $u_2 = time$. A PCA model with six principal components was sufficient to achieve 95 percent variance explained and multivariate regression was used to map the inputs to the PCA scores.

4.5.3 Sensitivity analysis

A continuous system is highly interactive, therefore each of these parameters (chosen to be estimated from each unit operation) will have different sensitivity towards the final objective of the overall system. A dynamic sensitivity analysis has been conducted on the different parameters, which have been estimated in order to determine the order of sensitivity of each of the entire unit operation. A perturbation has been introduced within these parameters and its effect on the final objective function has been determined. The sensitive parameters will have more effect on the process. Since the sensitivity analysis is dynamic in nature, the effect of the parameters on the process variables can be analyzed over the entire time period. The process variables considered for optimization are CSD, rate of filtration ($\dot{V}$), rate of drying(m_v), RSD and API composition at mixer outlet. The parameters which have been chosen from each unit operation have been perturbed from $+6\%$ to -6% with a step size of 2 and the absolute percentage changes in the process variables have been analyzed as given in Equation (4.29) [93]:

$$\textit{Absolute percentage change in } \Omega^{Total} = 100\frac{abs(Y_o^j(t) - Y_i^j(t))}{Y_o^j(t)} \tag{4.29}$$

where $Y_o^j(t)$ is value of the objective function at base value of the jth parameter and $Y_i^j(t)$ is the value of the objective function in ith perturbation of the jth parameter. Figure 4.14 presents a 2D visualization for the effect of perturbation of different parameters on the objective function at the final time point. Figure 4.15 gives a 3D

visualization of the same at different time points. It can be seen from both the figures that mixer rpm is the most sensitive parameter. Cooling schedule for crystallization is the second most sensitive followed by filter pressure and drying gas temperature. This observation is consistent with the fact that quality of the final product (pharmaceutical formulation) is decided by the RSD and API composition at the mixer outlet. RSD dictates the uniformity of the blend and API composition dictates the content of the active ingredient in the product. These two CQAs depend on how efficient the mixing process is. One of the important process parameters for mixing is the mixer rotational speed (rpm). This should be optimized in order to attain maximum productivity where product quality is ensured. CSD of the API crystals is also important since it will influence the physical properties (size of crystals) of API which in turn will affect the mixing efficiency. Hence it is necessary to choose the optimum cooling schedule during crystallization so that the desired CSD can be obtained.

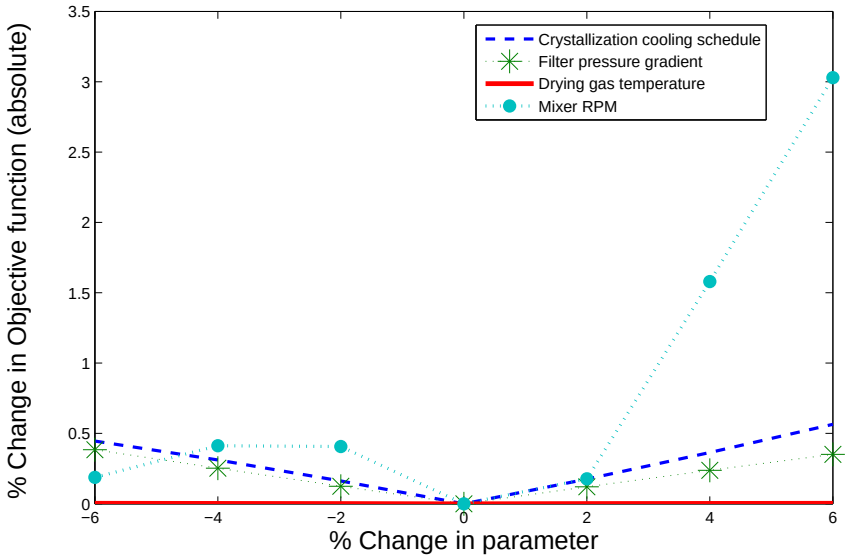

Figure 4.14: 2D visualization of sensitivity analysis

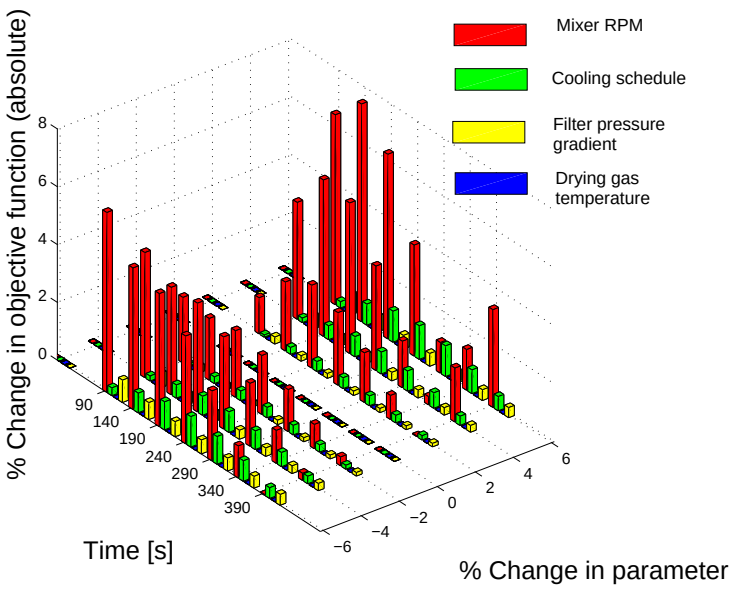

Figure 4.15: 3D visualization of sensitivity analysis

4.5.4 Optimization results

The objective function has been minimized and the parameter values have been estimated for effective operation of the process. Figure 4.16 gives the value of the objective function over time. It can be seen from the graph that the objective function value drops from a very high initial value (100461.2) to a very small final value (0.551003). Table 4.3 lists the optimized value of each parameter along with their initial guesses and upper and lower bounds. In order to maintain an optimal process performance, the mixer RPM should be kept at 215, the temperature of the drying gas should be 398K and the filter pressure should be 0.11kPa. For the crystallization operation, a cooling crystallization routine has been adopted. The temperature of the solution is reduced as crystallization takes place. Figure 4.17 presents the optimum cooling schedule. As can be seen from the figure, the cooling profile has steep slopes. This is because the simulation could not be run for longer time due to computational intensive nature of the DEM simulations. As a result smaller time interval has been used in the optimization framework formulated on $gPROMS^{TM}$ for demonstration of the concept. However

for practical implementation, one can run the DEM simulation for longer time using increased computational power and larger time steps can be used in the optimization framework to reduce the steepness of the cooling profile.

Conventionally a heuristic/empirical approach is typically used in pharmaceutical industries and therefore this optimization approach will provide better method to identify the optimum operating parameters of the process that will lead to the desired product quality. The optimization study demonstrates that this modeling tool can be used for extraction of optimum processing conditions in a continuous processing plant and can be implemented in real plant for an effective operation and improved product quality.

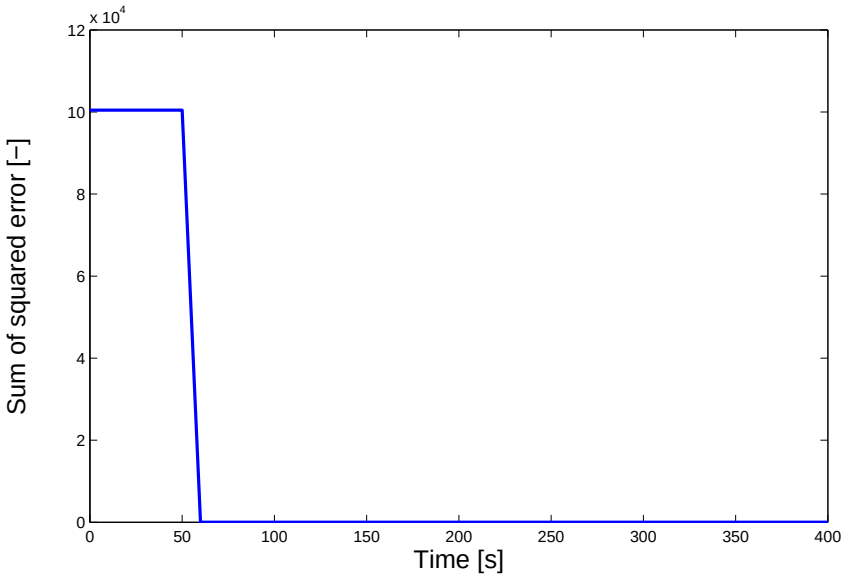

Figure 4.16: Objective function vs time

4.5.5 Comparison of the optimized operating condition with other operating condition

In this section an operating condition with linear cooling schedule has been considered during crystallization and the mixer rpm has been maintained at 250. In this case the velocity values at 250 rpm have been obtained from DEM. A DEM simulation has

Parameter	Final Value	Initial Guess	Lower Bound	Upper Bound
RPM	215	200	195	240
Drying gas temperature	398K	400K	300K	1000K
Filter Pressure	0.11kPa	0.08kPa	0.05kPa	0.15kPa

Table 4.3: Optimized Values

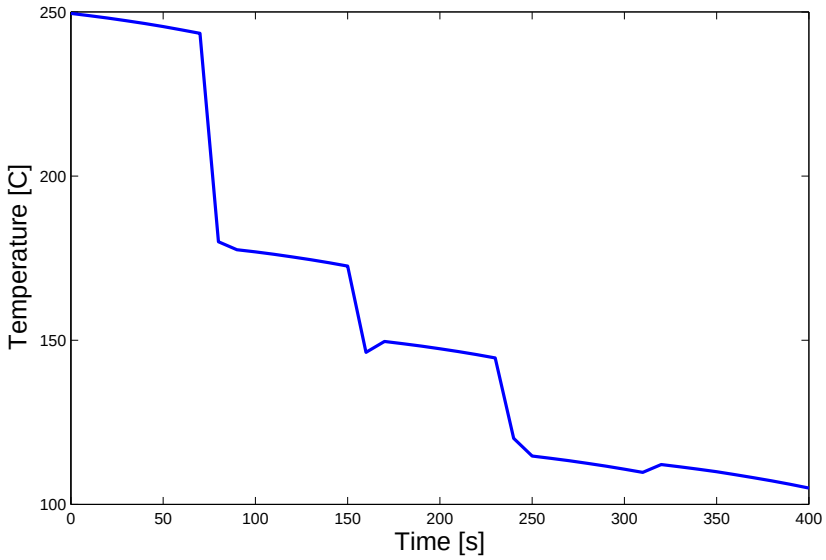

Figure 4.17: Cooling schedule for crystallization

been run for mixer at 250 rpm and the model has been post processed to obtain the velocity values which are fed into the PBM as inputs. Figure 4.3 gives a schematic of how DEM and PBM can be coupled. The crystallization model will give the CSD of the API crystals which is an input to the DEM model. Once the DEM simulation is run, the particle velocity values are extracted and fed to the mixer model in order to obtain the final CQAs (RSD and API composition). In a linear cooling schedule, the temperature is reduced linearly with time as opposed to the optimized profile. A linear cooling profile has been studied previously and information regarding this exist in literature [125, 126]. Figure 4.18 gives a comparison between the two temperature cooling schedules. This particular operating condition has been compared against the optimized operational schedule as proposed in this work.

The CSD of the crystals obtained from crystallizer and CQAs (e.g. RSD and API composition) of the final product from the mixer at this operating condition have been studied and compared with the optimized operating condition. Figures 4.19a and 4.19b present RSD variation with time and mixer length respectively. It can be seen that the optimized RSD is lower for both cases. This implies that the product obtained under optimal condition is more uniform and well mixed. Figure 4.20 presents comparison of the CSDs. The optimized CSD profile has a mean diameter of 45.43 μm and standard deviation of 23.15 whereas the linear profile has a mean of 42.25 μm and standard deviation of 24.27. This implies that the optimized profile is comparatively narrower. A narrow CSD profile implies more uniformity in the crystal size. Figure 4.21 gives the variation in API composition with time. The desired API composition in the pharmaceutical blend is 0.4. Hence it is desired that at steady state, the API content of the product obtained from the mixer is 40%. It can be seen that the optimized profile approaches the expected value gradually and finally reaches steady state. The API composition for the linear operating condition also approaches the expected value but it fluctuates and is noisy in nature. It does not reach the steady state.

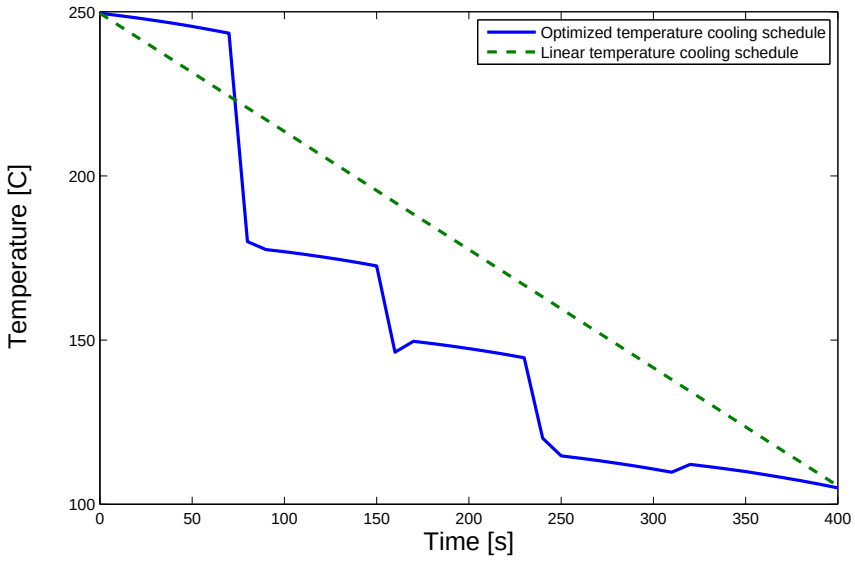

Figure 4.18: Temperature Profiles

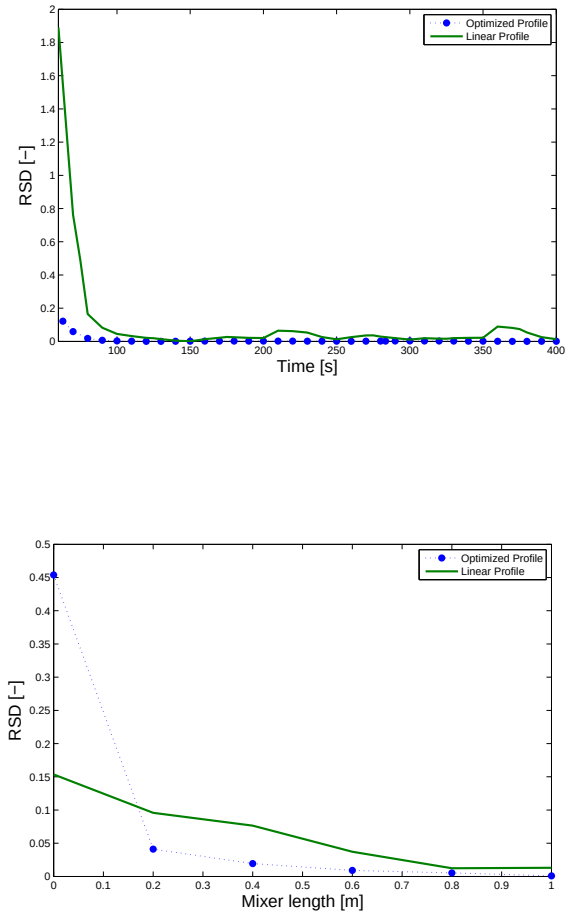

Figure 4.19: (a) RSD vs Time at mixer outlet and (b) RSD vs mixer length at time end-point

4.6 A hybrid MPC-PID control system design

noindent Hybrid control strategies have been suggested as a promising scheme for plant-wide control [112, 127, 128], but it is yet to be applied in pharmaceutical industries. Therefore, this work presents a scenario where the control loops have been designed with an advanced control system (MPC) or simple PID control depending on the complexity of the dynamics. It has been already shown by Singh et al. [108] (for a downstream tablet manufacturing framework) that a combined MPC-PID approach results in an improved control loop performance when compared to a PID only or MPC only control

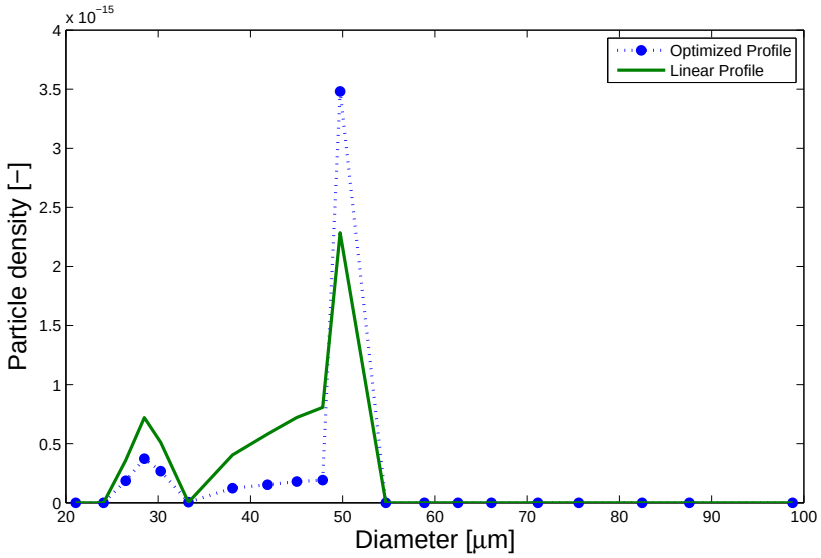

Figure 4.20: Comparison of CSDs

scheme. The hybrid scheme has been demonstrated with the aid of a MPC-PID cascade arrangement where the MPC acts in a supervisory mode and PID is the regulatory slave controller (secondary controller). In a cascade controller set-up, the output of the supervisory controller is used to obtain the set point of the secondary controller, which in turn manipulates the final actuator. For example, in the MPC-PID cascade system, the manipulated variables of the MPC become the set points of the underlying PID controllers, executed in a distributed control system (DCS). A cascade control system often proves efficient for pharmaceutical processes [108].

4.6.1 Design strategy of the control system

This section provides the details on the selection of the control variables and pairing with the suitable actuators and the design of the MPC and PID controllers.

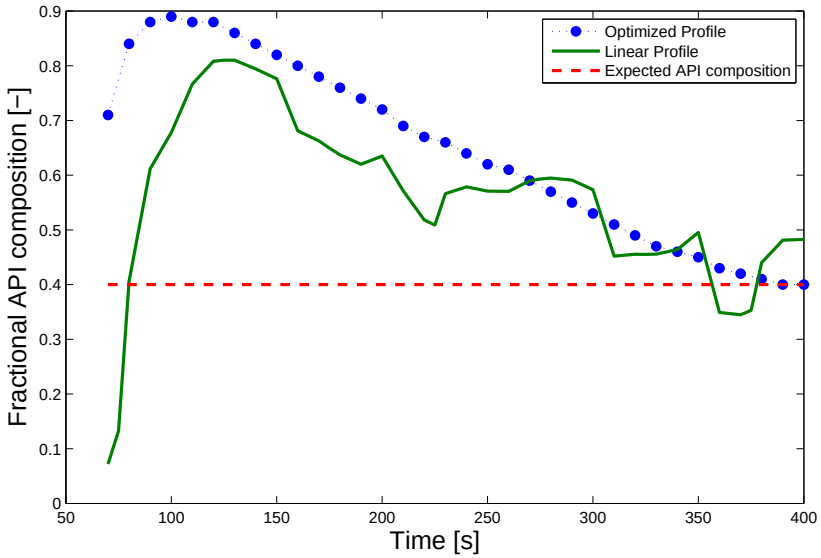

Figure 4.21: Comparison of API composition

Selection of the control variables and pairing with suitable actuators

As mentioned earlier, any flowsheet model is a highly interactive system. In such a system, most of the process variables may have an effect on each other. However, it may not be possible to control each and every one of them. Therefore, only those variables have been selected which have shown considerable effect on the overall process performance. The control variables have been decided based on the sensitivity study conducted previously. Table 4.4 lists the control variables and the chosen actuators for each unit operation.

The cooling temperature schedule is the critical process variable in case of crystallization operation. Solubility (or saturation concentration) of a solute depends on the operating temperature and it reduces with decrease in temperature. Therefore a cascade control scheme (consisting of a slave and master controller) has been considered for crystallization. The saturation concentration has been controlled with the help of a master controller. The actuator of the master controller is the operating temperature which has been controlled by the slave controller. Therefore the output of the

Process	Control Variable	Actuators (Manipulating Variable)
Crytallization	Temperature cooling schedule Saturation concentration	Coolant temperature
Drying	Drying gas temperature	Super-heated steam temperature
Blending	API composition Holdup	Excipient flowrate Weir height

Table 4.4: List of control and manipulated variables for each unit operation

master controller provides the set point to the slave controller. The actuator for the slave controller is cooling water temperature (passed through the coolant jacket around the crystallizer). The cascade loop has been demonstrated with the aid of a hybrid MPC-PID design, where MPC is the supervisory controller and used to control the saturation concentration. PID is the secondary controller used to control the operating temperature. A cascade control loop has been shown to have an enhanced performance over single loop control in many instances [93]. For example under certain scenarios (e.g., when a large dead time is involved; or when a disturbance affects an intermediate variable which has a considerable influence on the main control variable; or the gain of the secondary process and the actuator is nonlinear), it is difficult to control the main control variable efficiently without controlling the intermediate variables. It is possible to control the intermediate variables as well with the help of the cascade control loop, which indicates that the overall performance will be better than a single loop control system.

No control loop has been shown for filtration because an ideal controller (where the desired set point has been achieved perfectly) has been assumed. In practice, a pressure gauge can be used to measure the pressure gradient across the filtration medium and the flow of air/exhaust can be adjusted to attain the required pressure gradient [129, 130].

The control variable in case of drying is the drying gas temperature. Air has been considered as the drying gas in this case. Air at atmospheric temperature can be heated upto a desired temperature in a heat exchanger using super-heated steam and then sent to the dryer. The actuator in case of drying is the super-heated steam temperature.

There are two control variables of interest in case of the mixer (i.e. fractional API

composition of the final pharmaceutical blend and holdup). Mixer holdup is an important control variable as it has been known to have considerable effect on the product RSD, which is used to quantify the uniformity of the final mixed product) [131]. It has been seen that both cooling temperature schedule (of the crystallization operation) and excipient flowrate has a considerable effect on the API composition. The cooling temperature schedule affects the API composition as it governs the crystal growth rate which in turn changes the outlet flowrate of the crystals. The holdup has been controlled by manipulating the weir length. It should be noted that the effect of the weir length on the holdup has been determined by running DEM simulations of the mixing operation. Several DEM simulations of the mixer have been run by varying the weir length (i.e. 10 mm, 30 mm and 50 mm). In EDEM^{TM}, a commercial mixer Gericke GCM250^{TM} with impeller blades in alternating forward and backward orientation has been simulated. The length and diameter of the mixer are 330 mm and 100 mm, respectively. A feed rate of 0.018 kg/s and an impeller speed of 250 rpm have been maintained. Normal particle size distribution with a mean radius of 1 mm with 5% standard deviation has been used. Each simulation has been run for 50 seconds. The DEM simulations have been post processed to obtain the mean residence time of the particles within the mixer. The holdup has been calculated from the input flowrate and the mean residence time. A transfer function has been fitted to relate the holdup with the weir length.

The actual flowsheet model developd in gPROMS^{TM} has been used as a virtual plant and transfer function models have been obtained from the same in order to relate the control variables with the manipulated variables. A step change has been given to the manipulated variables in order to obtain the dynamic response of the control variables. A control relevant transfer function model has been fitted to relate the control and manipulated variables. The control loops have been designed using the Simulink^{TM} feature of MATLAB^{TM} with the help of built-in PID and MPC controller algorithms. The software computes a linear MPC plant model from the actual Simulink^{TM} model for designing an initial controller.

4.6.2 Design of controller

PID is most commonly used controller in the manufacturing industry because of its simplicity (ease of implementation and use). There are 3 important tuning parameters for PID controller (i.e. gain (Kc), reset time/integral time (τ_I) and rate/derivative term (τ_D)). The difference between the set point and measured control variable at any time point is the error ($\epsilon(t)$). The controller parameters have been tuned using Ziegler-Nichols tuning technique, which is a heuristic approach [132].

An advanced MPC consisting of four inputs and four outputs has been designed for the API separation and purification process using MPC toolbox of MATLAB^{TM}. The MPC is based on optimization of an objective function within a moving horizon therefore it is also called receding horizon scheme. The formulated MPC objective function is given in appendix which consists of weighted square sum of control variable deviations, weighted squared sum of controller adjustments, and weighted squared sum of manipulated variable deviations. As required for MPC, a linear time invariant (LTI) model has been first developed in Simulink using detailed process model and then this model has been imported to MPC toolbox for MPC configuration and design. MPC uses the developed linear model to generate the future process response within a prediction horizon and through optimization it generates the actuator signal within a control horizon. The prediction horizon (P) and control horizon (M) has been decided such that its difference is significantly greater than the ratio of the maximum process delay (td_{max}) and control interval (t) ($P - M >> td_{max}/t$) as suggested in scientific literature [108]. The MPC performance depends significantly on its tuning parameters which are output weights, input weights and rate weights. The output weight decides, which control variable needs to be given more weightage over the others, the input weights help to maintain the actuator at nominal value for consistent performance and rate weights decide the step size of the control action. Increasing the rate weight leads to smaller steps of controller action and therefore better process performance but at the expense of higher computational power and optimization time. The MPC tuning parameters have been tuned using the optimization based method (Integral time averaged

error (ITAE) [132]) available within the optimization toolbox of MATLAB^{TM}. After MPC configuration, the closed-loop performance has been assessed for set point tracking and disturbance rejection before importing the designed MPC to the Simulink^{TM} based process flowsheet model which conceptually represents the virtual manufacturing plant where the PID based slave controller is already implemented. The performance of the hybrid MPC-PID scheme is then evaluated for set point tracking and disturbance rejection. After satisfactory performance, the inputs and outputs of the process model can be easily switched with the plant inputs and outputs through MATLAB^{TM} OPC toolbox, as shown by Singh et al. [110].

The control limit has been considered to be 2% more or less than the set point (as suggested in scientific literature [93]). The results have been reported for 2000 seconds (approximately 33 minutes). It should be noted that the measurement noise has been taken into consideration while studying the set point tracking ability of the controller. The controller performance has been quantified by calculating the ITAE using Equation (4.30). While evaluating the performance of a controller, it is important to know the absolute error over the entire period of control action (in order to know how the controller behavior is over time). Absolute error is the magnitude of the exact difference between the set point and the measured value. The integral time square error (ITSE) can also be considered, however it is less sensitive compared to ITAE. Similarly, integral of the absolute error (IAE) or the integral square error (ISE) can also be used. However, ITAE produces smaller oscillations compared to IAE and ISE and it also includes the 'time' term [133]. Therefore, ITAE has been chosen as the criterion of comparison.

$$ITAE = \int_0^t t \ |(setpoint - measured\ variable)|dt \tag{4.30}$$

4.6.3 Control system design

In this section a pictorial representation of the developed control system is presented. A hybrid MPC-PID cascade control loop has been proposed for crystallization. The other control variables (i.e. drying gas temperature, API composition and holdup) have been controlled via MPC only. Figure 4.22 is the integrated process along with the control

loops. The control loop for the crystallization step is a cascade arrangement. C_{sat} is measured and fed to the MPC block which generates the set point for the cooling schedule (T(setpoint)) for the PID (controller 001). The slave controller controls the temperature cooling schedule (T) by manipulating the temperature of the cooling water (T_c) flowing through the cooling jacket. The drying gas temperature (T_{gas}) is measured and fed to the MPC block which generates the control signal by manipulating the super heated steam temperature (T_s) which heats the air in a heat exchanger. The hot air is then sent to the dryer. The API composition at the mixer outlet is measured and fed to the MPC block which manipulates the excipient flowrate to maintain the API composition at a desired set point. The holdup has been controlled by the MPC block by manipulating the weir length. Table 4.5 lists the controller tuning parameters. In case of PID (controller 001), a high value of the reset time signifies a low value of the integral term. Therefore, only the proportional and derivative terms are the most effective in this case. It can be seen that the output weights (MPC parameter) of all the control variables is 1, which means that same weightage has been given to all the control variables. The value of rate weight for every control variable is 0.1. It should be noted that in case of the MPC, the control interval is 1s, prediction horizon is 10s and control horizon is 2s.

In the case of the crystallization process, saturation concentration is the control variable for the master controller. The output of the master controller (temperature cooling schedule) provides the set point to the slave controller, which controls the cooling temperature schedule by manipulating the coolant temperature (passed through the coolant jacket around the crystallizer). The slave controller has been retained as a simple regulatory PID (which controls the temperature cooling schedule) and MPC acts as the master controller (which controls the saturation concentration). Therefore, the output of MPC (temperature cooling schedule) acts as the set point for the slave controller. In the case of the cooling crystallization, the operating temperature of the system is decreased so that the saturation concentration or the solubility decreases and the solute precipitates out of the solution to form crystals. Therefore the set point for saturation concentration has been decreased over time following a linear function.

PID parameters			
Control loop	Gain (K_c)	Reset Time (τ_I)	Rate (τ_D)
Crystallization (slave loop)	-0.166 ($K - ml/mg$)	2.95E4s	1.09E4s
MPC parameters			
Control loop	Input Weight	Rate Weight	Output Weight
Crystallization (Master loop)	0	0.1	1
Drying	0	0.1	1
Mixing (API composition)	0	0.1	1
Mixing (Holdup)	0	0.1	1

Table 4.5: List of controller Tuning Parameters

Figure 4.23 illustrates the saturation concentration. It can be seen from the plot that the controller is able to maintain the variable at the specified set point within the specified control limits. ITAE calculated for saturation concentration is 1.995E5.

In the case of the drying operation, the drying gas temperature is the control variable and the superheated steam temperature is the manipulating variable. The set point has been specified as 500K. It can be seen from figure 4.24 that the controller is able to maintain the drying gas temperature at the desired set point, within the control limits. ITAE calculated for drying gas temperature is 2.86E6.

In the case of the mixing process, two control variables have been considered (API composition and holdup). It has been mentioned before that the temperature cooling schedule affects the API composition of the final mixed product. The manipulating variables for API composition are excipient flowrate and crystallization operating temperature. In the case of holdup, the weir length is the manipulating variable. The set points for API composition and holdup are 0.15 and 6 kg respectively. Figure 4.25a and 4.25b present the controller performance for API composition and holdup respectively. It can be seen from the plots that the controller performance is satisfactory. ITAE calculated for the API composition and holdup are 1.195E3 and 4.3E4 respectively.

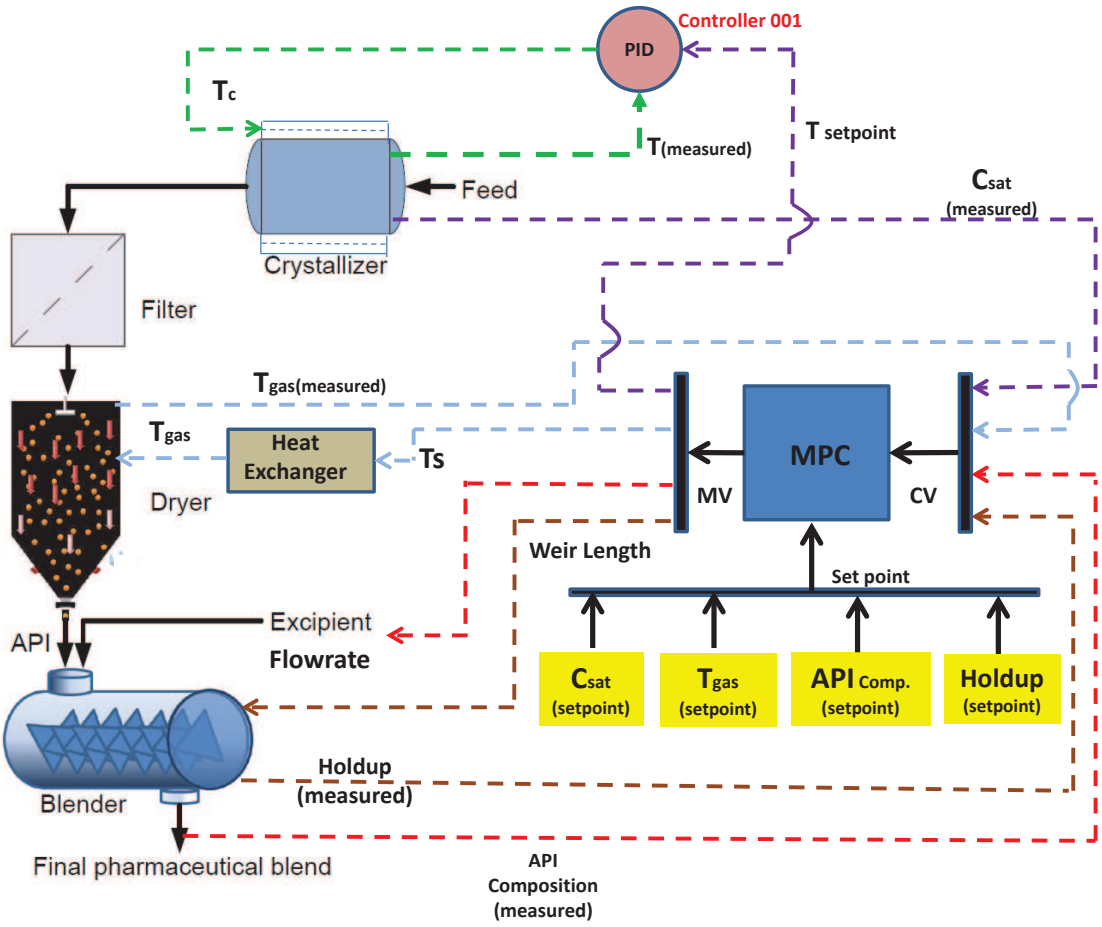

Figure 4.22: Pictorial representation of the closed loop continuous process

4.7 Chapter Conclusions

For the first time, a DEM-PBM multiscale integrated flowsheet model for continuous downstream processing of APIs has been developed. This model connects the purification processes of API production with a downstream pharmaceutical manufacturing process (mixing). With this model it will be easier for the pharmaceutical processing industries to understand the propagation of upstream process parameters and material properties on the downstream product attributes. The flowsheet model has been shown to generate results which qualitatively track the trend of the different variables of interest for each unit operation and CQAs (e.g. RSD and API composition). The model has been optimized and the optimal values of the important process parameters have been suggested. This optimized operational schedule has been compared with

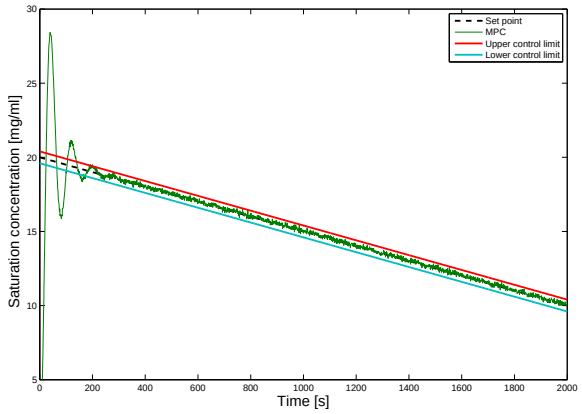

Figure 4.23: Hybrid MPC-PID performance of saturation concentration

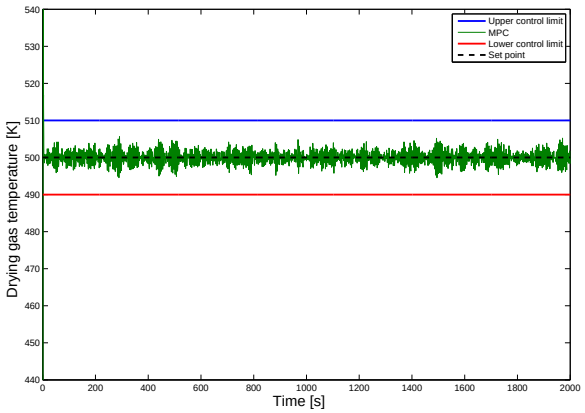

Figure 4.24: Hybrid MPC-PID performance of drying gas temperature

another schedule with different process conditions. It is seen that the optimized schedule gives better performance. An advanced hybrid MPC-PID control system has been developed. A cascade loop has been demonstrated for the control of the crystallization operation. The designed control system is able to track the step change in set points and reject unknown disturbances. This flowsheet can be extended further by adding other operations for downstream processing (e.g. granulation, roller compaction, tablet compaction and tablet dissolution) for a complete quantitative analysis of continuous purification and downstream processing of solid dosage forms.

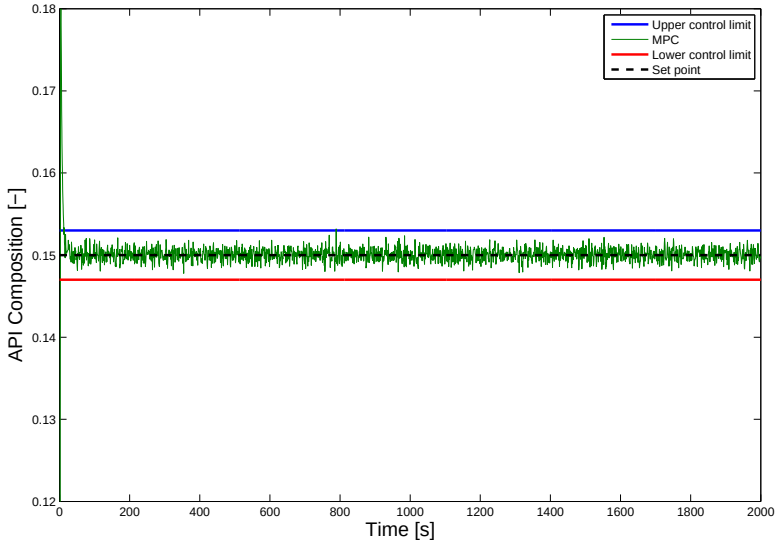

(a) API composition

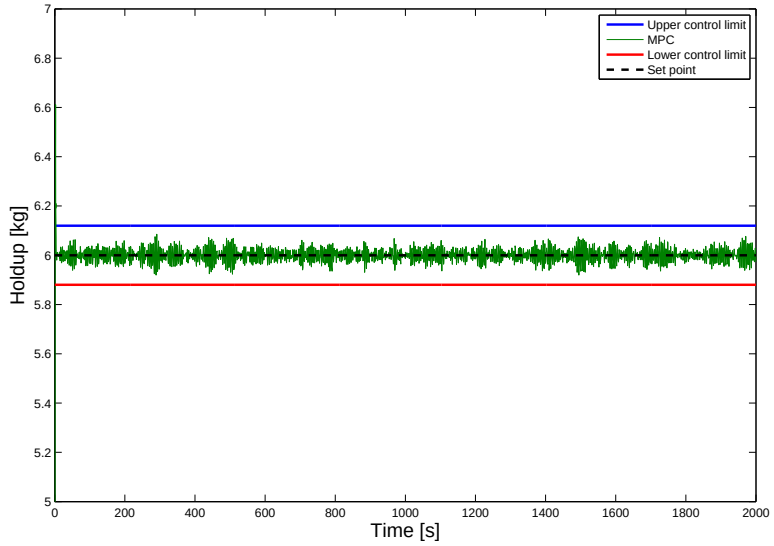

(b) Holdup

Figure 4.25: Hybrid MPC-PID performance of mixing process

Chapter 5

Development of a multiscale CFD-DEM-PBM description of a continuous fluidized bed wet granulation process

- **M. Sen**, D. Barrasso, R. Singh, R. Ramachandran, 2014. A multiscale hybrid CFD-DEM-PBM description of a fluid bed granulation process, Processes, 2, 89-111.

The purpose of this aim is to develop a multiscale CFD-DEM-PBM model for fluid bed granulation process using a dynamic two-way coupling and incorporating multiscale information such that the model can be used to study the detailed process dynamics. The model can be used effectively to study the different flow regimes and determine the evolution of important process variables (i.e. average particle diameter, particle size distribution and particle liquid content.

Granulation is widely applicable in industries which deal with powder handling processes (e.g. food, pharmaceutical, catalyst, fertilizer industries etc.). In pharmaceutical industries gramulation is often used as a unit operation present in the tablet manufacturing framework, and comes after the mixing operation. During granulation process, fine powder particles form agglomerates which are granules of larger size with improved properties (e.g. flowability, uniform composition etc.). In pharmaceutical industries, wet granulation is an important unit operation in the downstream tablet manufacturing process, since it has a significant effect on the mechanical properties of the tabletting material (e.g. hardness, dissolution rate). As a result, the understanding of the process dynamics of this particular unit operation is critical. An inefficient operation of the granulation process leads to high batch rejection rates (if operated in batch mode) or high recycle ratio (if operated in continuous mode) [134]. Since fluid bed granulation process consists of both solid and fluid phases, it is desired to model both the phases

individually and understand how they interact with each other. The fluid phase can be treated as a continuum and the flow dynamics can be described with the help of continuity equation and equation of motion. On the other hand, solid particles are discrete entities which will require the implementation of DEM techniques in order to capture their flow dynamics. Such types of flow which include both fluid and solid phases can be simulated efficiently with the help of CFD-DEM coupling. CFD will account for fluid flow whereas the same can be done for the solid phase using DEM. Establishing a connection between the flow field of the fluidizing medium and the contact pattern of the particles which in turn will dictate the aggregation rate will provide a detailed process dynamics of the fluid bed granulation process. A multiscale modeling scheme in this case is required.

The CFD model has been solved using Fluent^{TM} (version 14.5.0) (ANSYS), DEM has been solved using EDEM^{TM} (version 2.5.1) and in order to link the PBM with DEM, a user-defined library model has been built using the application programming interface within EDEM^{TM}.

In order to facilitate agglomeration during granulation process, a liquid binder is added and granulation takes place as a result of three rate processes (1.wetting and nucleation, 2. consolidation and aggregation and 3. breakage and attrition) [62]. Based on these rate processes, a granule can be classified by three internal properties (e.g. size, liquid content and porosity). In a FBG (fluid bed granulator), the particles are fluidized in order to ensure maximum contact between the liquid and the powder particles. At first the particles are rendered wet when they come in contact with the liquid binder and form granule nuclei. As the wet particles collide with one another, they form liquid bridges resulting in aggregation of small sized particles to form a larger sized particle. Similarly, particle breakage occurs because of the presence of shear stresses, compressive and tensile forces within the granulator due to particle-particle interaction or particle-wall (vessel interior wall) interaction, which can break a particle into smaller fragments.

The particle wetting rates in a FBG is highly dependent on the particle flow pattern which in turn is affected by the flow field of the fluidizing gas [135]. The flow behavior

of the powder within the granulator also depends on the geometry of the vessel. Several attempts are being made to understand the granular flow pattern but many aspects of it (i.e. a more detailed study of the vessel geometry, fluid flow field, collision frequencies etc.) using sophisticated modeling tools and techniques are yet to be developed [136]. The physical properties of the granules that are important in deciding the compactibility of the granules and which also affect the mechanical strength of the tablets, are particle liquid content, particle size, particle surface area and pore diameter. Porosity relates to the void spaces present in the particle and it is an important particle property because the surface liquid content of a particle will depend on its porosity and the surface liquid content will further decide the particle's aggregation rate. Porous particles can easily deform during compaction to create new bonding surfaces, thus affecting the tablet hardness [137]. Hardness of the tablet also depends on the granule surface area [138]. An appropriate design and operation of the granulation process can help to control the PSD and also help to achieve the desired flow characteristics of the particles. Improved granule characteristics will lead to efficient operation of the other unit operations present in the tablet manufacturing framework [14] and also help to achieve better product quality.

PBMs have been used extensively in order to model granulation process [139]. PBMs are used to calculate the rate processes (e.g. aggregation, consolidation and breakage) during granulation, but certain information, used in calculation of mechanistic aggregation and breakage kernels (i.e. effect of particle properties, spatial effect, collision frequency, particle velocity etc.) cannot be determined from a PBM alone. A DEM on the other hand is able to determine these entities. Such a PBM-DEM coupled model for particle aggregation has been reported [68].

Since a CFD-DEM approach has been used to study several complex particle-fluid flow systems [140, 141, 142], it is an effective tool to model fluid bed granulation. Interested readers are referred to the review presented by [143] on the discrete particle modeling of fluid beds. A combined CFD-DEM approach was first presented by [144] for simulating plug flow through horizontal pipes. Since then, there have been several works reported in scientific literature [145, 146, 147]. Liquid-solid interactions have been studied in case

of gas bubble formation in a gas-liquid-solid system [148, 149, 150]. Similar studies have been reported in case of gas and liquid fluidized beds in the bubbling regimes where a rigorous two way coupling framework has been introduced to explain the fluid-particle interaction [151, 152]. Fernandez et al. used CFD-DEM coupling in case of centrifugal separation systems [153]. Previous studies have been carried out in CFD-DEM coupling in case of granulation and are well documented [135, 154]. A direct numerical simulation model for a three phase flow in case of wet granulation, consisting of solid, liquid and gas has been developed by [15]. The liquid-gas flow has been solved using one of the CFD multi-phase solvers, and a solid particle flow is solved by DEM.

A CFD-PBM framework has been already implemented in order to model size change taking place in a particle-fluid system [155, 156] and a PBM derived from kinetic theory of granular flow (KTGF) has been developed by [157] for fluidized melt granulation. Hydrodynamic modeling of wet granulation process in a FBG using CFD principles has been reported by [158]. However there is a major scope still open to study a CFD-DEM-PBM coupled framework, which will capture a detailed interaction between the phases and quantify the size change. Such a multiscale model formulation has been reported by [159] for agglomerate breakage in fluid bed. The present work aims at capturing the particle aggregation during a granulation process in a FBG. The framework can be further developed in future by adding particle breakage along with the aggregation.

5.1 Multiscale model development

This section illustrates the mathematical equations and modeling techniques of each domain of the coupled framework. The CFD model calculates the fluid flow-field and the DEM adds it to the force-field calculation for each particle. The PBM obtains the various information required to calculate the rate processes from DEM to quantify the size change and update the PSD.

5.1.1 CFD model for the fluidizing medium

The fluid phase has been simulated using FLUENT^{TM}. The flow model chosen is that of a laminar viscous flow. The governing equations for incompressible flow are given in Equations (5.1)- (5.2) [135, 160]:

Navier-Stokes Equation

$$\frac{\partial \epsilon \mathbf{u}}{\partial t} + \nabla.(\epsilon \mathbf{u}\mathbf{u}) = -\frac{1}{\rho}\epsilon \nabla p - \frac{\mu}{\rho}\nabla^2.(\epsilon \mathbf{u}) + \mathbf{g} - S_p \tag{5.1}$$

and Equation of continuity

$$\nabla.(\epsilon \mathbf{u}) = 0 \tag{5.2}$$

where ϵ is the solid volume fraction, $\mathbf{u}$ is the fluid velocity, ρ is the fluid density, p is flow pressure, μ is the viscosity, S_p is the source term and $\mathbf{g}$ is gravity. The fluidizing medium in this case has been considered to be air and the fluid velocity at the inlet has been kept constant at 30 m/s. The fluid velocity at the inlet has been scaled as a function of the particle size in DEM to simulate observed experimental fluidization in a granulator. The inlet velocity has been determined by running several simulation trials such that the particles are fluidized and the effect of gravity can be nullified. In real granulation process, the particle size is in microns. But in the simulation, the initial particle size is in millimeters (i.e. 2mm diameter), which is much higher than the initial particle size used in real granulation process. As the simulation bed weighs more, therefore a higher air velocity is required to counter the effect of gravity. The solution methods used for calculating the momentum and particle volume fraction is first order upwind [161]. A first order Implicit scheme has been selected for the transient formulation. The boundary conditions have been set as follows:

- Flow near wall is laminar and the velocity varies linearly with the distance from wall.
- A no slip boundary condition has been set at the wall.

- A velocity inlet boundary condition has been used for the air entering the geometry.
- An outlet-vent boundary condition has been used at the geometry exit.

5.1.2 Discrete element model

DEM essentially uses Newton's laws of motion (as shown in Equation (5.3) and (5.4)) to simulate the particle force fields (namely contact forces and body forces [34]). The contact forces are due to particle-particle or particle-boundary (vessel internal wall) contacts whereas the body forces are any external force fields (i.e. gravity or fluid flow field in case of fluid bed granulation) acting on the particles. The net force F_{total} is calculated for each particle at a time interval which is approximately in the order of 10^{-5} or 10^{-6} seconds and the new particle state is calculated by numerically solving Newton's law and Euler's equations of rotational motion. The simulation uses a damped Hertzian normal contact model with Mindlin-Deresiewicz/Coulomb friction tangential force model. A detailed discussion on the contact models along with the governing equations have been provided by [34].

$$m_i \frac{dv_i}{dt} = F_{total} \tag{5.3}$$

$$F_{total} = \sum F_{contact} + \sum F_{body} \tag{5.4}$$

The DEM has been simulated using EDEM^{TM}. The geometry of the FBG has been imported within EDEM^{TM} and the initial PSD has been created. The initial PSD is uniform such that all particles are of fixed size (1 mm in radius). A virtual particle factory plate has been introduced within the geometry in the lower half and the particles are created at a generation rate of 50,000 particles per second. The liquid addition has been captured in EDEM^{TM}. The liquid droplets have been modeled as solid particles with similar properties as the initial powder particles. Liquid particles have been created continuously at a rate of 50,000 particles per second from a virtual plate placed in the

upper half of the granulator. It should be noted that the liquid addition has been started at time equal to 0.2s in order to let the particles fluidize first. The feed rate and the number of particles have been set in a way such that the simulation speed is fast and a reasonable granulation is achieved within the simulation time (when compared qualitatively with the experimental results [162, 163]). In a FLUENT^{TM}-EDEM^{TM} coupled simulation, it is important that the particle size is comparable with the mesh size (i.e. the particle size shouldn't be very large compared to the mesh size) [164]. For example in this work the primary particle diameter is 2mm and the mesh size is 4mm. These parameters have been fixed by running several trial simulations.

The change in particle size and new PSD is calculated using the PBM in the subsequent time steps as will be explained later. Whenever a liquid particle collides with a powder particle, it is deleted from the system and the liquid content of the particle increases by the liquid particle volume. If two liquid particles collide with each other, a single droplet with volume equal to the total volume of the two particles is formed. It should be noted that as the liquid particles are deleted from the system immediately upon contact, therefore EDEM^{TM} does not consider the contact forces due to these particles in the simulation. The EDEM^{TM} tracks the collisions occurring in between different particles and the information is stored in form of an array, which is made use by the PBM for calculating the new population distribution function at every population balance time step. Table 5.1 gives the material properties and the other parameters for particle-particle and particle-wall interaction.

The density of the powder material is 1030 kg/m^3 (which is similar to that of a pharmaceutical active ingredient (S)-Ibuprofen [165, 166]). Detailed information on the exact range of parameter values (particle-particle and particle-wall interaction parameters of EDEM^{TM}) for S-Ibuprofen is not available in literature, hence the values have been adapted from [34], who simulated fines in a continuous mixer, and from the work of [167].

Particle properties	
Shear modulus	$1E6Nm^{-2}$
Poisson's ratio	0.25
Density	$1030kgm^{-3}$
Particle-particle interactions	
Coefficient of restitution	0.2
Coefficient of static friction	0.5
Coefficient of rolling friction	0.01
Granulator walls	
Material	Steel
Shear modulus	$7.6E8Nm^{-2}$
Poisson's ratio	0.29
Density	$7800kgm^{-3}$
Particle-wall interactions	
Coefficient of restitution	0.2
Coefficient of static friction	0.5
Coefficient of rolling friction	0.01

Table 5.1: DEM simulation parameters

5.1.3 Population balance model for FBG

The present study considers the particle size change only, therefore the internal coordinates (represented using solid and liquid volume) have been retained and the spatial coordinates have been dropped from the PBE. At present only the particle aggregation has been accounted for and breakage has been neglected. Equation (2.1) has been modified accordingly to obtain Equation (5.5) as shown below:

$$\frac{\partial}{\partial t}F(s,l,t) + \frac{\partial}{\partial l}\left[F(s,l,t)\frac{dl}{dt}\right] = \Re_{aggregation} \tag{5.5}$$

The first and second terms of the equation represent evolution of the particle distribution function with respect to time and rate of liquid addition respectively. s and l are the volumes of solid and liquid (per particle), respectively and $\frac{dl}{dt}$ is the liquid addition rate. The liquid addition has been captured implicitly in EDEM^{TM}. Therefore the liquid addition term has been omitted from Equation (5.5) and the PBE has been further modified as shown in Equation (5.6):

$$\frac{\partial}{\partial t}F(s,l,t) = \Re_{aggregation} \tag{5.6}$$

The aggregation rate process is defined in Equations (5.7) to (5.9)

$$\Re_{aggregation} = \Re_{formation} - \Re_{depletion} \tag{5.7}$$

where

$$R_{formation} = \frac{1}{2}\int_0^s \int_0^l \beta(s-s', l-l', s', l', t)F(s-s', l-l', t)F(s', l', t)dl'ds' \tag{5.8}$$

$$R_{depletion} = \int_0^\infty \int_0^\infty \beta(s, l, s', l', t)F(s', l', t)F(s, l, t)dl'ds' \tag{5.9}$$

$\beta(s, l, s', l', t)$ is the aggregation kernel, as given in Equation (5.10). The aggregation kernel has been defined as a function of the collision frequency (C) and collision efficiency ψ. The collision frequency (which is a function of particle size [64]) is calculated based on the number of collisions occurring between the particle groups which can be obtained from EDEM^{TM} based on the particle properties.

$$\beta(s, l, s', l', t) = C(s, l, s', l', t)\psi(s, l, s', l') \tag{5.10}$$

The collision frequency is an important parameter. As previously mentioned, it is already known to be a function of particle size [64], but a study has been conducted by the authors showing collision frequency as a function of the PSD as well. The effect of the particle size is captured in the collision frequency which in turn controls the aggregation rate. Therefore, the aggregation rate kernel of this model depends on the PSD at any point of time. Collision frequency can be calculated as shown in Equation (5.11) [64]:

$$C(s,l,s',l',t) = \frac{N_{coll}(s,l,s',l',t)}{F(s,l,t)F(s',l',t)\Delta t} \tag{5.11}$$

In the above equation, N_{coll} is the total number of collision between two particle types represented by solid and liquid bins ($F(s,l,t)$ and $F(s',l',t)$) during the time interval Δt.

A simple expression (as shown in Equation (5.12)) has been adapted for collision efficiency based on the works of Biggs et al. [168]:

$$\psi(s,l,s',l') = \begin{cases} \psi_0, & LC(s,l) \geq LC_{min} or LC(s',l') \geq LC_{min} \\ 0, & LC(s,l) < LC_{min} or LC(s',l') < LC_{min} \end{cases} \tag{5.12}$$

Here LC stands for liquid content of the particles and LC_{min} is the minimum liquid content required for the particle coalescence. The above expression essentially means that if the liquid content of any two particles is greater than or equal to the minimum value (specified as 0.2 in this case), then the particles may aggregate to form a new particle upon collision depending on the value of the collision efficiency (which has been kept at a constant value of 0.01 in this study). The liquid content and collision efficiency values have been chosen such that the process variables show qualitative similarity in trend when compared to experimental results [163].

The PBM has been implemented by creating a custom contact model and custom factory for particle aggregation and liquid addition within the EDEM^{TM} simulation. The initial particles (both liquid and solid) which are created within EDEM^{TM} has a uniform solid and liquid volume respectively. Since a particle consists of both solid and liquid part, therefore the internal coordinate has been discretized linearly based on the particle's solid and liquid volume (also referred to as 'bins').

5.1.4 Information exchange in the coupling framework

The information exchanged over the coupled network along with the model assumptions have been summarized in this section. The model assumptions have been listed below:

- The PBM considers aggregation only, breakage and consolidation has not been incorporated since FBG processes are low shear processes with reduced consolidation and breakage (similar approach has been followed by [169]).
- A simple aggregation kernel has been formulated based on collision frequency and collision efficiency (adapted from [64]).
- The collision efficiency in the aggregation kernel is size independent, non-mechanistic and conditional based on the liquid content of the powder particles (adapted from [168]).
- Liquid addition has been captured in EDEM^{TM} by creating particles which get deleted from the system upon contact.

Figure 5.1 shows a schematic of the main CFD-DEM-PBM coupling framework and the DEM-PBM framework has been magnified to show the ongoing steps within it. The CFD-DEM framework has been developed by coupling EDEM^{TM} and FLUENT^{TM} through the commercially available coupling interface between them. CFD simulates the flow-field of the fluidizing air. When the solution converges, the fluid flow-field is passed to the CFD-DEM coupling interface which then calculates the drag force acting on each particle. The calculated drag force is then transferred to the DEM solver which updates the particle flow-field to obtain the new particle positions (or state). It should be noted that the PBM has been coded within EDEM^{TM} using the Application programming interface. The PBM time step is greater than the DEM time step. Therefore as the DEM solver performs the iteration, PBM waits till the PBM time step is reached. The number of collisions between each pair of solid and liquid bins over the time interval is recorded within the DEM simulation. This information is transferred to the PBM when the PBM time step is reached. The PBM uses this information to calculate the aggregation kernel as given by Equations (5.7)- (5.12). Each time the PBM is solved, a new PSD is calculated. This new PSD is then implemented within the DEM simulation for the subsequent DEM time step until the next PBM step is encountered. The DEM solver iterates until the CFD time step ends. The CFD-DEM coupling interface then

takes the information of the new particle position (or state) from the DEM solver, updates the solid volume fraction in each fluid cell and passes the information to the CFD solver. The CFD solver again iterates over the next time step until the solution converges and the same steps are repeated. The EDEM^{TM} time step should be always less than the FLUENT^{TM} time step and it is suggested that the EDEM^{TM} time step is kept between (1/10)th to (1/100)th of the FLUENT^{TM} time step for stability [164]. In this case, the CFD time step is 2E-3 seconds and the DEM time step is 3.25E-5 seconds. It means that the DEM solver iterates approximately 61 times within one CFD time step. The PBM time step is 0.25 seconds (i.e. PBM is solved every 0.25 seconds). The framework has been simulated for 2 seconds. Therefore the PBM has been solved 8 times in this simulation time. The PBM time step is an important factor and has been decided after running a few simulation trials. It is important to choose the time-step in a way such that:

1. A reasonable number of collisions occur among the particles between any two subsequent time steps.

2. The PBM is solved a reasonable number of times such that there is a more consistent distribution of the particle size (as seen in Figure 5.10)

If the PBM time step is too low, then the model will not be able to capture enough number of collisions which results in difficulty of computational tractability of PBM. A resolution study of the PBM time step and its effect on PSD has been carried out (details have been provided in the results and discussion section (section 4.3)).
The coupled framework has been run for a time period of 2 seconds which took approximately 6 hours of CPU time, running on an Intel Core i7-2600 CPU processor (3.4 GHz) with 16 GB of RAM.

5.1.5 Model outputs

This section presents a brief description of the model outputs which are PSD, average fractional liquid content and average diameter.

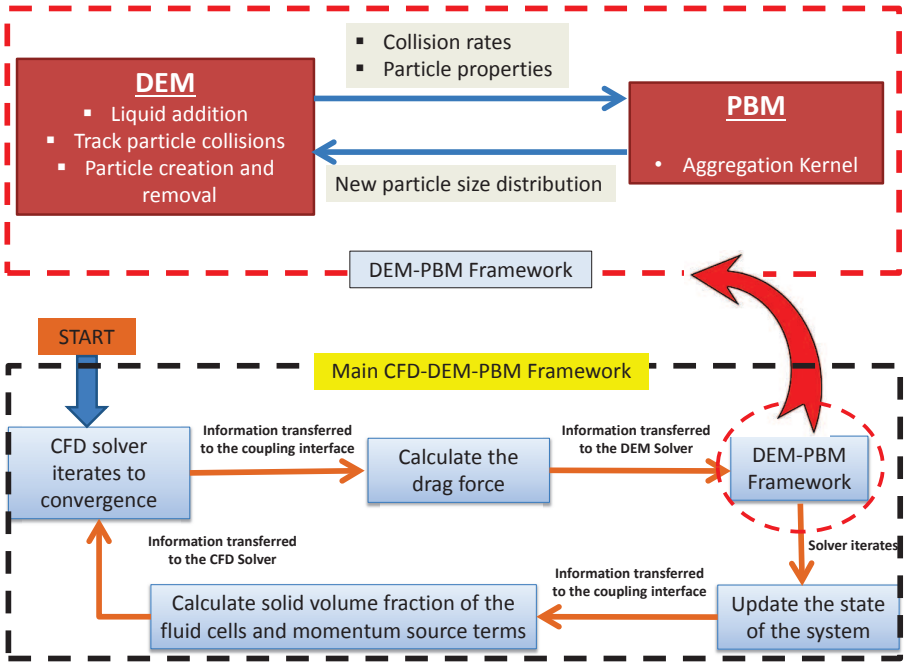

Figure 5.1: Schematic of the coupled multiscale framework

The PSD has been obtained by post-processing the simulation data. The diameter of each particle present in the system at any particular time point can be obtained from EDEM^{TM}. Several size classes are defined by ranges of the diameter and each bin from the PBM are grouped in these size classes. The total mass of particles in each of these size classes is determined individually and each of them is further normalized by dividing with the overall mass of particles to obtain a mass frequency as seen in equation (5.13). The mass frequency can be plotted with respect to the size classes in order to obtain the PSD.

$$\mu_m(t) = \sum_{L_m \leq D_{ij} < L_{m+1}} \left(\frac{F(s_i, l_j, t)}{\sum_{i=1}^{ns} \sum_{j=1}^{nl} F(s_i, l_j, t)} \right) \frac{\rho V_m}{\sum_{m=1}^{nm} \rho V_m} \tag{5.13}$$

where μ_m is the mass frequency of mth size class (which is a function of particle diameter), ρ is the density, ns is the number of solid bins, nl is the number of liquid bins, V_m is the particle volume in m th size class, nm is the number of size classes and D_{ij} is the particle diameter corresponding to the ith solid bin and jth liquid bin.

Similarly the average diameter (D_{avg}) can be calculated as shown in equation (5.14):

$$D_{avg}(t) = \frac{\sum_{i=1}^{ns}\sum_{j=1}^{nl} F(s_i, l_j, t)(6(s_i + l_j)/\pi)^{1/3}}{\sum_{i=1}^{ns}\sum_{j=1}^{nl} F(s_i, l_j, t)} \tag{5.14}$$

The average fractional liquid content (x_{avg}) can be calculated as shown in equation (5.15):

$$x_{avg}(t) = \frac{\sum_{i=1}^{ns}\sum_{j=1}^{nl} F(s_i, l_j, t)(l_j/(s_i + l_j)}{\sum_{i=1}^{ns}\sum_{j=1}^{nl} F(s_i, l_j, t)} \tag{5.15}$$

5.2 Results and discussion

This section includes the discussion on the model geometry and the results obtained from the coupled framework. The simulation steps have been highlighted briefly as shown below.

5.2.1 Simulation procedure

This section lists the procedure followed while setting up the coupled simulation, in a nutshell.

1. The geometry has been made using ANSYS Design Modeler^{TM}.
2. The geometry has been meshed using ICEM-CFD^{TM}.
3. The mesh file has been imported within FLUENT^{TM}.
4. The mesh has been converted into Polyhedra domain.
5. The gravity is defined in the correct direction and a transient simulation is selected.
6. The flow model has been selected to be viscous laminar.
7. The coupling server has been started.
8. The FLUENT^{TM} is coupled with EDEM^{TM} for the desired fluid domain by selecting the Eulerian-Eulerian option.

9. The coupling server will automatically import the geometry with the specified direction of gravity in EDEM^{TM} and set the source terms in x-momentum, y-momentum and z-momentum calculation. The value of the simulation parameters of the coupling interface has been set as follows:

    - Sample points: The number of points used by FLUENT^{TM} to calculate the volume fraction of the fluid cell. This value has been set at 10, which means that a large particle can transfer its volume between 10 cells. This particular parameter decides the stability and speed of the simulation. A higher value of sample point may increase the stability but decrease the simulation speed.
    - Relaxation factor: The relaxation factors again help with stability and convergence of the solution. Reducing the value helps to increase stability and achieve convergence. Both momentum-MTM-under-relaxation factor and volume under-relaxation factor have been set at 0.7.

10. The inlet fluid velocity has been defined as 30 m/s.

11. The custom contact model and custom factory (for PBM calculation) have been imported within EDEM^{TM}.

12. The material properties, particle-particle and particle-wall interaction parameters as given in table 5.1 have been set in EDEM^{TM}.

13. The initial PSD has been created in EDEM^{TM}.

14. The liquid particles have been created in EDEM^{TM} (the liquid addition starts at 0.2s).

15. Once the EDEM^{TM} simulation is set up, initialize the solution in FLUENT^{TM}.

16. Run the calculation.

5.2.2 Model geometry

The measurement details of the model geometry has been given in figure 5.2. Figure 5.2 also presents the mesh, which has been done in ICEM-CFD^{TM}. The geometry has been

meshed using the tetra/mixed meshing tools with a grid size of 4mm. The mesh has been converted into polyhedra domain after importing it in FLUENT^{TM}. As shown in figure 5.2, the geometry has been divided into five fluid domains or cell zones (inlet domain, fluid inlet domain, main fluid domain, fluid outlet domain and outlet domain). The CFD-DEM coupling has been performed for the cell zone (main fluid domain). Every time the simulation leaves Fluent^{TM} and enters EDEM^{TM}, all the relevant data in the linked zones are passed to EDEM^{TM}. Reducing the number of linked zones will reduce the amount of data transferred between the two softwares and thus increase the simulation speed. Therefore the simulation has been linked for the 'main fluid domain' only. Although the coupling has been done for the 'main fluid domain', the particles are free to move around throughout the geometry, but only the data from the 'main fluid domain' are passed to EDEM^{TM}. The results/plots reported in the manuscript are for the 'main fluid domain' only. It should be noted that the spatial co-ordinates have not been considered in the PBM. The main idea is to present a CFD-DEM-PBM framework which is able to capture the granulation dynamics. Therefore the assumption is that the 'main fluid domain' is representative of the whole geometry.

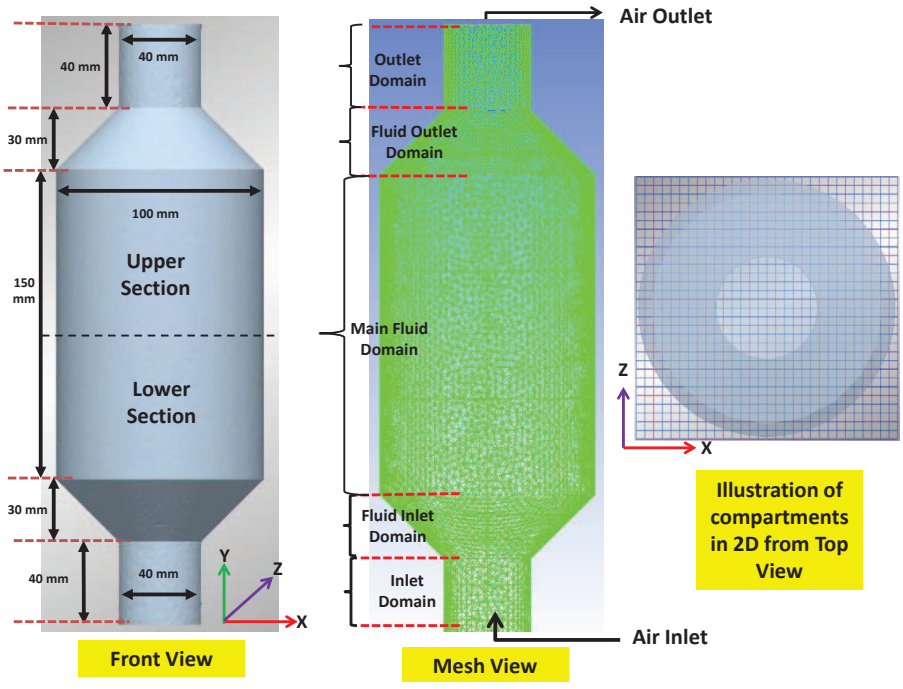

Figure 5.2: Model Geometry and mesh of the FBG

5.2.3 Multiscale model results

The multiscale model has been simulated to obtain the average diameter and liquid content of the particles as a function of time. This model can be also used to study the distribution of particle velocity and particle liquid content, which will help to understand the flow pattern and liquid content of the solid particles. Since the aggregation rate depends on the liquid content of the particles, therefore it is important to study these aspects. It will also help in understanding the impacts of the equipment design and improve it for a better operational efficiency.

In order to analyze the particle flow pattern and liquid distribution, the 'main fluid domain' has been divided equally into two sections (upper half and lower half). Each half has been divided into several compartments and the DEM simulation has been post processed to obtain the particle velocity in each of these compartments. As shown in figure 5.2, the geometry has been divided into 30 grids in both x and z direction and 1 grid in y direction, such that there are $30 \times 1 \times 30$ compartments in total. Figure 5.2 gives an illustration of the compartments in 2D as seen from the top view. Figure 5.3 shows the contour plots of the particle velocities (i.e. the resultant velocity of the three components v_x, v_y and v_z) averaged over different time intervals. Figure 5.3a and figure 5.3b present the particle velocities for both lower and upper halves, averaged over time 0s-0.5s and 0.5s-1s respectively. It can be seen that the velocity of the particles increases with time. However the lower section shows a more uniform distribution of velocity compared to the upper section. The plot for upper section in figure 5.3a shows a non-uniform distribution with high velocity present sporadically in few locations and the velocity values in most of the compartments are closer to zero. This is because the particles are being injected into the system from a virtual plate placed in the lower half and it takes about 0.4 seconds for the bed to be fully fluidized. Similarly figures 5.3c and 5.3d present the particle velocity distribution in both the halves averaged over time 1s-1.5s and 1.5s-2s respectively. These plots also show that the particle velocity increases with time as the bed gets fully fluidized and presents a more uniform velocity distribution in the upper half. It can be also noted that an absolute steady state in the

particle velocity is not being realized. This is due to the mechanics of the granulation process (as the partcles interact with each other and the boundary in numerous ways, it is difficult to obtain an absolute steady state).

Figure 5.4a and 5.4b show the particle liquid content distribution averaged over 0s-0.5s (initial time of simulation) and 1.5s-2s (final time of simulation). Figure 5.4a shows a non-uniform distribution over a higher range for the upper part, with the values in most of the compartments lying close to zero (similar observation has been made in the velocity distribution as well). The distribution becomes comparatively uniform with time as seen in figure 5.4b. The liquid content of the particles in the upper part is more than the liquid content of the particles present in the lower part. This is because the liquid droplets are being injected into the system from a virtual plate located near the upper half of the granulator, hence only a few of them are able to penetrate through the void space and reach the lower half. This shows that the binder liquid distribution is highly dependant on the particle flow pattern, which in turn also affects the aggregation rate (particle liquid content is an important factor in deciding the granulation rate processes).

Figures 5.5 and 5.7 present snapshots of the particles within the granulator taken at different time points based on their liquid content and relative diameter respectively.

As previously mentioned, the amount of liquid present in the particles is an important attribute as it controls the rate process, which in turn will decide the increase in particle size. The snapshots (figure 5.5) of the liquid content have been taken at 1s and 2s. The particles have been colour coded based on its fractional liquid content. It can be seen that more particles are getting wet with time. This is because the particle velocity increases with time and a more uniform velocity distribution is obtained throughout the granulator (also seen from the contour plots) resulting in more contacts between the liquid and solid particles. So the average liquid fraction (i.e. the ratio of liquid volume to the total volume of a particle, where total volume is equal to the summation of liquid volume and solid volume of a particle) increases with time and levels off gradually as can be seen in figure 5.6 (plot of particle liquid content versus time). Since the particles are free to move around (in all domains), therefore there are particles exiting the ‘main

fluid domain‘. Initially there is a steep increase in the liquid content because the bed takes some time to be fully fluidized. As a result the number of particles in the ‘main fluid domain‘ is still increasing and more particles are getting wet with time. But as the bed is fully fluidized, an approximate steady state is being realized in the ‘main fluid domain‘. It should be noted that in this model, the liquid droplets which have been created are of comparable size to the solid particles. Therefore an assumption has been made that one liquid particle can wet only one solid particle. Under certain circumstances, where the powder particles are much smaller than the liquid particles, it is possible that one liquid droplet wets more than one powder particle (depending on the liquid to solid volume ratio). This feature can be included in the coupled framework in future.

Figure 5.7 presents the snapshot of the relative particle diameter taken at 1s and 2s. It can be seen that the number of large sized particles increase with time. This can be again explained on the basis of the particle movement pattern. With time, the velocity distribution becomes more uniform and the contact between the particles increases which results in aggregation. Figure 5.8 is a plot for the average diameter as a function of time. It is seen that the average diameter of the particles increase with time. Figure 5.9 is a plot for the PSD taken at different time points. It can be seen that a gradual progression towards larger sized particles is being realized during granulation.

The trends observed in this study are qualitatively consistent with experimental results [162, 163]. The studies show that the granulation is being achieved as the particle liquid content increases. They present bimodal particle size distributions that broaden over time by starting with finer primary particles.

In order to show the effect of PBM time step, two more simulatons have been run with PBM time step equal to 0.2s (PBM has been solved 10 times) and 0.4s (PBM has been solved 5 times) and compared with the base case (PBM time step equal to 0.25s, where PBM has been solved 8 times). Figure 5.10 presents the PSDs obtained at the final time point (time=2s) from each simulation. It can be seen that the PSD for the largest PBM time step (0.4s) has a lower frequency of very large particles (due to the presence of the highest peak). This is because the PBM has been solved only 5 times during the

simulation thus limiting the opportunities for large particles to collide and aggregate with each other. On the other hand, PSDs with smaller PBM time step (0.2s and 0.25s) show a more consistent distribution suggesting more accuracy. Therefore it is essential to perform a comparative analysis of the model predicted data obtained by running the simulation with different PBM time step, with experimental data.

5.3 Chapter Conclusions

This work presents a multiscale model for granulation, using information from different scales of CFD, DEM and PBM techniques. Granulation has been extensively modeled following a PBM approach, which groups a lump of particles in different classes (based on size, porosity etc.), but this particular framework tracks the flow-field of each particle with the help of DEM. The CFD aspect helps to add in the drag force acting on the particles due to the flow field of the fluidizing medium. The aggregation kernel is a function of the collision efficiency and collision frequency, which in turn depends on the particle size distribution. An empirical expression, based on the liquid content has been used to determine the collision efficiency. Future effort will be to introduce a mechanistic approach in determining the collision efficiency based on relative velocity of the colliding particles, particle mass and liquid content. The PBM which has been implemented is two-dimensional which can track the change in particle size as well as liquid content of the particles. The liquid addition has been captured implicitly in the DEM and the aggregation kernel has been decided based on the information provided by the DEM on collision frequency and particle liquid content. PBM calculates the new PSD at every PBM time step, which has been implemented in the DEM by removing old particles and creating new ones. The model can be used effectively to study the material flow pattern, different flow regimes (usually encountered in dense granular systems), binder distribution pattern, the effect of equipment geometry (see if dead zones are present) and key performance criteria (i.e. average diameter and liquid content). This model can be used to study the effect of material properties as well, which can be an interesting future investigation. This coupled model is detailed as it is able to store information from different scales and can be used as an effective tool to understand the process

dynamics of a fluid bed granulation process.

It should be noted that this coupled multiscale model is computationally intensive and therefore can not be integrated into the flowsheet model (as developed in specific aim III) efficiently in the present form. However, this multiscale model can be used to build a ROM for the CFD-DEM bit, which can then be incorporated into the PBM. The coupled ROM-PBM can be effectively integrated into the flowsheet model.

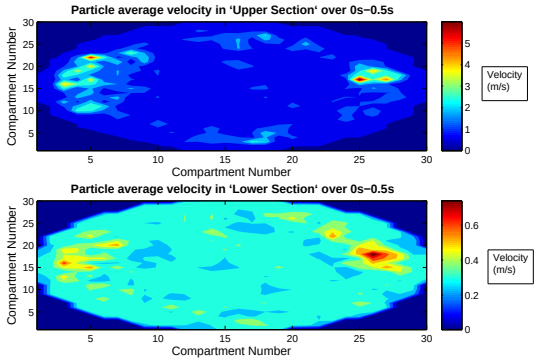

(a) Velocity distribution over 0s-0.5s

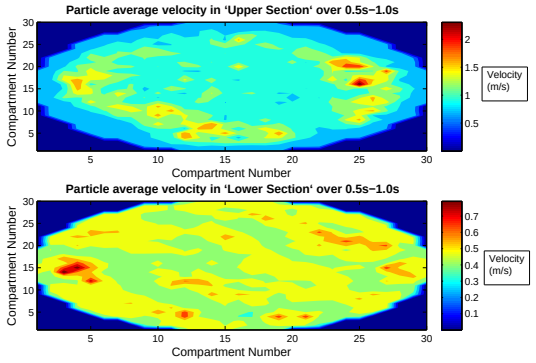

(b) Velocity distribution over 0.5s-1.0s

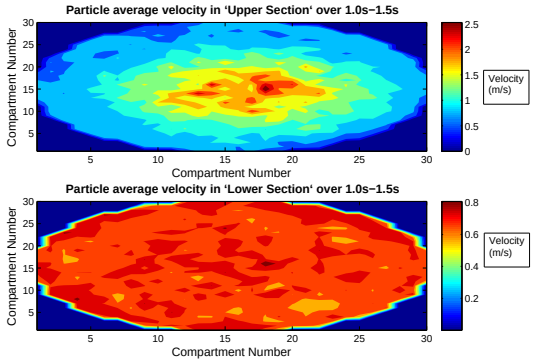

(c) Velocity distribution over 1.0s-1.5s

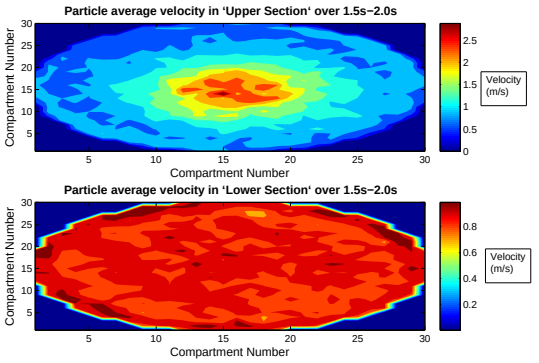

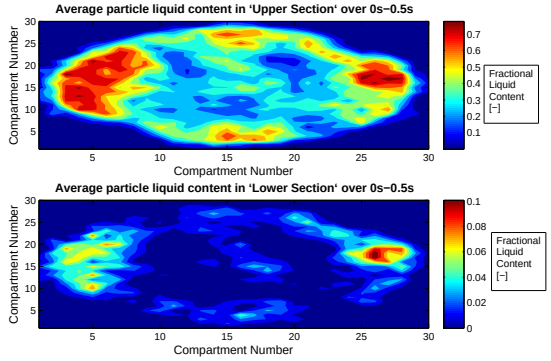

(a) Liquid content over 0s-0.5s

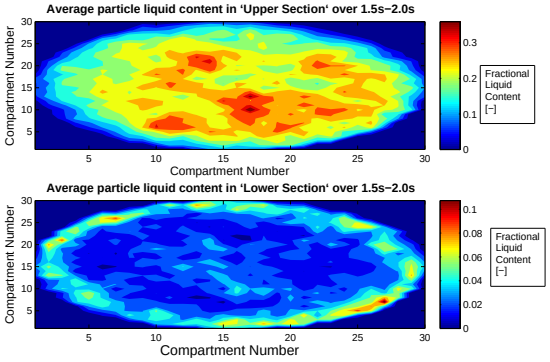

(b) Liquid content over 1.5s-2.0s

Figure 5.4: Plots for particle liquid content distribution

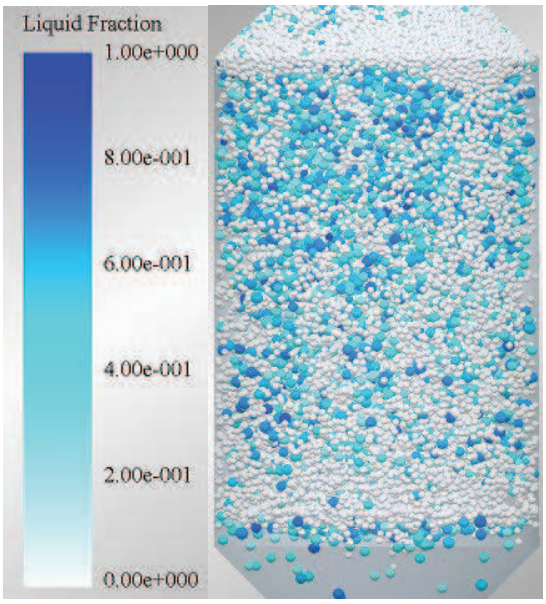

(a) Particle liquid content at time=1s

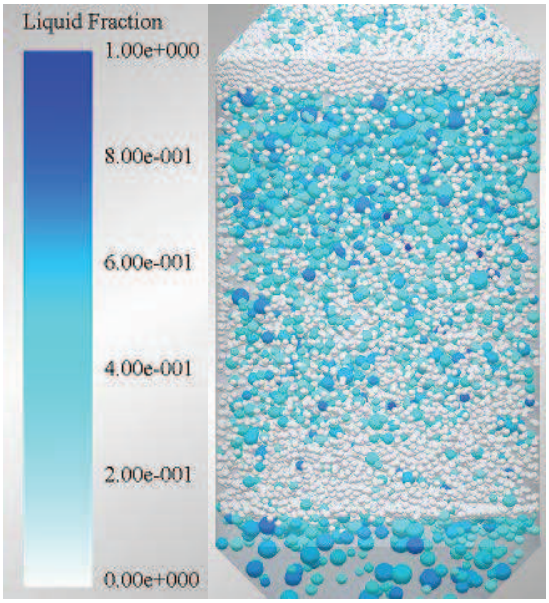

(b) Particle liquid content at time=2s

Figure 5.5: EDEM^{TM} snapshots of liquid content

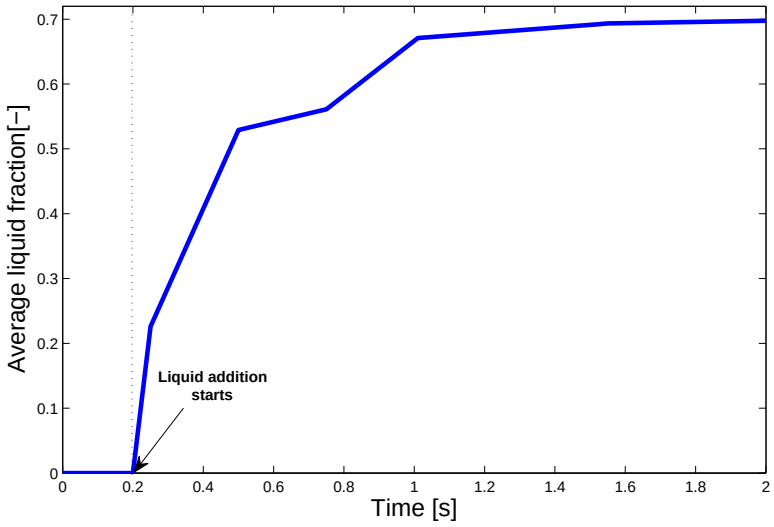

Figure 5.6: Liquid content vs time

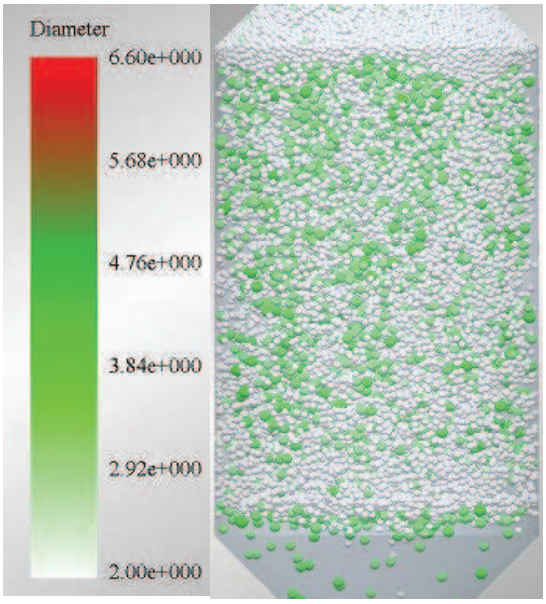

(a) Particle diameter at time=1s

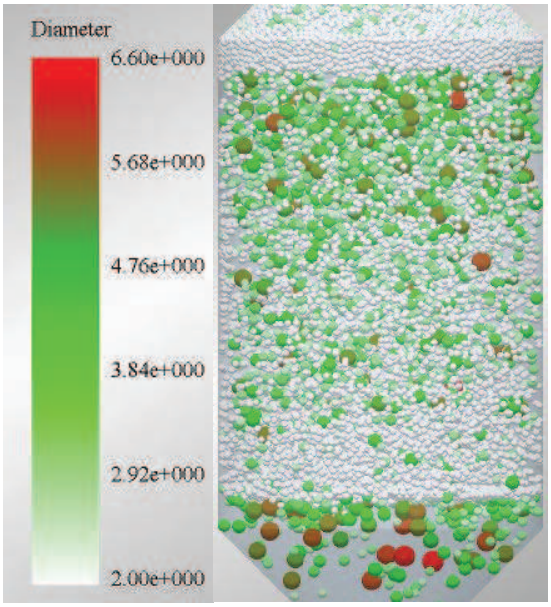

(b) Particle diameter at time=2s

Figure 5.7: EDEM^{TM} snapshots of particle diameter

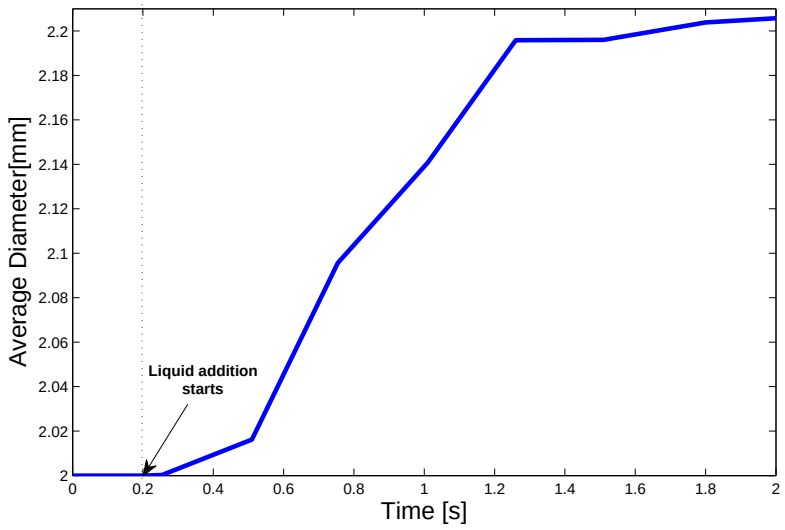

Figure 5.8: Average diameter vs time

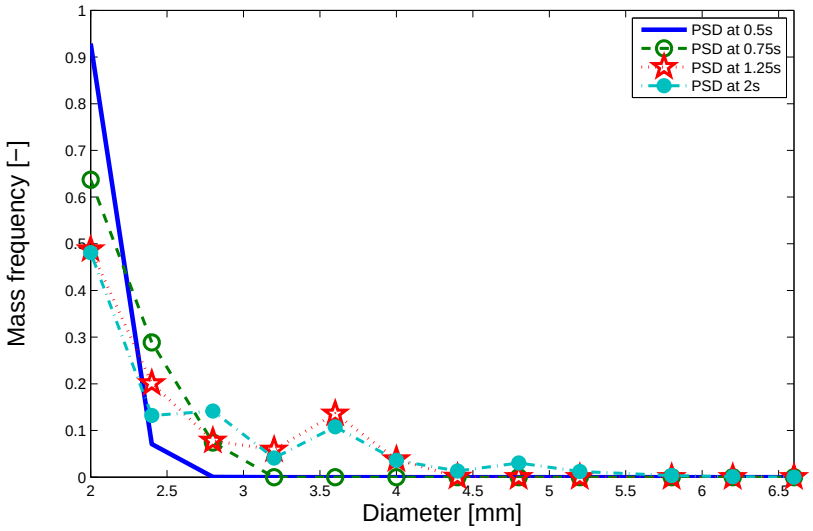

Figure 5.9: PSD at different time points

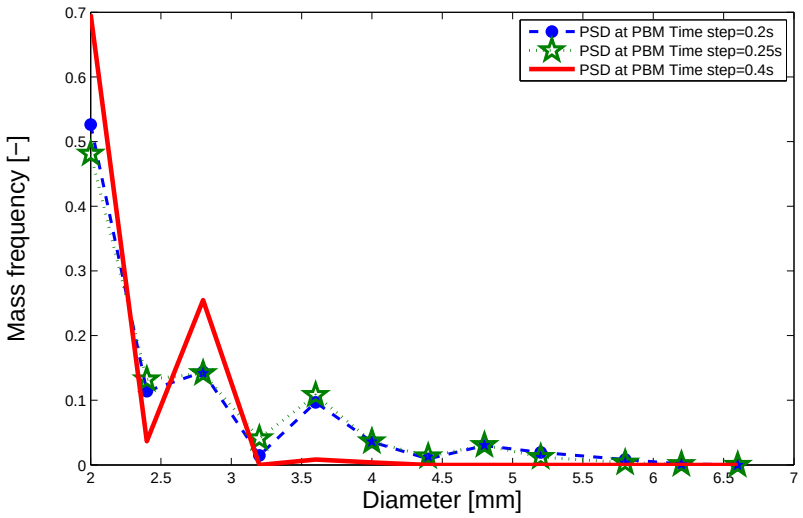

Figure 5.10: PSDs for different PBM time step

Chapter 6

Thesis conclusions and future directions

This dissertation is aimed at utilizing different modeling techniques (i.e. CFD, DEM and PBM) in order to develop a detailed integrated and multiscale model for a continuous manufacturing framework that can be implemented towards efficient pharmaceutical manufacturing processes. This work introduces mechanistic models developed from first-principles which has been shown capable of capturing detailed dynamics of the process. The multiscale frameworks which have been demonstrated are capable of storing information from various scales (micro, meso and macro). These multiscale frameworks are highly efficient for modeling powder systems, since a bulk powder flow consists of discrete particles which behave or interact with other neighboring particles or the equipment geometry in different manner. The multiscale models thus developed have been integrated in a continuous manner in order to demonstrate a continuous processing framework that can be implemented in pharmaceutical industries. This work presents an integrated flowsheet model which establishes a connection between the upstream API purification/processing steps and downstream tablet manufacturing process. This flowsheet can be used to study the effect, the upstream process parameters have on the downstream product attributes. It is a well known fact that PAT and QbD tools can be easily implemented in case of continuous processing schemes which will enhance the product quality and also reduce the production of rejects. As the continuous processing is being implemented in the pharmaceutical industries, this flowsheet model can be used as a tool for virtual experimentation for performing design, optimization and control related studies. Since design and optimization related studies require several runs or trials, therefore such a virtual platform will save time and resources which is

otherwise not possible with real experimentation. The flowsheet model consists of crystallization, filtration, drying and mixing, where crystallization, filtration and drying are upstream API purification operations and mixing is a downstream tablet manufacturing operation.

A PBM has been developed for a continuous mixing process (detailed in specific aim I), which has been experimentally validated and a multiscale one-way DEM-PBM coupled model has been suggested for the same (detailed in specific aim II). The PBM can be used for process or equipment design as has been demonstrated in specific aim I. The output variables (mixed product CQAs) from PBM has been shown to demonstrate quantitative agreement with the experimental trends and give a high prediction certainty. The results from the multiscale framework has been shown to give excellent qualitative agreement when compared with the results of a full DEM simulation as well as experimental trends. Therefore the mixing model is highly effective in capturing the detailed physics of the operation. This mixing model has been further integrated in a continuous flowsheet model as discussed in specific aim III. A two-dimensional PBM has been written for the crystallization operation, which is able to capture crystal growth in two directions. The crystallization model has been validated experimentally in order to determine the kinetic parameters. As described in specific aim III, the flowsheet model is multiscale in nature as well, since it incorporates particle level information into the PBM. The usage of the flowsheet model has been demonstrated by performing an optimization and design related study (detailed in specific aim III). An efficient control strategy has been suggested for the same by implementing a hybrid MPC-PID platform. The flowsheet can be further extended by including a granulation operation after mixing. Granulation is often present in the downstream tablet manufacturing framework and is used for size enlargement of the fine particles in order to improve their flowability and physical properties. A dynamic concurrent coupled CFD-DEM-PBM multiscale modeling framework as been developed for a fluid bed wet granulation process (as detailed in specific aim IV). This model is able to capture the detailed interaction between the fluid and solid phases and able to simulate the particle size change

with the help of PBM. The FBG model has been shown to be able to capture the different flow regimes within the granultor and product quality attributes (PSD, average particle diameter, liquid content. A ROM can be developed from the multiscale model developed for the fluid bed granulation process. The ROM can be further incorporated in the flowsheet model.

The FDA has introduced QbD and PAT principles, which mandate that the product quality should be built by design at every manufacturing stage. This approach is a promising alternative when compared to the traditional trial-and-error approach, where the quality of the final product is matched with the regulatory guidelines. The application of the required GMP ensures good end product quality. QbD and PAT principles help reduce the overall time-to-market and cost of health-care. Therefore products that conform to quality in accordance to the regulatory guidelines (as dictated by the QbD and PAT principles) can be produced via an efficiently designed and controlled continuous processing framework. An overall idea of this work is to present different modeling tools and techniques which can be used to enhance the design of the manufaturing processes used in the pharmaceutical industries and can be used to aid in the smooth transition of these industires from a batch to continious processing schemes.

6.1 Future directions

The present flowsheet model can be further extended by adding the other relevant unit operations which include chemical synthesis of the API followed by its separation, purification, after which the API crystals are sent to the formulation and tabletting stages. This will give a full fledged continuous framework, which can be further used for performing optimization study and for designing an efficient control system as demonstrated in specific aim III. At present the flowsheet includes only the API separation, purification and pharmaceutical blend formulation stages. However it forms the basis for further extension.

References

[1] S. D. Schaber, D. I. Gerogiorgis, R. Ramachandran, J. M. B. Evans, P. I. Barton, B. L. Trout, Economic analysis of integrated continuous and batch pharmaceutical manufacturing: A case study, Industrial and Engineering Chemistry Research 50 (2011) 10083–10092.

[2] H. Leuenberger, New trends in the production of pharmaceutical granules: batch versus continuous processing, European Journal of Pharmaceutics and Biopharmaceutics 52 (2001) 289–298.

[3] F. Boukouvala, A. Dubey, A. Vanarase, R. Ramachandran, F. J. Muzzio, M. Ierapetritou, Computational approaches for studying granular dynamics of continuous blending processes - ii, Macromolecular Materials and Engineering 296 (2011) 000–000.

[4] K. Plumb, Continuous processing in the pharmaceutical industry: Changing the mindset, Chemical Engineering Research and Design 83 (2005) 730–738.

[5] R. Ramachandran, J. Arjunan, A. Chaudhury, M. Ierapetritou, Model-based control-loop performance assesment of a continuous direct compaction pharmaceutical process, Journal of Pharmaceutical Innovation 6 (2011) 249–263.

[6] H. Leuenberger, G. Betz, Chapter 15: Granulation process control-production of pharmaceutical granules: The classical batch concept and the problem of scale-up, In: AD Salman, J Seville, M Hounslow, editors. Handbook of powder technology: granulation vol 11 (2007) 705–733.

[7] H. Leuenberger, Scale-up in the 4th dimension in the field of granulation and drying or how to avoid classical scale-up, Powder Technology 130 (2003) 225–230.

[8] J. Werani, M. Grunberg, C. Ober, H. Leuenberger, Semicontinuous granulation-the process of choice for the production of pharmaceutical granules, Powder Technology 140 (2004) 163–168.

[9] G. Betz, P. Junker-Purgin, H. Leuenberger, Batch and continuous processing in the production of pharmaceutical granules, Pharmaceutical Development and Technology 8 (2003) 289–297.

[10] F. Boukouvala, V. Niotis, R. Ramachandran, F. Muzzio, M. G. Ierapetritou, An integrated approach for dynamic flowsheet modeling and sensitivity analysis of a continuous tablet manufacturing process: an integrated approach, Computers and Chemical Engineering 42 (2012) 30–47.

[11] G. V. Reklaitis, J. Khinast, F. J. Muzzio, Pharmaceutical engineering science-new approaches to pharmaceutical development and manufacturing, Chemical Engineering Science 65 (2010) 4 – 7.

[12] I. T. Cameron, F. Y. Wang, C. D. Immanuel, F. Stepanek, Process systems modeling and applications in granulation: A review, Chemical Engineering Science 60 (2005) 3723–3750.

[13] S. Mascia, P. L. Heider, H. Zhang, R. Lakerveld, B. Benyahia, P. I. Barton, R. D. Braatz, C. L. Cooney, J. M. B. Evans, T. F. Jamison, K. F. Jensen, A. S. Myerson, B. L. Trout, End-to-end continuous manufacturing of pharmaceuticals: Integrated synthesis, purification, and final dosage formation, Angewandte Chemie International Edition 52 (2013) 12359–12363.

[14] F. Boukouvala, A. Chaudhury, M. Sen, R. Zhou, L. Mioduszewski, M. G. Ierapetritou, R. Ramachandran, Computer-aided flowsheet simulation of a pharmaceutical tablet manufacturing process incorporating wet granulation, J Pharm Innov (2013) DOI 10.1007/s12247–012–9143–9.

[15] K. Washino, H. S. Tan, M. J. Hounslow, A. D. Salman, A new capillary force model implemented in micro-scale CFD-DEM coupling for wet granulation, Chemical Engineering Science (2013) http://dx.doi.org/10.1016/j.ces.2013.02.006.

[16] B. Remy, Granular flow, segregation and agglomeration in bladed mixers, Ph.D. thesis, Rutgers, The State University of New Jersey (2010).

[17] A.U. Vanarase and F.J. Muzzio, Effect of operating conditions and design parameters in a continuous powder mixer, Powder Technology 208 (2011) 26 – 36.

[18] P. M. Portillio, M. G. Ierapetritou, S. Tomassone, C. Mc Dade, D. Clancy, P. P. C. Avontuur, F. J. Muzzio, Quality by design methodology for development and scale-up of batch mixing processes, J Pharm Innov 3 (2008) 258–270.

[19] P. M. Portillio, A. U. Vanarase, A. Ingram, J. K. Seville, M. G. Ierapetritou, F. J. Muzzio, Investigation of the effect of impeller rotation rate, powder flow rate, and cohesion on the powder flow behavior in a continuous blender using pept, Chemical Engineering Science 65 (2010) 5658–5668.

[20] H. Berthiaux, K. Marikh, Modeling continuous powder mixing by means of the theory of markov chains, Particulate Science & Technology 22 (2004) 379–389.

[21] O. S. Sudah, W. A. Chester, J. A. Kowalski, J. W. Beeckman, F. J. Muzzio, Quantitative characterization of mixing processes in rotary calciners, Powder Technology 126 (2002) 166–173.

[22] H. Wu, E. J. Heilweil, A. S. Hussain, M. A. Khan, Process analytical technologies (PAT) - effects of instrumental and compositional variables in terahertz spectral data quality to characterize pharmaceutical materials and tablets, Computer Aided Chemical Engineering 343 (2007) 148–158.

[23] F. Boukoulava, F. J. Muzzio, M. G. Ierapetritou, Predictive modeling of pharmaceutical processes with missing and noisy data, AIChE Journal 56 (2010) 2860–2872.

[24] P. M. Portillio, M. G. Ierapetritou, F. J. Muzzio, Effects of rotation rate, mixing angle, and cohesion in two continuous powder mixers - a statistical approach, Powder Technology 194 (2009) 217–227.

[25] P. M. Portillio, F. J. Muzzio, M. Ierapetritou, Characterizing powder mixing processes utilizing compartment models, International Journal of Pharmaceutics 320 (2006) 14–22.

[26] P. M. Portillio, M. G. Ierapetritou, S. Tomassone, C. Mc Dade, D. Clancy, P. P. C. Avontuur, F. J. Muzzio, Using compartment modeling to investigate mixing behavior of a continuous mixer, J Pharm Innov 3 (2008) 161–175.

[27] Y. Gao, F. Muzzio, M. G. Ierapetritou, Characterization of feeder effects on continuous solid mixing using fourier series analysis, AIChE Journal 57 (2011) 1144–1153.

[28] Y. Gao, M. G. Ierapetritou, F. J. Muzzio, Investigation on the effect of blade patterns on continuous solid mixing performance, The Canadian Journal of Chemical Engineering 89 (2010) 969–984.

[29] Y. Gao, A. Vanarase, F. Muzzio, M. Ierapetritou, Characterizing continuous powder mixing using residence time distribution, Chemical Engineering Science 66 (2011) 417–425.

[30] P. M. Portillio, F. J. Muzzio, M. Ierapetritou, Hybrid-DEM compartment modeling approach to granular mixing, AIChE Journal 53 (2007) 119–128.

[31] B. Freirich, J. Li, J. D. Litster, C. Wassgren, Incorporating particle flow information from discrete element simulations in population balance models of mixer-coaters, Chemical Engineering Science 66 (2011) 3592–3604.

[32] A. Sarkar, C. R. Wassgren, Simulation of a continuous granular mixer:effect of operating conditions on flow and mixing, Chemical Engineering Science 64 (2009) 2672–2682.

[33] A. Sarkar, C. R. Wassgren, Continuous blending of cohesive granular material, Chemical Engineering Science 65 (2010) 5687–5698.

[34] A. Dubey, A. sarkar, M. Ierapetritou, C. R. Wassgren, F. J. Muzzio, Computational approaches for studying the granular dynamics of continuous blending processes,1-dem based methods, Macromolecular materials and engineering 296 (2011) 290307.

[35] B. Remy, Granular flow, segregation and agglomeration in bladed mixers, Ph.D. thesis, Rutgers, The State University of New Jersey (2010).

[36] P. Marchal, R. David, J. P. Klein, J. Villermaux, Crystallisation and precipitation engineering - I. An efficient method for solving population balances in crystallisation and agglomeration, Chemical Engineering Science 43 (1988) 59–67.

[37] F. Puel, G. Févotte, J. P. Klein, Simulation and analysis of industrial crystallization processes through multidimensional population balance equations. part 1: a resolution algorithm based on the method of classes, Chemical Engineering Science 58 (2003) 3715–3727.

[38] R. Gunawan, I. Fusman, R. D. Braatz, High resolution algorithms for multidimensional population balance equations, AIChE Journal 50 (2004) 2738–2749.

[39] D. L. Ma, D. K. Tafti, R. D. Braatz, High-resolution simulation of multidimensional crystal growth, Industrial and Engineering Chemistry Research 41 (2002) 6217–6223.

[40] C. D. Immanuel, F. J. Doyle III, Solution technique for a multi-dimensional population balance model describing granulation processes, Powder Technology 156 (2005) 213–225.

[41] J. M. H. Poon, C. D. Immanuel, F. J. Doyle III, J. D. Litster, A three-dimensional population balance model of granulation with a mechanistic representation of the nucleation and aggregation phenomena, Chemical Engineering Science 63 (2008) 1315–1329.

[42] J. M. H. Poon, R. Ramachandran, C. F. W. Sanders, T. Glaser, C. D. Immanuel, F. J. D. III, J. D. Litster, F. Stepanek, F. Y. Wang, I. T. Cameron, Experimental validation studies on a multi-scale and mult-dimensional population balance model of batch granulation, Chemical Engineering Science 64 (2009) 775–786.

[43] R. Ramachandran, C. D. Immanuel, F. Stepanek, J. D. Litster, F. J. D. III, A mechanistic model for granule breakage in population balances of granulation: theoretical kernel development and experimental validation, Chemical Engineering Research and Design 87 (2009) 598–614.

[44] R. Ramachandran, P. I. Barton, Effective parameter estimation within a multidimensional population balance model framework, Chemical Engineering Science 65 (2010) 4884–4893.

[45] D. Ramkrishna, Population Balances, Academic Press, San Diego, 2000.

[46] P. D. Christofides, Control of nonlinear distributed process systems: Recent development and challenges, AICHE Journal 47 (2001) 514–518.

[47] C. D. Immanuel, F. J. Doyle III, Computationally efficient solution of population balance models incorporating nucleation, growth and coagulation: application to emulsion polymerization, Chemical Engineering Science 52 (2003) 3681–3698.

[48] H. S. Tan, M. J. V. Goldschmidt, R. Boerefijn, M. J. Hounslow, A. D. Salman, J. A. M. Kuipers, Building population balance model for fluidized bed melt granulation: lessons from kinetic theory of granular flow, Powder Technology 30 (2004) 103–109.

[49] I. Goldhirsch, Introduction to granular temperature, Powder Technology 182 (2008) 130–136.

[50] B. Chaudhuri, A. Mehrotra, F. J. Muzzio, M. S. Tomassone, Cohesive effects in powder mixing in a tumbling blender, Powder Technology 165 (2006) 105–114.

[51] A. Gorsek, P. Glavic, Design of batch versus continuous processes: part 1: single-purpose equipment, Chemical Engineering Research and Design 75 (1997) 709–717.

[52] H. Leuenberger, New trends in the production of pharmaceutical granules: batch versus continuous processing, European Journal of Pharmaceutics and Biopharmaceutics 52 (2001) 289 – 298.

[53] S. Adam, D. Suzzi, C. Radeke, J. G. Khinast, An integrated quality by design (QbD) approach towards design space definition of a blending unit operation by discrete element method (DEM) simulation, European Journal of Pharmaceutical Sciences 42 (2011) 106–115.

[54] T. Gracia, G. Cook, R. Nosal, PQLI key topics - criticality, design space and control strategy, Journal of Pharmaceutical Innovation 3 (2008) 60–68.

[55] R. Lionberger, S. L. Lee, L. Lee, A. Raw, L. X. Yu, Quality by design: Concepts for ANDAs, The AAPS Journal 10 (2008) 268–276.

[56] R. Nosal, T. Schultz, PQLI definition of criticality, Journal of Pharmaceutical Innovation 3 (2008) 69–78.

[57] L. Yu, Pharmaceutical quality by design: Product and process development, understanding and control, Pharmaceutical Research 25 (2008) 781–791.

[58] R. Singh, K. V. Gernaey, R. Gani, Model-based computer-aided framework for design of process monitoring and analysis systems, Computers and Chemical Engineering 33 (2009) 22–42.

[59] R. Singh, K. V. Gernaey, R. Gani, ICAS-PAT: A software for design, analysis and validation of PAT systems, Computers and Chemical Engineering 34 (2010) 1108 – 1136.

[60] J. Glassey, K. V. Gernaey, C. Clemens, T. W. Schulz, R. Oliveira, G. Striedner, C. F. Mandenius, Process analytical technology (PAT) for biopharmaceutical, Biotechnology Journal 6 (2011) 369–377.

[61] Y. Saito, X. F. Fan, A. Ingram, J. P. K. Seville, A new approach to high-shear mixer granulation using positron emission particle tracking, Chemical Engineering Science 66 (2011) 563–569.

[62] S. M. Iveson, J. D. Litster, K. Hapgood, B. J. Ennis, Nucleation, growth and breakage phenomena in agitated wet granulation process: a review, Powder Technol. 117 (2001) 3–39.

[63] J. Bouffard, F. Bertrand, J. Chaouki, A multiscale model for the cimulation of granulation in rotor-based equipment, Chemical Engineering Science 81 (2012) 106–117.

[64] J. A. Gantt, E. P. Gatzke, A stochastic technique for multidimensional granulation modeling, AIChE Journal 52 (2006) 3067–3077.

[65] A. Reinhold, H. Briesen, Discrete element modeling for multiscale simualtion of aggregation processes. in: Tenth international symposium on process systems engineering, PSE2009.

[66] A. Abbas, J. A. Romagnoli, Multiscale modeling, simulation and validation of batch cooling crystallization, Separation and Purification Technology 53 (2007) 153–163.

[67] E. Weinan, B. Enquist, X. T. Li, W. Q. Ren, E. Vanden-Eijnden, Heterogenous multiscale methods: a review, Communications in computational physics 2 (2007) 367–450.

[68] A. reinhold, H. Briesen, Numerical behavior of a multiscale aggregation model-coupling population balances and discrete element models, AIChE Journal 70 (2012) 165–175.

[69] A. Hassanpour, H. Tan, A. Bayly, P. Gopalkrishnan, B. Ng, M. Ghadiri, Analysis of particle motion in a paddle mixer using discrete element method (dem), Powder Technology 206 (2011) 189–194.

[70] A. Dubey, A. U. Vanarase, F. J. Muzzio, Effect of process parameters on the performance of a continuous blender: A DEM based study, AIChE Journal (2012) doi:10.1002/aic.13770.

[71] H. K.-E., E. Simsek, S. Rickelt, S. Wirtz, V. Scherer, Review and extension of normal force models for the discrete element method, Powder Technol. 171 (2007) 157173.

[72] J. Shafer, S. Dippel, D. E. Wolf, Force schemes in simulations of granular materials, J de Phys. I 6 (1996) 5–20.

[73] H. K.-E., M. Sturm, S. Wirtz, V. Scherer, Selection of an appropriate time integration scheme for the discrete element method (dem), Comput. Chem. Eng. 32 (2008) 2263–2279.

[74] K. M. Aoki, T. Akiyama, Simulation studies of pressure and density wave propagation in vertically vibrated beds of granules, Phys Rev E 52 (1995) 3288–3291.

[75] H. K.-E., E. Smirk, S. Wirtz, V. Scherer, Modeling of granular flow and combined heat transfer in hoppers by the discrete element method (dem), Journal of pressure vessel technology 128 (2006) 439–444.

[76] N. V. Brilliantov, F. Spahn, J. Hertzcsh, T. Poschel, Model for collisions in granular gases, Phys. Rev. E 53 (1996) 5382–5392.

[77] C. Thornton, Z. M. Ning, A theoretical model for the stick/bounce behaviour of adhesive, elastic-plastic spheres, Powder Technol. 99 (1998) 154–162.

[78] W. R. Ketterhagen, J. S. Curtis, C. R. Wassgren, B. C. Hancock, Modeling granular segregation in flow from quasi-three-dimensional, wedge-shaped hoppers, Powder Technol. 179 (2008) 126–143.

[79] W. R. Ketterhagen, J. S. Curtis, C. R. Wassgren, A. Kong, P. J. Narayan, B. C. Hancock, Granular segregation in discharging cylindrical hoppers: A discrete element and experimental study, Chemical Engineering Science 62 (2007) 6423–6439.

[80] J. A. Gantt, I. T. Cameron, J. D. Litster, E. P. Gatzke, Determination of coalescence kernels for high-shear granulation using dem simulations, Powder Technol. 170 (2006) 53–63.

[81] D. K. Kafui, C. Thornton, Fully-3d dem simulation of fluidised bed spray granulation using an exploratory surface energy-based spray zone concept, Powder Technol. 184 (2008) 177–188.

[82] X. An, R. Yang, K. Dong, A. Yu, Dem study of crystallization of monosized spheres under mechanical vibrations, Computer Physics Communications 182 (2011) 1989–1994.

[83] A. U. Vanarase, Design, modeling and real-time monitoring of continuous powder mixing processes, Ph.D. thesis, Rutgers, The State University of New Jersey (2011).

[84] A. Drud, A GRG code for large sparse dynamic nonlinear optimization problems, Mathematical Programming 31 (1985) 153 – 191.

[85] A. Drud, Conopt-a large scale GRG code, ORSA Journal on Computing 6 (1992) 207 – 216.

[86] R. Ramachandran, P. I. Barton, Effective parameter estimation within a multi-dimensional population balance model framework, Chemical Engineering Science 65 (2010) 4884 – 4893.

[87] M. Sen, R. Singh, A. Varanase, J. John, R. Ramachandran, Multi-dimensional population balance modeling and experimental validation of continuous powder mixing processes, Chemical Engineering Science 80 (2012) 349–360.

[88] A. Vanarase, M. Alcal, J. Rozo, F. Muzzio, R. Romaach, Real-time monitoring of drug concentration in a continuous powder mixing process using nir spectroscopy, Chemical Engineering Science 65 (21) (2010) 5728 – 5733.

[89] Y. Gao, F. Muzzio, M. G. Ierapetritou, Investigation on the effect of blade patterns on continuous solid mixing performance., The Canadian Journal of Chemical Engineering 89 (2010) 969 – 984.

[90] P. M. Portillo, M. G. Ierapetritou, F. J. Muzzio, Effects of rotation rate, mixing angle, and cohesion in two continuous powder mixers–a statistical approach, Powder Technology 194 (2009) 217 – 227.

[91] R. Gunawan, I. Fusman, R. D. Braatz, Parallel high-resolution finite volume simulation of particulate processes, AIChE Journal 54 (2008) 1449–1458.

[92] S. Ganesan, L. Tobiska, An operator-splitting finite element method for the efficient parallel solution of multidimensional population balance systems, Chemical Engineering Science 69 (2011) 59–68.

[93] R. Singh, M. Ierapetritou, R. Ramachandran, An engineering study on the enhanced control and operation of continuous manufacturing of pharmaceutical tablets via roller compaction, Int J Pharm 438 (2012) 307–326.

[94] I. Alaathar, E. Hartge, S. Heinrich, J. Werther, Modeling and flowsheet simulation of continuous fluidized bed dryers, Journal of Powder Technology (2012) http://dx.doi.org/10.1016/j.powtec.2012.03.048.

[95] B. Benyahia, R. Lakerveld, P. I. Barton, A plant-wide dynamic model of a continuous pharmaceutical process, Industrial & engineering chemistry research 51 (2012) 15393–15412.

[96] D. Bertsimas, O. Nohadani, K. M. Teo, Robust optimization for unconstrained simulation-based problems, Operations Research 58 (2010) 161–178.

[97] B. Y. Shekunov, P. York, Crystallization processes in pharmaceutical technology and drug delivery design, Journal of Crystal Growth 211 (2000) 122–136.

[98] C. Wibowo, K. D. Samant, L. Young, Integrated approach to crystallization process design for fine chemicals and pharmaceuticals, Computer Aided Chemical Engineering 21 (2006) 749–754.

[99] F. Boukouvala, F. J. Muzzio, M. G. Ierapetritou, Dynamic data-driven modeling of pharmaceutical processes, Ind Eng Chem Res (2011) 6743–6754.

[100] A. E. Cervera-Padrell, T. Skovby, S. Kiil, R. Gani, K. V. Gernaeya, Active pharmaceutical ingredient (API) production involving continuous processes a process system engineering (PSE)-assisted design framework, Journal of Powder Technology 82 (2012) 437–456.

[101] R. Lakerveld, B. Benyahia, R. D. Braatz, P. I. Barton, Model-based design of a plant-wide control strategy for a continuous pharmaceutical plant, AIChE Journal (2013) DOI: 10.1002/aic.14107.

[102] X. Z. Wang, L. Liu, R. Li, R. J. Tweedie, K. Primrose, J. Corbett, F. McNeil-Watson, Online monitoring of nanoparticle suspensions using dynamic light scattering, ultrasound spectroscopy and process tomagraphy, Comp Aided Chem Eng. 26 (2009) 351–356.

[103] M. J. Lee, D. Y. Seo, H. E. Lee, I. C. Wang, W. S. Kim, M. Y. Jeong, G. J. Choi, In line NIR quantification of film thickness on pharmaceutical pellets during a fluid bed coating process, International Journal of Pharmaceutics 403 (2010) 66–72.

[104] J. Huang, C. Goolcharran, K. Ghosh, A quality by design approach to investigate tablet dissolution shift upon accelerated stability by multivariate methods, European Journal of Pharmaceutics and Biopharmaceutics 78 (2011) 141–150.

[105] B. A. Ogunnaike, W. H. Ray, Process dynamics, modeling, and control, Oxford University Press, NY, USA, 1994.

[106] J. Richalet, Industrial applications of model based predictive control, Automatica 29 (1993) ‘1251–1274.

[107] C. E. Garcia, D. M. Prett, M. Morari, Model predictive control: theory and practice-a survey, Automatica 25 (1989) 335–348.

[108] R. Singh, M. Ierapetritou, R. Ramachandran, System-wide hybrid MPC-PID control of a continuous pharmaceutical tablet manufacturing process via direct compaction, European Journal of Pharmaceutics and Biopharmaceutics 85 (2013) 1164–1182.

[109] R. Ramachandran, J. Arjunan, A. Chaudhury, M. G. Ierapetritou, Model-based control loop performance assessment of a continuous direct compaction pharmaceutical processes, Journal of Pharmaceutical Innovation 6 (2012) 249–263.

[110] R. Singh, D. Barrasso, A. Chaudhury, M. Sen, M. Ierapetritou, R. Ramachandran, Closed-loop feedback control of a continuous pharmaceutical tablet manufacturing process via wet granulation, Journal of Pharmaceutical Innovation (2014) DOI 10.1007/s12247–014–9170–9.

[111] R. Singh, A. Sahay, F. Muzzio, M. Ierapetritou, R. Ramachandran, Systematic framework for onsite design and implementation of the control system in continuous tablet manufacturing process, Computers and Chemical Engineering (2013) Accepted for publication.

[112] B. Pregelj, S. Gerksic, Hybrid explicit model predictive control of a nonlinear process approximated with a piecewise affine model, Journal of Process Control 20 (2010) 832–839.

[113] G. R. Harrison, P. W. Todd, S. R. Rudge, D. Petrides, Bioseparations science and engineering, Oxford University Press, 2003.

[114] A. Chaudhury, P. Pandey, R. Ramachandran, A multi-dimensional population balance model validation approach to high-shear wet granulation (HSWG) processes, AIChE Annual Meeting, Minneapolis, USA, Oct. 17-21.

[115] H. Miki, T. Terashima, Y. Asakuma, K. Maeda, K. Fukui, Inclusion of mother liquor inside KDP crystals in a continuous MSMPR crystallizer, Separation and Purification Technology 43 (2005) 71 – 76.

[116] W. L. Mccabe, J. C. Smith, P. Harriott, Unit operations of chemical engineering, McGraw-Hill, 2001.

[117] A. Mezhericher, A. Levy, I. Borde, Modelling of particle breakage during drying, Chemical Engineering and Processing 47 (2008) 1404 – 1411.

[118] M. Sen, A. Chaudhury, R. Singh, J. John, R. Ramachandran, Multi-scale flowsheet simulation of an integrated continuous purification-downstream pharmaceutical manufacturing process, Int J Pharm 445 (2013) 29–38.

[119] M. Mirmehrabi, S. Rohani, An approach to solvent screening for crystallization of polymorphic pharmaceuticals and fine chemicals, Journal of pharmaceutical sciences 94 (2005) 1560–1576.

[120] gPROMS model builder, gPROMS 3.4.0 documentation, Process system enterprise (PSE) http://www.psenterprise.com/gproms.html.

[121] D. Sarkar, S. Rohani, A. Jutan, Multi-objective optimization of seeded batch crystallization processes, Chemical Engineering Science 61 (2006) 5282–5295.

[122] F. Boukouvala, Y. Gao, F. Muzzio, M. G. Ierapetritou, Reduced-order discrete element method modeling, Chemical Engineering Science (2013) http://dx.doi.org/10.1016/j.ces.2013.01.053.

[123] F. Boukouvala, R. Ramachandran, A. Vanarase, F. J. Muzzio, M. G. Ierapetritou, Computer aided design and analysis of continuous pharmaceutical manufacturing processes, Computer Aided Chemical Engineering 29 (2011) 216–220.

[124] Y. Lang, A. Malacina, L. T. Biegler, S. Munteanu, J. I. Madsen, S. E. Zitney, Reduced order model based on principal component analysis for process simulation and optimization, Energy & Fuels (2009) 1609 – 1706.

[125] R. Riesen, Process optimization using an automatic laboratory reactor, Document of Mettler-Toledo GmbH, Schwerzenbach, Switzerland () 1–8.

[126] K. L. Choong, R. Smith, Optimization of batch cooling crystallization, Chemical Engineering Science 59 (2004) 313–327.

[127] G. Zhu, M. A. Henson, B. A. Ogunnaike, A hybrid model predictive control strategy for nonlinear plant-wide control, Journal of Process Control 10 (2000) 449–458.

[128] C. Song, B. Wu, P. Li, A hybrid model-based optimal control method for nonlinear systems using simultaneous dynamic optimization strategies, Journal of Process Control 22 (2012) 852–860.

[129] A. Robles, M. V. Ruano, J. Ribes, J. Ferrer, Advanced control system for optimal filtration in submerged anaerobic mbrs (SAnMBRs), Journal of Membrane Science 430 (2013) 330–340.

[130] R. H. Peiris, H. Budman, C. Moresoli, R. L. Legge, Fouling control and optimization of a drinking water membrane filtration process with real-time model parameter adaptation using fluorescence and permeate flux measurements, Journal of Process Control 23 (2013) 70–77.

[131] A. Hammond, M. Smith, The role of PAT, condition monitoring and adaptive control in delivering QbD, AIChE Annual Meeting, Pittsburg, PA, USA, October 28-November 2.

[132] G. Stephanopoulos, Chemical Process Control, Prentice-Hall,Inc., NJ, USA, 2006.

[133] W. C. Schultz, V. C. Rideout, Control system performance measures: Past, present and future,, IRE Trans. on Automatic Control AC-6 (1961) 22–35.

[134] F. Y. Wang, I. T. Cameron, Review and future directions in the modelling and control of continuous drum granulation, Powder Technology 124 (2002) 238–253.

[135] L. Fries, S. Antonyuk, S. Heinrich, S. Palzer, DEM-CFD modeling of a fluidized bed spray granulator, Chemical Engineering Science 66 (2011) 23402355.

[136] B. H. Ng, Y. L. Ding, M. Ghadiri, Modelling of dense and complex granular flow in high shear mixer granulator- a CFD approach, Chemical Engineering Science 64 (2009) 3622–3632.

[137] Y. Habib, L. L. Augsburger, R. F. Shangraw, Production of inert cushioning beads: effect of excipients on the physicomechanical properties of freeze-dried beads containing microcrystalline cellulose produced by extrusion-spheronization, International Journal of Pharmaceutics 233 (2002) 67–83.

[138] S. L. Cantor, S. Kothari, O. M. Y. Koo, Evaluation of the physical and mechanical properties of high drug load formulations: Wet granulation vs. novel foam granulation, Powder Technology 195 (2009) 15–24.

[139] D. Barrasso, S. Walia, R. Ramachandran, Multi-component population balance modeling of continuous granulation processes: A parametric study and comparison with experimental trends, Powder Technology 241 (2013) 85–97.

[140] D. G. Rong, M. Horio, Behavior of particles and bubbles around immersed tubes fluidized bed at high temperature and pressure: a DEM simulation, International Journal of Multiphase Flow 27 (2001) 89–105.

[141] C. H. Ibsen, E. Helland, B. H. Hjertager, Comparison of multifluid and discrete particle modelling in numerical predictions of gas particle flow in circulating fluidised beds, Powder Technology 149 (2004) 29–41.

[142] K. W. Chu, A. B. Yu, Numerical simulation of the gas-solid flow in three dimensional pneumatic conveying bends, Industrial & Engineering Chemistry Research 47 (2008) 7058–7071.

[143] N. G. Deen, M. S. Annaland, M. A. Van der Hoef, J. A. M. Kuipers, Review of discrete particle modelling of fluidized beds, Chemical Engineering Science 62 (2007) 28–44.

[144] Y. Tsuji, T. Tanaka, T. Ishida, Lagrangian numerical-simulation of plug flow of cohesionless particles in a horizontal pipe, Powder Technology 71 (1992) 239–250.

[145] Z. Y. Zhou, S. B. Kuang, K. W. Chu, A. B. Yu, Assessments of CFD-DEM models in particlefluid flow modelling, Journal of fluid mechanics 661 (2010) 482–510.

[146] E. Helland, R. Occelli, L. Tadrist, Numerical study of cluster formation in a gasparticle circulating fluidized bed, Powder Technology 110 (2000) 210–221.

[147] M. J. Rhodes, X. S. Wang, M. Nguyen, P. Stewart, K. Liffman, Use of discrete element method simulation in studying fluidization characteristics: influence of interparticle force, Chemical Engineering Science 56 (2001) 69–76.

[148] Y. Li, J. Zhang, L.-S. Fan, Numerical simulation of gas-liquid-solid fluidization systems using a combined CFD-VOF-DPM method: bubble wake behavior, Chemical Engineering Science 54 (1999) 5101–5107.

[149] Y. Li, G. Yang, J. Zhang, L.-S. Fan, Numerical studies of bubble formation dynamics in gasliquidsolid fluidization at high pressures, Powder Technology 116 (2001) 246–260.

[150] C. Chen, L.-S. Fan, Discrete simulation of gasliquid bubble column and gasliquidsolid fluidized beds, AIChE Journal 50 (2004) 288–301.

[151] A. D. Renzo, F. P. D. Maio, Homogeneous and bubbling fluidization regimes in DEM-CFD simulations: Hydrodynamic stability of gas and liquid fluidized beds, Chemical Engineering Science 62 (2007) 116–130.

[152] T. Tsuji, K. Yabumoto, T. Tanaka, Spontaneous structures in three-dimensional bubbling gas-fluidized bed by parallel DEM-CFD coupling simulation, Powder Technology 185 (2008) 132–140.

[153] X. R. Fernandez, H. Nirschl, Simulation of particles and sediment behaviour in centrifugal field by coupling CFD and DEM, Chemical Engineering Science (2013) http://dx.doi.org/10.1016/j.ces.2013.02.039.

[154] L. Fries, S. Antonyuk, S. Heinrich, D. Dopfer, S. Palzer, Collision dynamics in fluidised bed granulators: A DEM-CFD study, Chemical Engineering Science 86 (2013) 108123.

[155] W.-C. Yan, Z.-H. Luo, A.-Y. Guo, Coupling of CFD with PBM for a pilot-plant tubular loop polymerization reactor, Chemical Engineering Science 66 (2011) 5148–5163.

[156] C. Drumm, M. M. Attarakih, H. Bart, Coupling of CFD with DPBM for an RDC extractor, Chemical Engineering Science 64 (2009) 721–732.

[157] H. S. Tan, M. J. V. Goldschimdt, R. Boerefijin, M. J. Hounslow, A. D. Salman, J. A. M. Kuipers, Building population balance model for fluidized bed melt granulation: lessons from kinetic theory of granular flow, Powder Technology 142 (2004) 103–109.

[158] P. Rajniak, F. Stepanek, K. Dhanasekharan, R. Fan, C. Mancinelli, R. T. Chern, A combined experimental and computational study of wet granulation in a wurster fluid bed granulator, Powder Technology 189 (2009) 190–201.

[159] M. Dosta, S. Antonyuk, S. Heinrich, Multiscale simulation of agglomerate breakage in fluidized bed, Ind. Eng. Chem. Res. 70 (2013) 165–175.

[160] R. B. Bird, W. E. Stewart, E. N. Lightfoot, Transport Phenomena, John Wiley & Sons (Asia) Pte. Ltd., Singapore, 2007.

[161] C. Hirsch, Numerical Computation of Internal and External Flows, John Wiley & Sons, NJ, USA, 1990.

[162] A. S. El Hagrasy, P. Cruise, I. Jones, J. D. Litster, In-line size monitoring of a twin screw granulation process using high-speed imaging, J Pharm Innov 8 (2013) 90–98.

[163] A. S. El Hagrasy, J. R. Hennenkamp, M. D. Burke, J. J. Cartwright, J. D. Litster, Twin screw wet granulation: Influence of formulation parameters on granule properties and growth behavior, Powder Technology 238 (2013) 108–115.

[164] EDEM CFD Coupling Interface, EDEM 2.5.1 documentation, DEM Solutions (2013) http://www.dem–solutions.com/.

[165] R. Mehvar, F. Jamali, Pharmacokinetic analysis of the enantiomeric inversion of chiral nonsteroidal antiinflammatory drugs, Pharm. Res. 5 (1988) 76–79.

[166] E. A. Meade, W. L. Smith, D. L. Dewitt, Differential inhibition of prostaglandin endoperoxide synthase (cyclooxygenase) isozymes by aspirin and other non-steroidal anti-inflammatory drugs, J. Biol. chem 9 (1993) 6610–6614.

[167] C. Mangwandi, Y. S. Cheong, M. J. Adams, M. J. Hounslow, A. D. Salman, The coefficient of restitution of different representative types of granules, Chemical Engineering Science 62 (2007) 437–450.

[168] C. Biggs, C. Sanders, A. Scott, A. Willemse, A. Hoffman, T. Instone, A. Salman, M. Hounslow, Coupling granule properties and granulation rates in high-shear granulation, Powder Technology 130 (2003) 162–168.

[169] L. Madec, L. Falk, E. Plasari, Modelling of the agglomeration in suspension process with multidimensional kernels, Powder Technology 130 (2003) 147–153.